INTERACTION NOTES

NOTE 437

JUNE 1984

A VARIATIONAL APPROACH TO DEVELOPING RELATIONSHIPS AMONG WIRE CURRENTS IN A CABLE BUNDLE

N. Engheta
F.C. Yang
K.S.H. Lee

DIKEWOOD
Division of Kaman Sciences Corporation
2800-28th Street, Suite 370
Santa Monica, California 90405

ABSTRACT

A deterministic approach based on the variational principle is employed to derive the relationships among the bulk cable current and its individual wire currents. These relationships can be utilized to develop as well as to verify pin specifications of a Line Replaceable Unit (LRU) via direct-drive tests, either onboard an aircraft or in a laboratory. A set of canonical problems involving 2-wire cable over a ground plane is studied in detail for the purpose of checking the derived relationships and of analyzing common- and differential-mode current distributions under various conditions. New experiments are suggested to verify as well as to improve the results reported herein.

INTERACTION NOTES

NOTE 437

JUNE 1984

A VARIATIONAL APPROACH TO DEVELOPING RELATIONSHIPS AMONG WIRE CURRENTS IN A CABLE BUNDLE

N. Engheta
F.C. Yang
K.S.H. Lee

DIKEWOOD
Division of Kaman Sciences Corporation
2800-28th Street, Suite 370
Santa Monica, California 90405

ABSTRACT

A deterministic approach based on the variational principle is employed to derive the relationships among the bulk cable current and its individual wire currents. These relationships can be utilized to develop as well as to verify pin specifications of a Line Replaceable Unit (LRU) via direct-drive tests, either onboard an aircraft or in a laboratory. A set of canonical problems involving 2-wire cable over a ground plane is studied in detail for the purpose of checking the derived relationships and of analyzing common- and differential-mode current distributions under various conditions. New experiments are suggested to verify as well as to improve the results reported herein.

PREFACE

We wish to thank Captain T. Marshall and Dr. C.E. Baum of the Air Force Weapons Laboratory and Dr. J.S. Shuster formerly at the Air Force Weapons Laboratory for their interest and suggestions in this effort. We also wish to thank Dr. A.G. DiLoreto of Dikewood for his advice and stimulating discussions on this work and Mr. R. Aguero of Dikewood for performing the numerical calculations.

CONTENTS

CONTENTS (Concluded)

I. INTRODUCTION

A "complete" EMP hardness statement for an aircraft or other vulnerable systems requires the knowledge of both the threat-induced stress or its bound and the susceptibility threshold level of every pin to every Line Replaceable Unit (LRU). The induced stresses can be obtained by measuring, in a system-level simulation test, the currents or the voltages on the wires connected to LRU's (and then using the appropriate extrapolation). The susceptibility thresholds can be obtained by performing onboard and/or laboratory direct-drive measurements. However, this is a prohibitive effort because of the large number of LRU pins contained in an aircraft.

Continually, attempts have been made to reduce the number of measurements required for a reliable hardness assessment. Since wires leading to LRU pins are usually lumped into bundles, one such attempt was to find relationships among the bounds of the cable bundle current and the bounds of the individual wire currents by using a statistical approach (Refs. 1,2). However, the samples used in the study were not large enough and the conclusions derived therefrom were not convincing. Furthermore, the bounding approach that was used, although appropriate for pin stress estimates, does not provide pin susceptibility thresholds.

In this report, a deterministic as well as a more general approach is undertaken. More specifically, analyses are performed to determine how currents or voltages on individual wires of a bundle can be established without measuring each wire current or voltage. It is expected that the number of required measurements will strongly depend on how a bundle is excited and configured. This dependence suggests that a deterministic approach is preferred over a statistical one.

In Section II, a detailed analysis is given as to how the individual wire currents can be determined without measuring the current in each wire . The analysis is based on a variational technique. Section III describes how the results presented in Section II can be used in direct-drive testing in general and for determining pin susceptibility thresholds in particular. This type of testing can be utilized for developing aircraft electronic component specifications as well as for verifying specification requirements. Sections II and III conclude with simple examples that illustrate the methodologies given Section IV is devoted to a detailed study of the currents on the cable wires and how the excitation mechanisms and cable configurations will affect the wire responses. Simple and useful rules for selecting the optimal measurement approach* is deduced from an analysis of 2-wire bundles. The variational technique introduced in Section II requires information on the impedances of the cable bundle at the pins. Unfortunately, the existing data base does not provide sufficient information to verify the rules deduced from the variational technique. Section V describes new experiments for the verification and improvement of the rules. The experiments are designed so that they can be performed either in a laboratory or in the EMP Test Aircraft (EMPTAC). A brief summary and conclusions of this report are given in Section VI.

*Optimality here is defined in terms of the number of measurements required to obtain meaningful estimates of each wire current.

II. DEDUCTION OF INDIVIDUAL WIRE CURRENTS FROM A LIMITED NUMBER OF MEASUREMENTS

When an aircraft is exposed to an EMP, high-intensity transients may be induced in cable bundles inside the aircraft. These bundles are connected to LRU's. One of the important problems relating to this EMP interaction is to find the intensities of the induced transients at the pins of these LRU's. These transients are the pin currents and the pin voltages. Obviously a procedure for quantifying all such transients based solely on measurements is not practical. Hence analytical techniques to reduce the number of measurements are urgently needed. One powerful technique is that of a variational principle, which requires the use of equivalent circuits at the LRU's. The definition of the equivalent circuits at an N-port LRU will first be given, and then follows the application of a variational principle to the problem at hand.

1. DEFINITION OF AN N-PORT EQUIVALENT CIRCUIT

Let a cable bundle with N wires be connected to an N-port LRU. This cable guides induced transients into the LRU (Fig. 1). The driving circuit can be replaced by an equivalent circuit, namely the Thevenin equivalent circuit with N voltage sources which can be denoted by a vector of dimension N in series with an NxN source impedance matrix ($Z_{S_{n,m}}$). The load impedance ($Z_{L_{n,m}}$) is also an NxN matrix (Fig. 2). Values for the N voltage sources contained in this circuit can be obtained by disconnecting all the wires from the LRU and then measuring all the voltages at the disconnection (Fig. 3a). That is

$$(V_{oc_n})^T = (V_{oc_1}, V_{oc_2}, \cdots, V_{oc_N}) \tag{1}$$

where $(\ )^T$ stands for transpose of a matrix. To find the elements of the source impedance matrix $Z_{S_{n,m}}$ we first disconnect all the wires from the LRU,

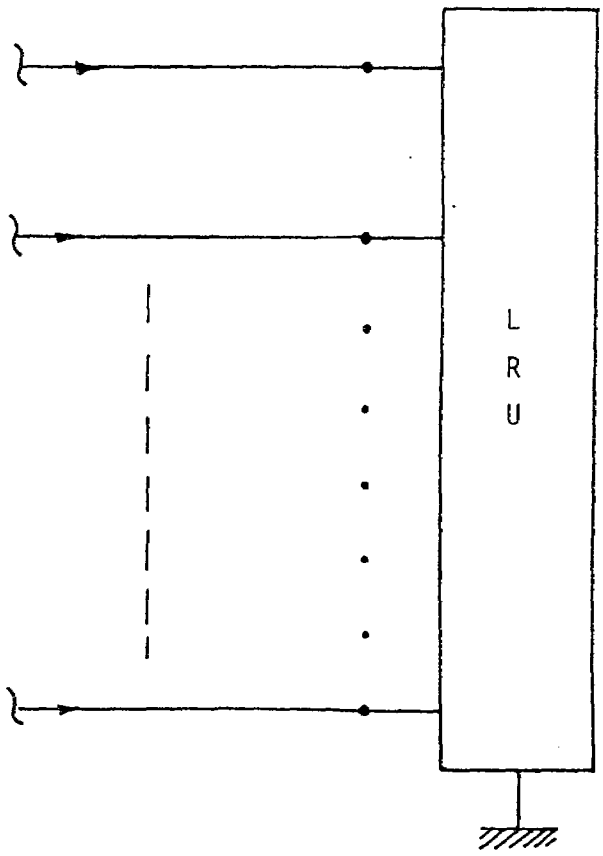

Figure 1. An N-port LRU with an N-wire cable bundle connected to it.

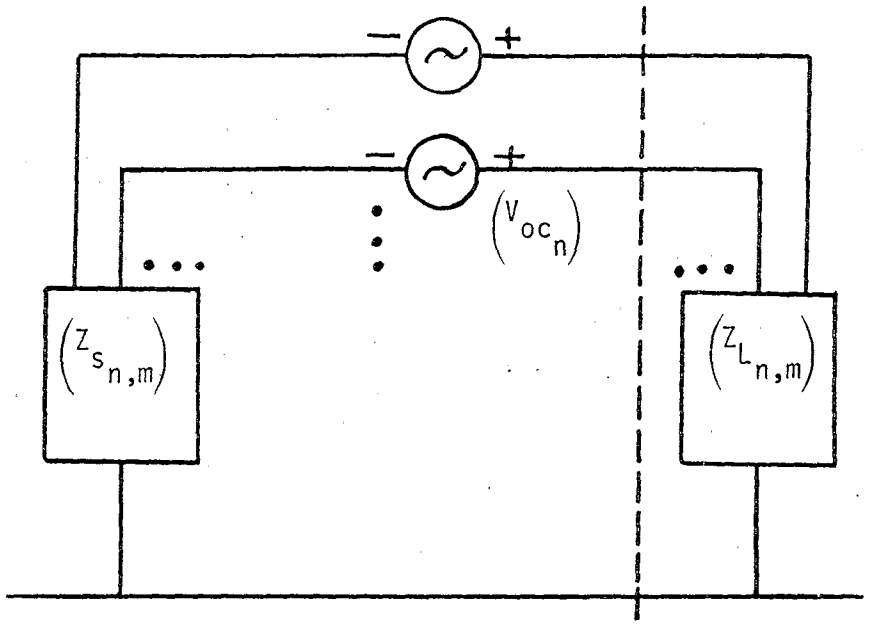

(a) The Thévenin equivalent circuit.

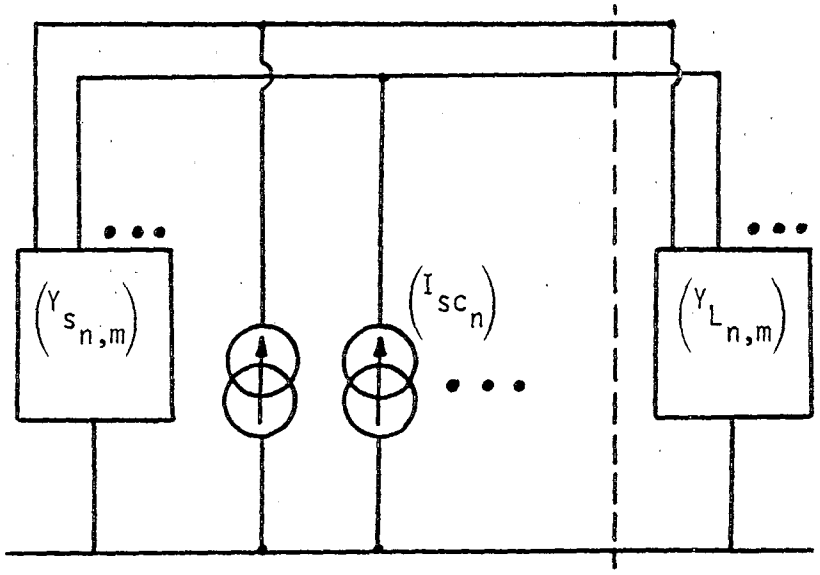

(b) The Norton equivalent circuit

Figure 2 . The equivalent circuits for the LRU in Figure 1 .

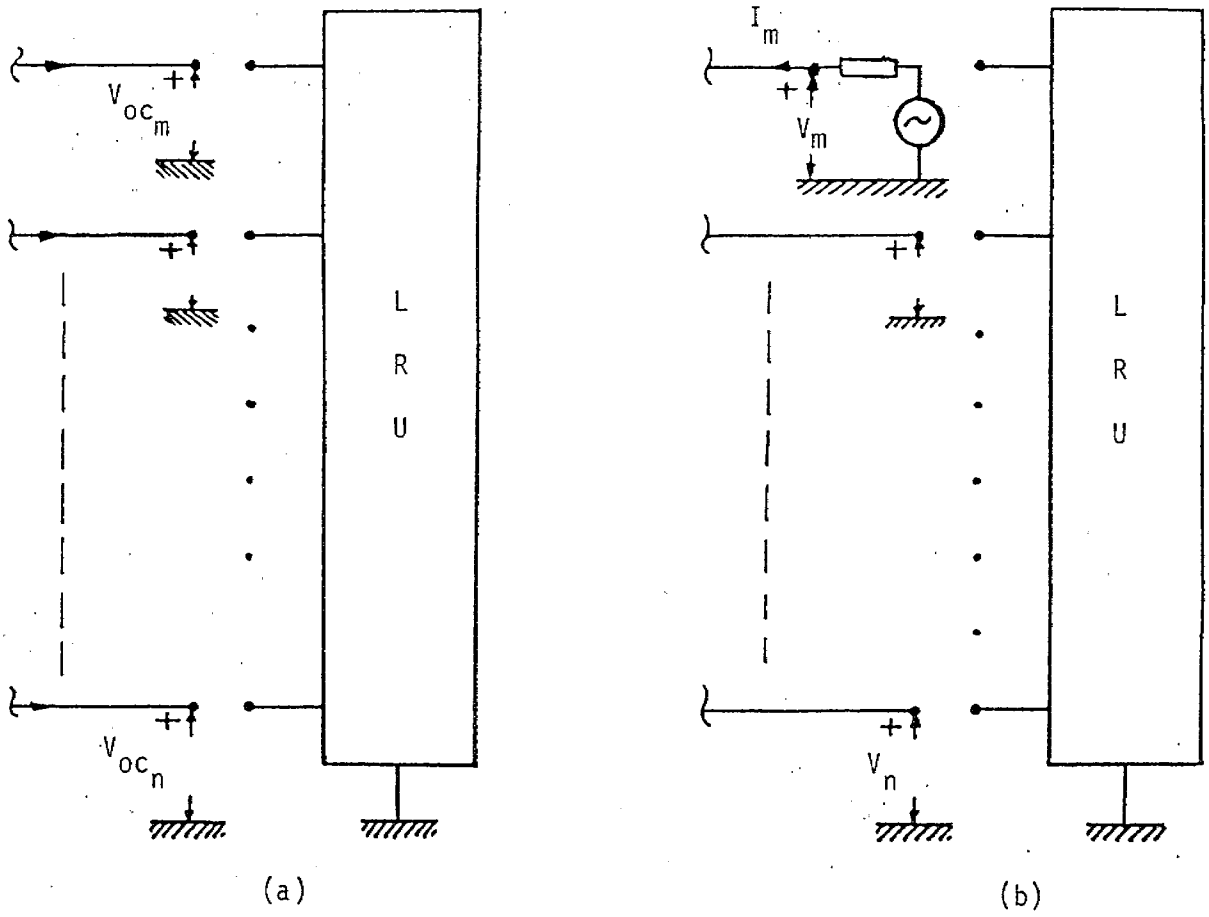

Figure 3. Experimental setups to measure (a) the open-circuit voltages, and (b) the source impedance element $Z_{s_{n,m}}$.

apply a source to the m-th wire and then measure the current on the m-th wire and the open-circuit voltage on the n-th wire while the rest of the wires remains open (Fig. 3b). With this procedure $Z_{s_{n,m}}$ is simply given by

$$Z_{s_{n,m}} = V_n/I_m \text{ when } I_1 = I_2 = \ldots = I_{m-1} = I_{m+1} = \ldots = I_N = 0 \text{ and } I_m \neq 0. \quad (2)$$

This method can also be used to obtain the load impedance matrix of the LRU.

Another equivalent circuit, namely the Norton equivalent circuit with current sources, can also be constructed. The current source vector can be found by shorting out all the wires and measuring all the currents flowing on them, regardless of the nature of excitation (Fig. 4a). In the Norton equivalent circuit $(Y_{s_{n,m}})$ is the inverse of $(Z_{s_{n,m}})$, i.e.,

$$(Y_{s_{n,m}}) = (Z_{s_{n,m}})^{-1} \quad (3)$$

Another way of finding the element $Y_{s_{n,m}}$ of the source admittance matrix is to disconnect all wires from the LRU, to apply a source to the m-th wire and to measure the voltage on the m-th wire and the short-circuit current on the n-th wire while the rest of the wires remains shorted (Fig. 4b). Then $Y_{s_{n,m}}$ is simply given by

$$Y_{s_{n,m}} = I_n/V_m \text{ when } V_1 = V_2 = \ldots = V_{m-1} = V_{m+1} = \ldots = V_N = 0 \text{ and } V_m \neq 0 \quad (4)$$

From the Thevenin equivalent circuits, we can write

$$(I_{L_n}) = ((Z_{L_{n\,m}}) + (Z_{s_{n,m}}))^{-1} \cdot (V_{oc_m}) \quad (5)$$

$$(V_{L_n}) = (Z_{L_{n,m}}) \cdot ((Z_{L_{m,p}}) + (Z_{s_{m,p}}))^{-1} \cdot (V_{oc_p}) \quad (6)$$

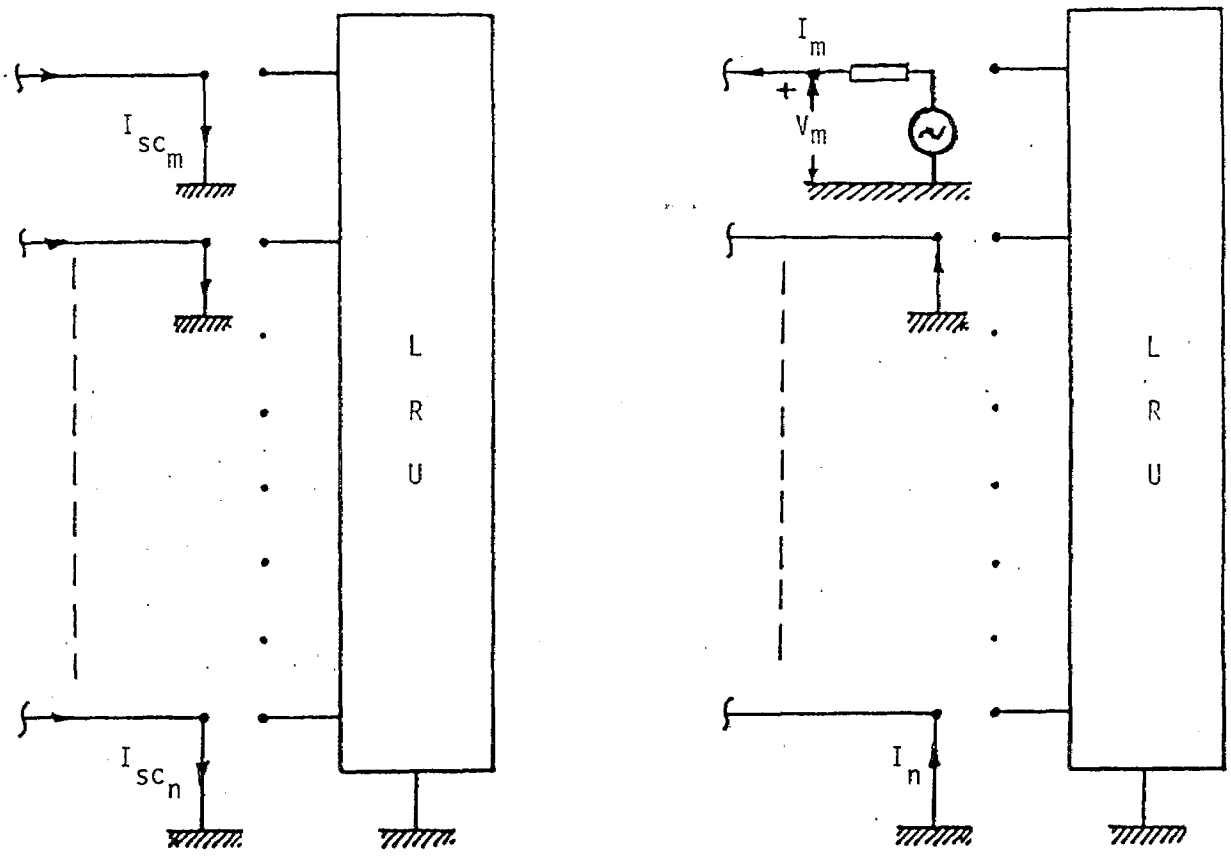

Figure 4. Experimental setups to measure (a) the short-circuit currents, and (b) the source admittance elements $Y_{s_{n,m}}$.

Similarly, from the Norton equivalent circuit we can write

$$(V_{L_n}) = ((Y_{L_{n,m}}) + (Y_{s_{n,m}}))^{-1} \cdot (I_{sc_m}) \tag{7}$$

$$(I_{L_n}) = (Y_{L_{n,m}}) \cdot ((Y_{L_{m,p}}) + Y_{s_{m,p}}))^{-1} \cdot (I_{sc_p}) \tag{8}$$

Since these two equivalent circuits should give the same load responses, we get, for $(Z_{L_{n,m}}) = (0_{n,m})$

$$(I_{L_n}) = (I_{sc_n}) = (Z_{s_{n,m}})^{-1} \cdot (V_{oc_m}) = (Y_{s_{n,m}}) \cdot (V_{oc_m}) \tag{9}$$

The load responses, (V_{L_n}) and (I_{L_n}), are the quantities of interest. However, it is very difficult, if not practically impossible, to find all the elements of (I_{L_n}) and (V_{L_n}) for the LRU. This is due to the fact that to find (I_{L_n}) or (V_{L_n}) for all excitations necessary for a reliable hardness assessment requires a large number of measurements. It is therefore desirable to quantify pin currents and pin voltages with fewer number of measurements. To make this possible, one needs to find the relationships among the fewer measured quantities and all the individual pin responses. The fewer measurements should be the ones that are easy to measure and expected to contain more information. Some of the candidate quantities for measurements are the cable bundle current I_B and the currents on wires that are expected to be strongly excited. In the following, the relationships will be developed when only the cable bundle current is measured, or when only one wire current is measured, or when one wire current and the cable bundle current are measured. The relationships can then easily be extended to cases with more number of measurements.

2. ONLY I_B MEASURED

It is known that currents and voltages in a circuit distribute themselves in such a way that the energy is stationary with respect to currents (Ref. 3). In addition to satisfying the condition of stationarity, constraints must be imposed for determining all the currents/voltages. The only constraint to be considered in this subsection is that the sum of the individual wire currents be equal to the measured bulk cable current I_B. The method of Lagrange Multipliers will now be used to find the relationship between I_B and the individual wire currents (Refs. 4, 5, 6). The energy function of the Thevenin equivalent circuit is given by

$$P = (I^*_{L_n})^T \cdot (Z_{t_{n,m}}) \cdot (I_{L_m}) \tag{10}$$

where $(Z_{t_{n,m}}) = (Z_{L_{n,m}}) + (Z_{s_{n,m}})$ which are generally complex matrices. We can rewrite P in terms of the elements of the matrices. That is

$$P = \sum_{n=1}^{N} \sum_{m=1}^{N} I^*_{L_n} Z_{t_{n,m}} I_{L_m} \tag{11}$$

The constraint is

$$I_B = \sum_{m=1}^{N} I_{L_m} \tag{12}$$

with I_{L_m} being the m-th pin current. Substituting

$$I_{L_m} = a_m + jb_m \tag{13}$$

$$I_B = I_{Br} + jI_{Bim} \tag{14}$$

into Equations 11 and 12, we obtain

$$P = \sum_{n=1}^{N} \sum_{m=1}^{N} (a_n - jb_n) Z_{t_{n,m}} (a_m + jb_m) \tag{15}$$

$$I_{Br} = \sum_{m=1}^{N} a_m \tag{16}$$

$$I_{Bim} = \sum_{m=1}^{N} b_m \tag{17}$$

Now, we must find the stationary points of the expression

$$f = \sum_{n=1}^{N} \sum_{m=1}^{N} (a_n - jb_n) Z_{t_{n,m}} (a_m + jb_m) + \lambda_1 (I_{Br} - \sum_{m=1}^{N} a_m) + \lambda_2 (I_{Bim} - \sum_{m=1}^{N} b_m) \tag{18}$$

where λ_1 and λ_2 are Lagrange Multipliers. Accordingly we should have

$$\frac{\partial f}{\partial a_n} = 0, \; n = 1, 2, \ldots, N \tag{19}$$

$$\frac{\partial f}{\partial b_n} = 0, \; n = 1, 2, \ldots, N \tag{20}$$

Consequently, we get

$$\sum_{m=1}^{N} Z_{t_{n,m}} (a_m + jb_m) + \sum_{m=1}^{N} (a_m - jb_m) Z_{t_{m,n}} - \lambda_1 = 0. \tag{21}$$

$$-j \sum_{m=1}^{N} Z_{t_{n,m}} (a_m + jb_m) + j \sum_{m=1}^{N} (a_m - jb_m) Z_{t_{m,n}} - \lambda_2 = 0 \tag{22}$$

Assuming that $(Z_{t_{n,m}})$ is a symmetric matrix, one can rewrite Equations 21 and 22 as

$$2(Z_{t_{n,m}}) \cdot (a_m) = \lambda_1 (1_n) \tag{23}$$

$$2(Z_{t_{n,m}}) \cdot (b_m) = \lambda_2 (1_n) \tag{24}$$

where

$(a_m)^T = (a_1, a_2, \cdots, a_N)$, $(b_m)^T = (b_1, b_2, \cdots, b_N)$, and $(1_n)^T = (1, 1, \cdots, 1)$.

(a_m) and (b_m) can thus be written as follows

$$(a_m) = \frac{1}{2}\lambda_1 (Y_{t_{m,n}}) \cdot (1_n) \tag{25}$$

$$(b_m) = \frac{1}{2}\lambda_2 (Y_{t_{m,n}}) \cdot (1_n) \tag{26}$$

where $(Y_{t_{n,m}}) = (Z_{t_{n,m}})^{-1}$. Substituting Equations 25 and 26 into Equation 16 and 17, and solving for λ_1 and λ_2 we find

$$\lambda_1 = \frac{2I_{Br}}{(1_n)^T \cdot (Y_{t_{n,m}}) \cdot (1_m)} \tag{27}$$

$$\lambda_2 = \frac{2I_{Bim}}{(1_n)^T \cdot (Y_{t_{n,m}}) \cdot (1_m)} \tag{28}$$

Consequently, by substituting into Equations 25 and 26 (a_m) and (b_m) are found to be

$$(a_m) = I_{Br} \frac{(Y_{t_{n,m}}) \cdot (1_n)}{(1_n)^T \cdot (Y_{t_{n,m}}) \cdot (1_m)} \tag{29}$$

$$(b_m) = I_{Bim} \frac{(Y_{t_{n,m}}) \cdot (1_n)}{(1_n)^T \cdot (Y_{t_{n,m}}) \cdot (1_m)} \tag{30}$$

Finally, we have arrived at the relationship between I_B and (I_{L_m}),

$$(I_{L_m}) = I_B \frac{(Y_{t_{m,n}}) \cdot (1_n)}{(1_n)^T \cdot (Y_{t_{n,m}}) \cdot (1_m)} \tag{31}$$

where

$$(Y_{t_{m,n}}) = (Z_{t_{m,n}})^{-1} = ((Z_{s_{m,n}}) + (Z_{L_{m,n}}))^{-1}$$

I_B is the measured bulk cable current and I_{L_m} is the current on wire m. As can be seen, from a knowledge of I_B, $(Z_{s_{n,m}})$ and $(Z_{L_{n,m}})$, (I_{L_m}) can be obtained. Using the Thevenin equivalent circuit, we can write

$$(V_{oc_n}) = (Z_{t_{n,m}}) \cdot (I_{L_m}) = I_B \frac{(1_n)}{(1_n)^T \cdot (Y_{t_{n,m}}) \cdot (1_m)} \tag{32}$$

Therefore, (I_{L_m}) obtained in Equation 31, will be the exact current vector, if the open-circuit voltages on all the wires are the same. Equations 31 and 32 hold true in the time domain when $(Z_{s_{m,n}})$ and $(Z_{L_{m,n}})$ are resistive for all frequencies.

3. ONLY ONE INDIVIDUAL WIRE CURRENT MEASURED

Another type of constraint that can be imposed is that the current of the most strongly excited individual wire, for example, I_k be given from measurement. That is

$$I_{L_k} = I_k \tag{33}$$

From Equations 13 and 33, we obtain

$$a_k = I_{kr} \tag{34}$$

$$b_k = I_{kim} \tag{35}$$

where I_{kr} and I_{kim} are real and imaginary parts of I_k, respectively. Now, we must find the stationary points of the expression

$$f = \sum_{n=1}^{N} \sum_{m=1}^{N} (a_n - jb_n) Z_{t_{n,m}} (a_m + jb_m) + \lambda_1 (I_{kr} - a_k) + \lambda_2 (I_{kim} - b_k) \tag{36}$$

where λ_1 and λ_2 are Lagrange Multipliers. Accordingly we should have, from Equations 19 and 20,

$$\sum_{n=1}^{N} Z_{t_{n,m}} (a_m + jb_m) + \sum_{m=1}^{N} (a_m - jb_m) Z_{t_{m,n}} - \lambda_1 \delta_{nk} = 0 \tag{37}$$

$$-j \sum_{m=1}^{N} Z_{t_{n,m}} (a_m + jb_m) + j \sum_{m=1}^{N} (a_m - jb_m) Z_{t_{m,n}} - \lambda_2 \delta_{nk} = 0 \tag{38}$$

Assuming that $(Z_{t_{m,n}})$ is a symmetric matrix, one can write Equations 37 and 38 as

$$2(Z_{t_{n,m}}) \cdot (a_m) = \lambda_1 \delta_{nk} \tag{39}$$

$$2(Z_{t_{n,m}}) \cdot (b_m) = \lambda_2 \delta_{nk} \tag{40}$$

a_m and b_m can thus be written as follows

$$a_m = \frac{1}{2} \lambda_1 Y_{t_{m,k}} \tag{41}$$

$$b_m = \frac{1}{2} \lambda_2 Y_{t_{m,k}} \tag{42}$$

Substituting Equations 41 and 42 into Equations 34 and 35, and solving for λ_1 and λ_2 we find

$$\lambda_1 = \frac{2I_{kr}}{Y_{t_{k,k}}} \tag{43}$$

$$\lambda_2 = \frac{2I_{kim}}{Y_{t_{k,k}}} \tag{44}$$

Therefore, a_m and b_m are

$$a_m = I_{kr} \frac{Y_{t_{m,k}}}{Y_{t_{k,k}}} \tag{45}$$

$$b_m = I_{kim} \frac{Y_{t_{m,k}}}{Y_{t_{k,k}}} \tag{46}$$

Finally, we arrive at the following important relationship.

$$I_{L_m} = I_k \frac{Y_{t_{m,k}}}{Y_{t_{k,k}}} \tag{47}$$

Using the Thevenin equivalent circuit, we get

$$(V_{oc_n}) = (Z_{t_{n,m}}) \cdot (I_{L_m})$$

$$= I_k \frac{\delta_{nk}}{Y_{t_{k,k}}} \tag{48}$$

Hence, (I_{L_m}) obtained from the above method will be accurate if the open-circuit voltages of all wires except the k-th wire are zero. Equations 47 and 48 hold true in the time domain when $(Z_{L_{m,n}})$ and $(Z_{s_{m,n}})$ are resistive for all frequencies.

4. ONLY BULK-CABLE CURRENT AND CURRENT ON ONE STRONGLY EXCITED WIRE MEASURED

Using an approach similar to the ones used in the previous cases, one obtains,

$$I_{L_n} = I_B \frac{Y_{t_{k,k}} \sum_{m=1}^{N} Y_{t_{n,m}} - Y_{t_{n,k}} \sum_{m=1}^{N} Y_{t_{k,m}}}{Y_{t_{k,k}} \left(\sum_{m=1}^{N} \sum_{p=1}^{N} Y_{t_{m,p}} \right) - \left(\sum_{m=1}^{N} Y_{t_{m,k}} \right) \left(\sum_{m=1}^{N} Y_{t_{k,m}} \right)} +$$

$$+ I_k \frac{Y_{t_{n,k}} \sum_{m=1}^{N} \sum_{p=1}^{N} Y_{t_{m,p}} - \left(\sum_{m=1}^{N} Y_{t_{m,k}} \right) \left(\sum_{m=1}^{N} Y_{t_{n,m}} \right)}{Y_{t_{k,k}} \left(\sum_{m=1}^{N} \sum_{p=1}^{N} Y_{t_{m,p}} \right) - \left(\sum_{m=1}^{N} Y_{t_{m,k}} \right) \left(\sum_{m=1}^{N} Y_{t_{k,m}} \right)} \tag{49}$$

where I_B and I_k are the measured bulk-cable and the k-th wire current, respectively (see Appendix A).

The above method can be applied to any other combination of current measurements as constraints for obtaining relationship among wire currents.

5. EXAMPLES:

Figure 5 depicts a two-wire configuration. The wires all have the same length , but they do not necessarily have the same displacement above the ground plane. The characteristic impedance matrix $(Z_{C_{n,m}})$ provides information about the line configuration. These wires are terminated at both ends with the load and terminating impedance matrices, $(Z_{L_{n,m}})$ and $(Z_{O_{n,m}})$, respectively. These wires are assumed to be excited by voltage and current sources

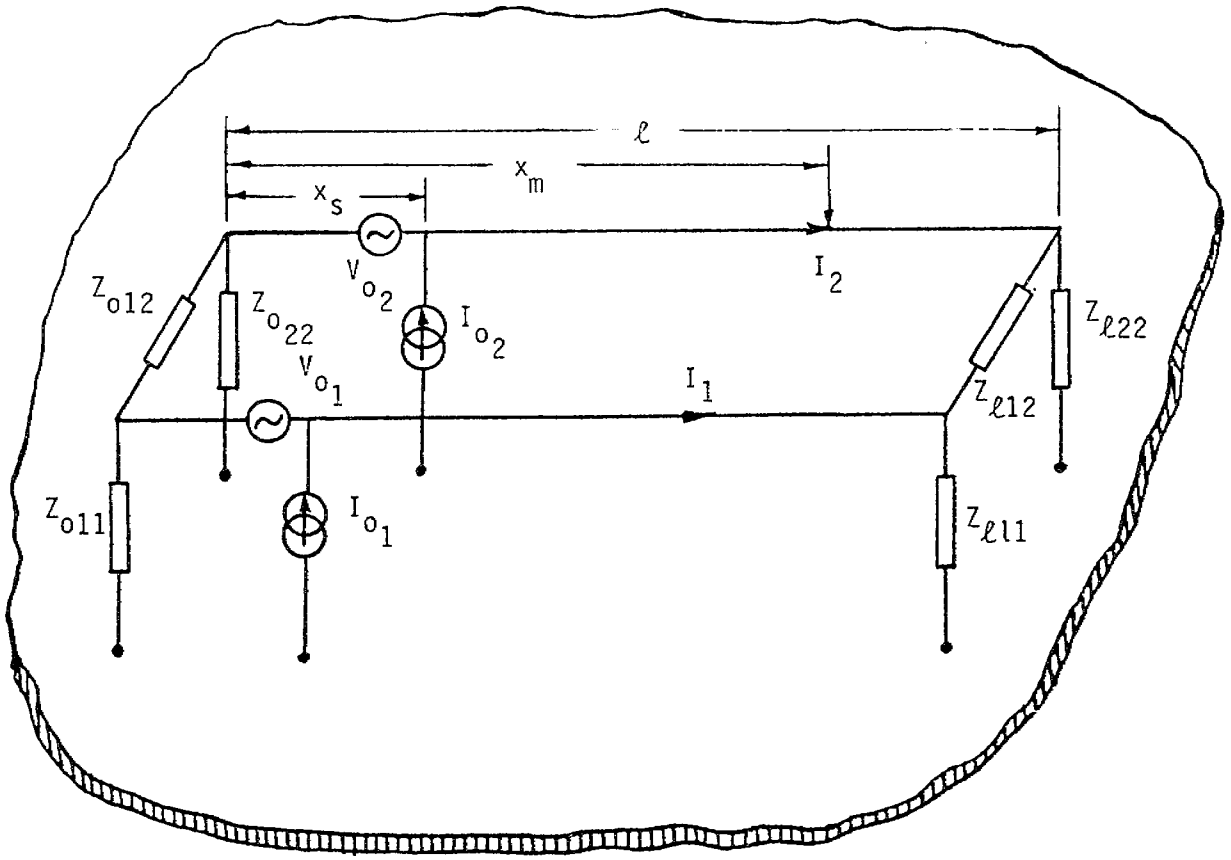

ℓ = wire length

x_s = source location

x_m = measurement location

$$(I_{o_n}) = \begin{pmatrix} I_{o_1} \\ I_{o_2} \end{pmatrix} \text{ current source}$$

$$(V_{o_n}) = \begin{pmatrix} V_{o_1} \\ V_{o_2} \end{pmatrix} \text{ voltage source}$$

$Z_{\ell 11}$, $Z_{\ell 12}$, $Z_{\ell 22}$ load impedances

Z_{o11}, Z_{o12}, Z_{o22} terminating impedances

Figure 5. Two-wire transmission line model.

denoted by (V_{o_n}) and (I_{o_n}). Computer codes have been developed to calculate currents and voltages at any point on these wires for arbitrary sources, load, terminating and characteristic impedances.

Let the sources take the following form.

$$V_{o_n}(t) = V_{o_n} \exp(-\alpha t)\sin(2\pi f_o t) \tag{50}$$

$$I_{o_n}(t) = I_{o_n} \exp(-\alpha t)\sin(2\pi f_o t) \tag{51}$$

where f_o = 2 MHz , $\alpha = 5 \times 10^6 \text{sec}^{-1}$, V_{o_n} = 1 volt and I_{o_n} = 1 mA. The chosen values for f_o and α are typical for the fundamental resonant mode of most aircraft (Ref. 7). Using the computer code, we find I_1 and I_2 at x_m = . These exact quantities will now be compared with those obtained from the variational technique described above. First, take the case where only I_B is measured, whose value is just $I_1 + I_2$. Using this I_B value in Equation 31 we obtain estimates of the wire currents, I_1' and I_2'. Next consider the case where only the current on wire #1 is measured. Using this current value as I_k in Equation 47, we obtain estimates of wire currents. I_1'' and I_2''.

Figures 6 and 7 present the plots of these currents for two different types of sources. Since the terminating impedance, ($Z_{o_{n,m}}$) at x = 0 is equal to the characteristic impedance ($Z_{c_{n,m}}$) , the open-circuit voltages of the two wires are about the same. Consequently, I_1' and I_2' obtained from I_B, alone are very much similar to I_1 and I_2 as they should. However, I_2'' is at variance with I_2. To quantify the accuracy associated with the currents estimated from only a lim ted number of measurements, we introduce a curve as shown in Figure 8 in which the horizontal axis indicates the number of measurements in a bundle of N wires and the vertical axis provides a measure of accuracy on the individual wire currents. The vertical axis extends from 0 to 100%. A

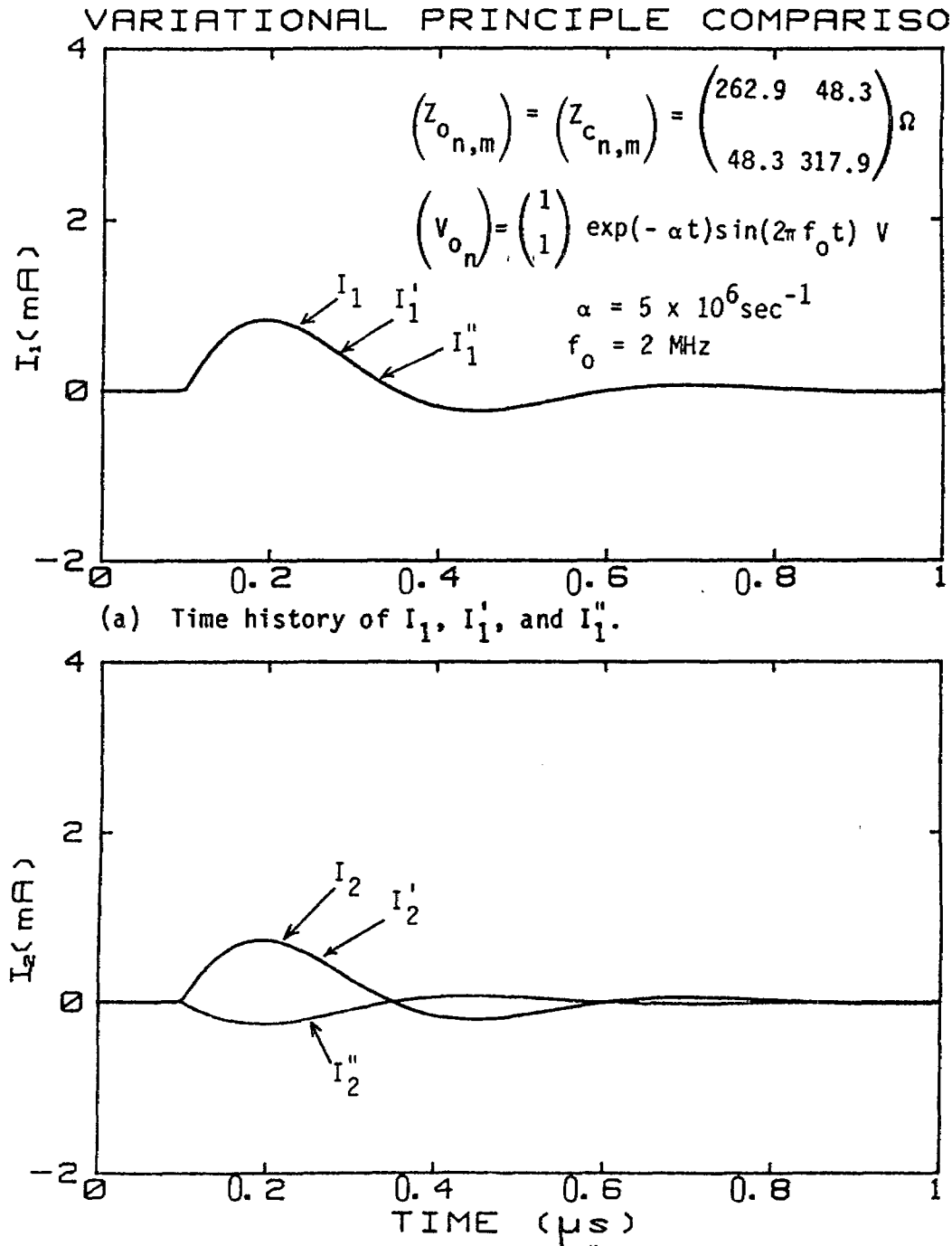

Figure 6. Exact wire currents (I_1, I_2) and estimated wire currents (I_1', I_2'; I_1'',I_2'') using two variational principle techniques when ℓ = 30 m, x_s = 0.25 m, x_m = 30 m, $Z_{\ell 11} = Z_{\ell 12} = Z_{\ell 22}$ = 400 Ω.

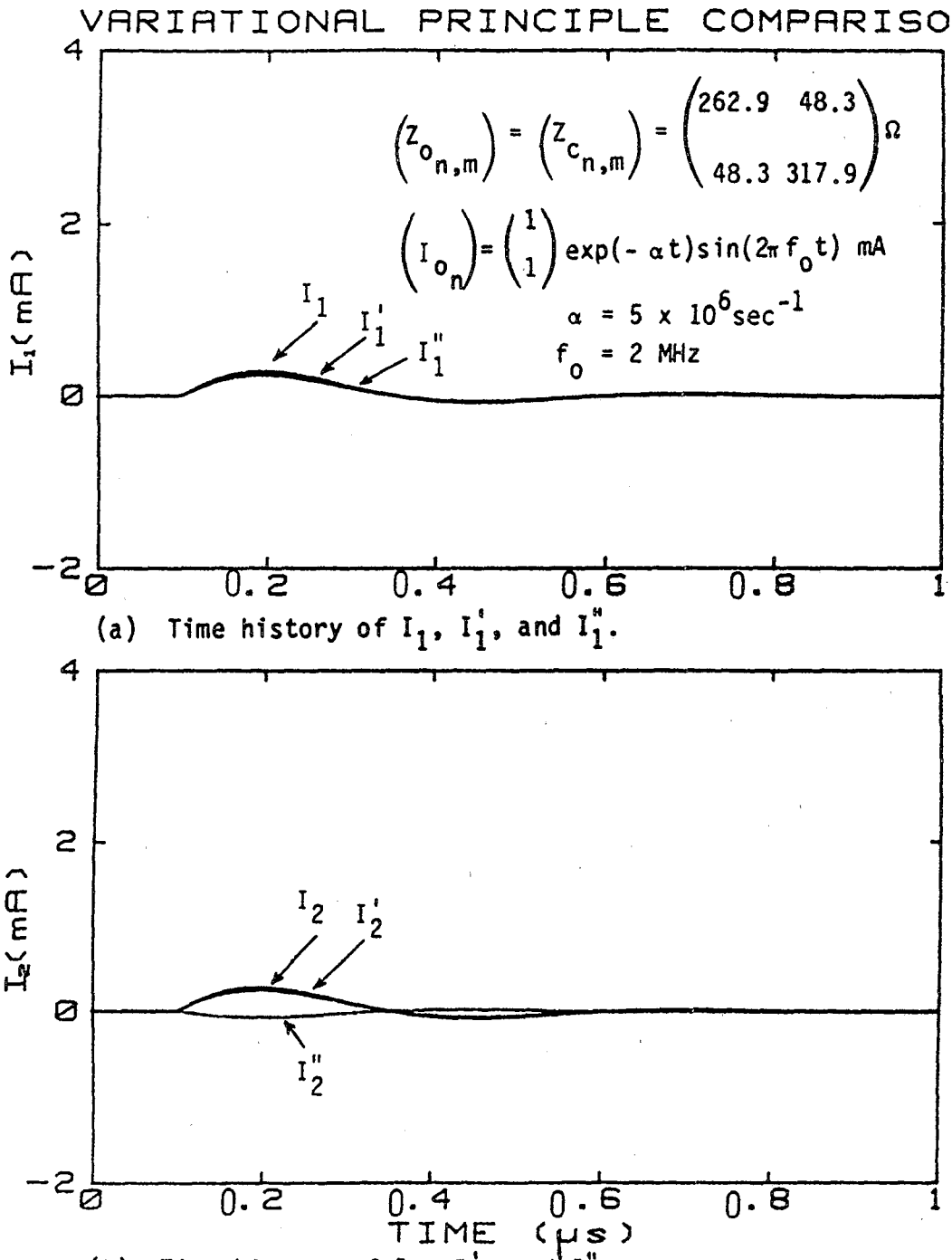

(a) Time history of I_1, I_1', and I_1''.

(b) Time history of I_2, I_2', and I_2''.

Figure 7. Exact wire currents (I_1, I_2) and estimated wire currents (I_1', I_2'; I_1'',I_2'') using two variational principle techniques when ℓ = 30 m, x_s = 0.25 m, x_m = 30 m, $Z_{\ell 11} = Z_{\ell 12} = Z_{\ell 22}$ = 400 Ω.

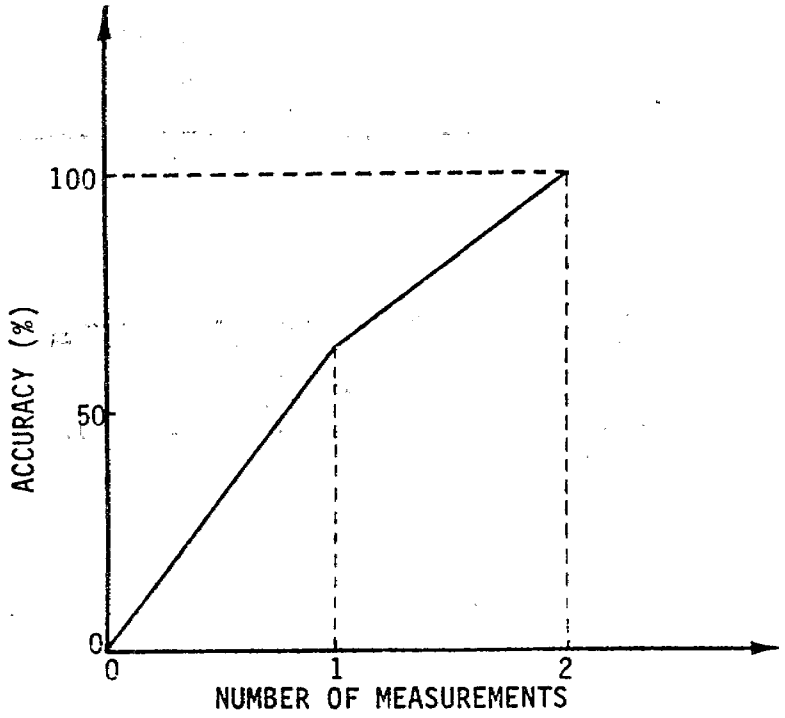

Figure 8. The accuracy measure versus the number of measurements for two-wire transmission line model.

vertical value of 100% indicates that there is no difference in the estimated value and the actual value. One accuracy gauge to be used for the vertical axis is

$$\text{Accuracy} = \min_{\text{all wires}} \left\{ \frac{2}{\pi} \cot^{-1} \left| \frac{\max|I_{\text{actual}}| - \max|I_{\text{calc.}}|}{\max|I_{\text{actual}}|} \right| \times 100\% \right\} \quad (52)$$

Figure 9 depicts the accuracy in terms of the relative error which is the argument of the inverse cotangent function. As can be seen, the relative error of 100%, i.e., $|I_{\text{calc.}}| = 2|I_{\text{actual}}|$, corresponds to an accuracy of 50%.

It is expected that the accuracy curve defined by Equation 52 be monotonically increasing with the number of measurements. In the two-wire transmission-line example the accuracy is 100% if the number of measurement is 2. However, if the number of measurement is 1, e.g., only an individual wire current is measured, then for I_2'' we obtain from Figure 6b a relative error of 62% which corresponds to accuracy ≈ 64%

Figures 10 and 11 show the cases where only one wire is excited and the terminating impedance ($Z_{o_{n,m}}$) is equal to the characteristic impedance ($Z_{c_{n,m}}$). In these cases the open-circuit voltage of the excited wire is nonzero and dominant over the others. Therefore I_1'' and I_2' are very much similar to I_1 and I_2, as can be seen from Figures 10 and 11. However, I_1' and I_2' are not equal to I_1 and I_2. The corresponding relative error and accuracy for I_1' in Figure 11 are 75% and 59%, respectively

Figures 12 and 13 show the cases where the terminating impedance ($Z_{o_{n,m}}$) at x=0 is not equal to the characteristic impedance ($Z_{c_{n,m}}$). As can be seen from Figure 12 where the two wires are excited, I_1' and I_2' obtained from I_B have a smaller maximum relative error. On the other hand, where one wire is excited (Fig. 13), I_1'' and I_2'' have a smaller maximum relative error.

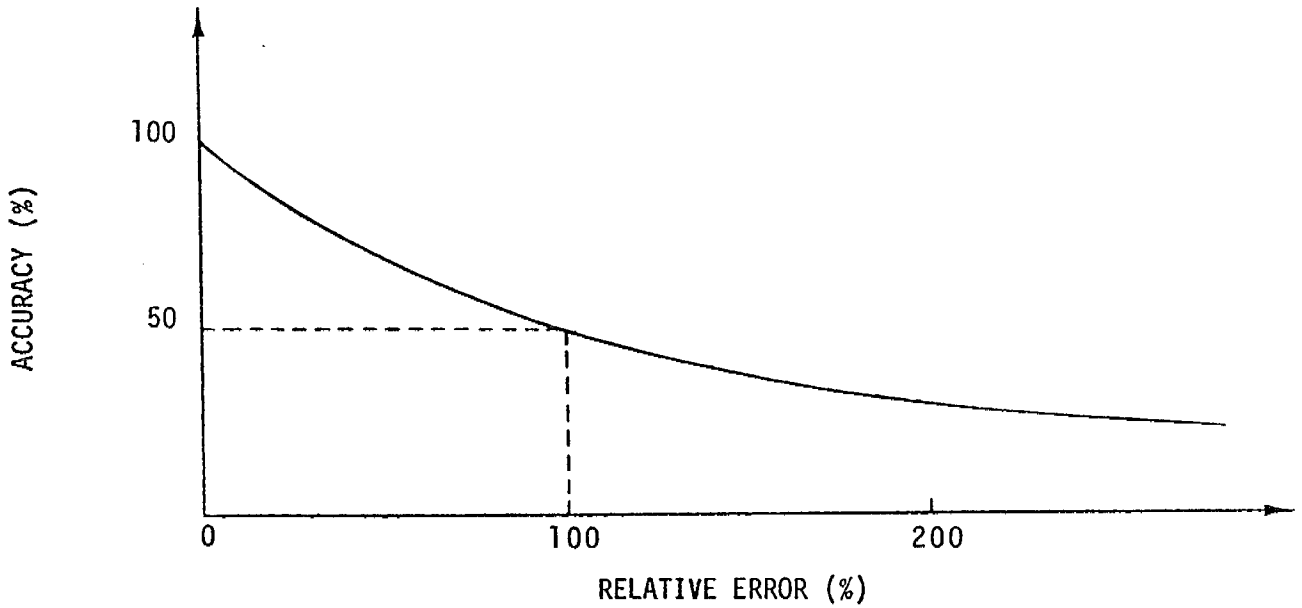

Figure 9. The accuracy measure versus the relative error.

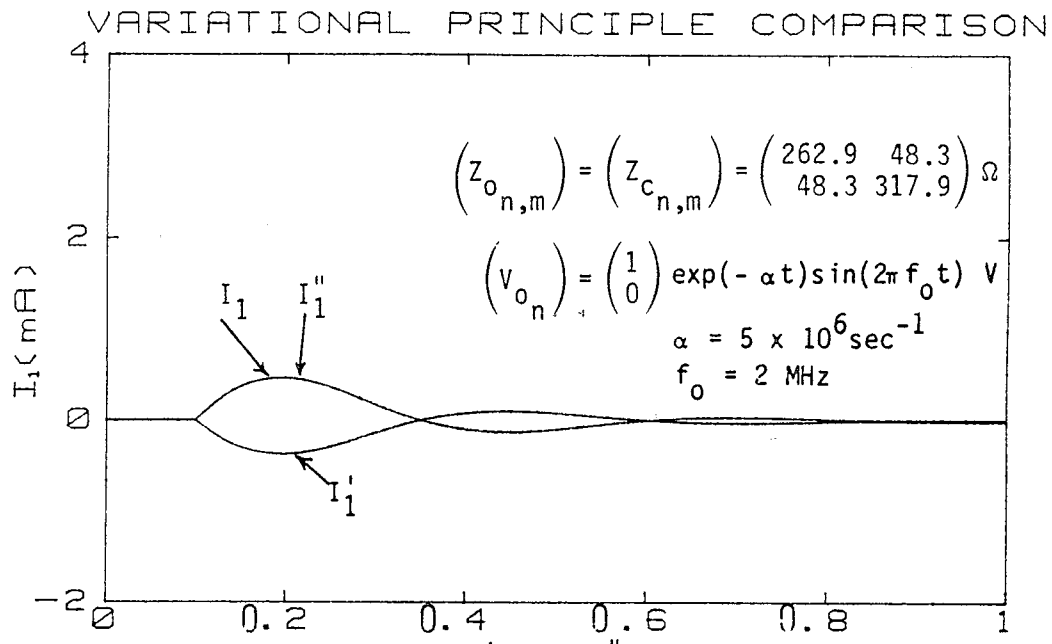

(a) Time history of I_1, I_1' and I_1''.

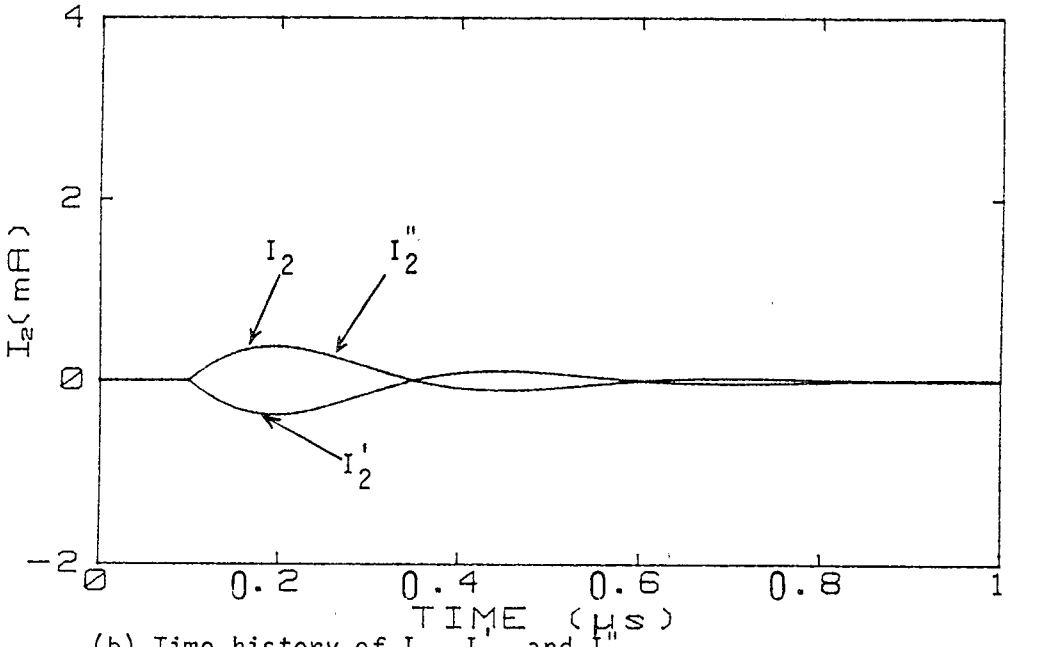

(b) Time history of I_2, I_2', and I_2''.

Figure 10. Exact wire currents (I_1, I_2) and estimated wire currents (I_1', I_2', I_1'', I_2'') using two variational principle techniques when ℓ = 30 m, x_s = 0.25 m, x_m = 30 m, $Z_{\ell 11} = Z_{\ell 12} = Z_{\ell 22}$ = 400 Ω.

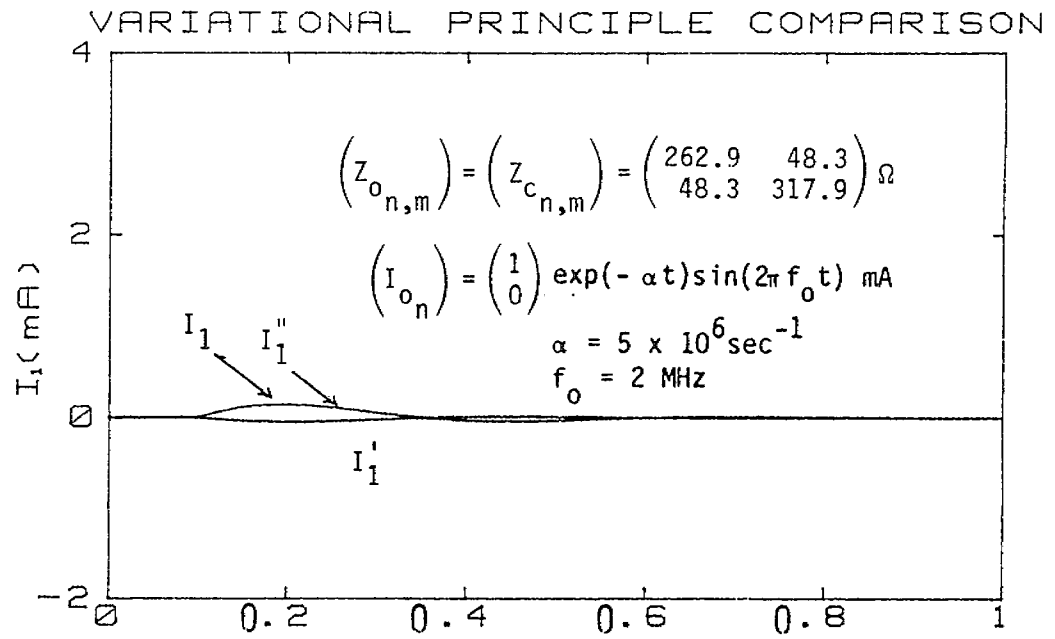

(a) Time history of I_1, I_1', and I_1''.

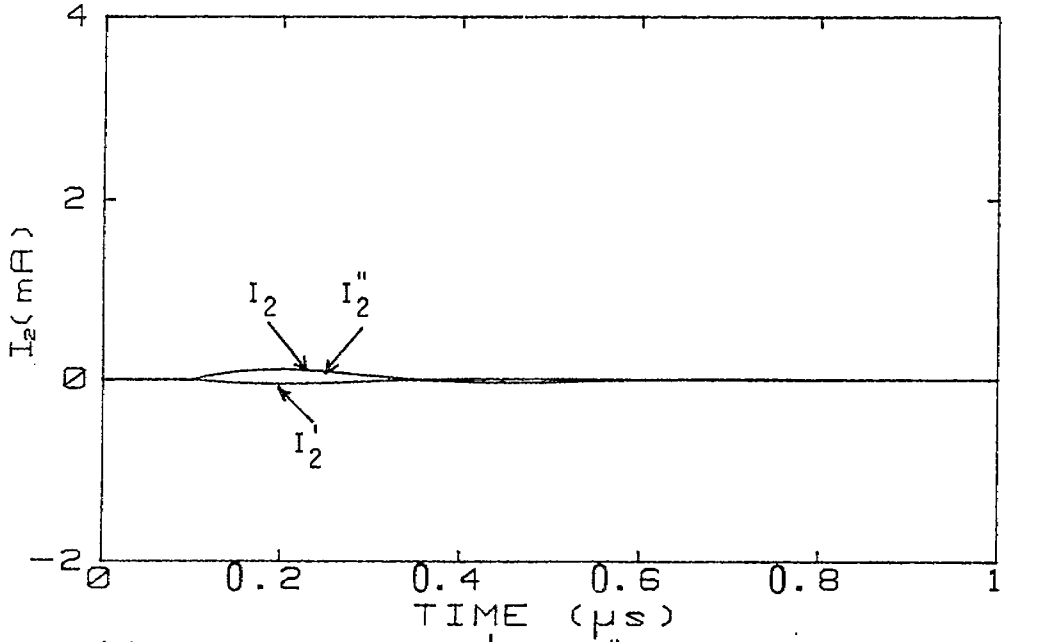

(b) Time history of I_2, I_2', and I_2''.

Figure 11. Exact wire currents (I_1, I_2) and estimated wire currents (I_1', I_2'; I_1'', I_2'') using two variational principle techniques when ℓ = 30 m, x_s = 0.25 m, x_m = 30 m, $Z_{\ell 11} = Z_{\ell 12} = Z_{\ell 22}$ = 400 Ω.

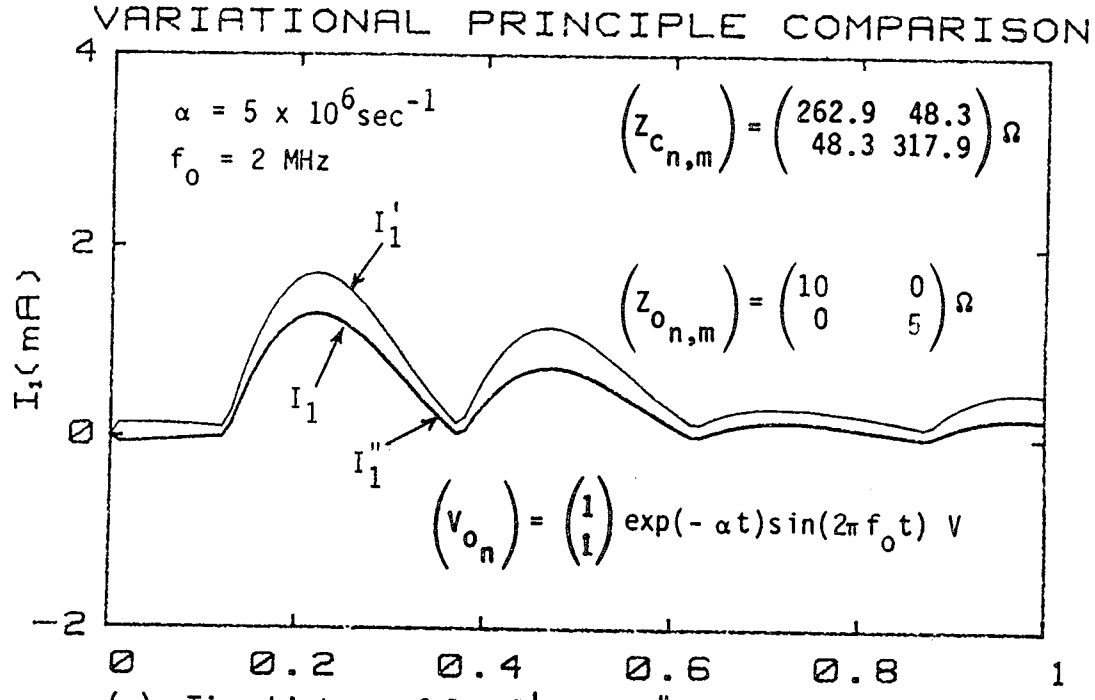

(a) Time history of I_1, I_1', and I_1''.

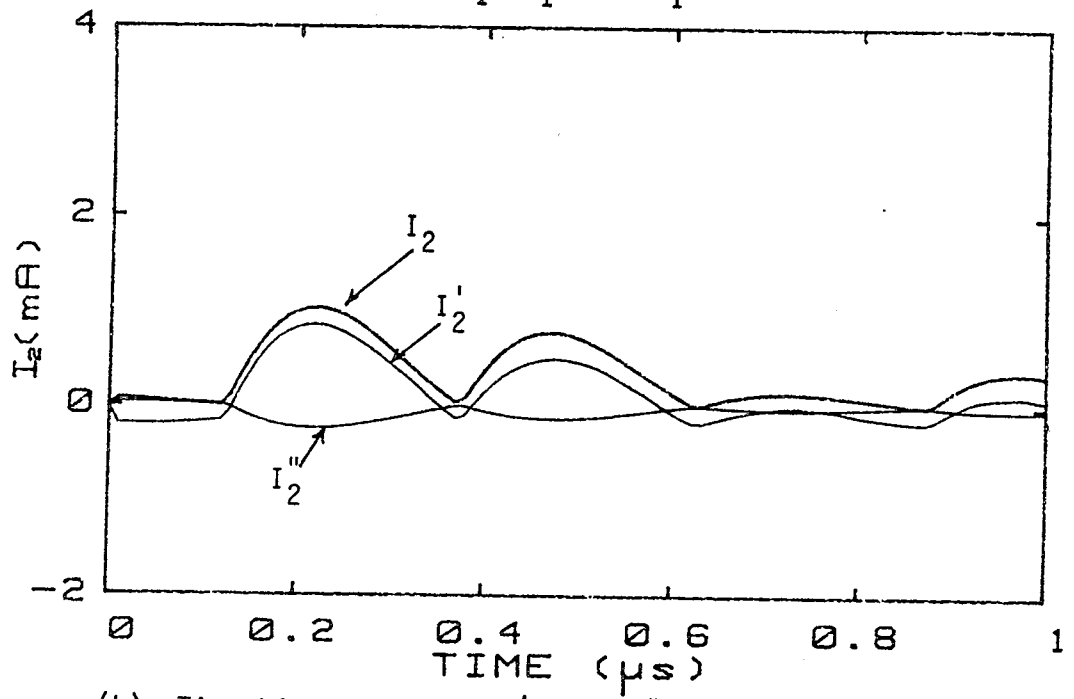

(b) Time history of I_2, I_2', and I_2''.

Figure 12. Exact wire currents (I_1, I_2) and estimated wire currents (I_1', I_2'; I_1'', I_2'') using two variational principle techniques when ℓ = 75 m, x_s = 37.5 m, x_m = 75 m, $Z_{\ell 11}$ = 100 Ω, $Z_{\ell 12}$ = 1 Ω and $Z_{\ell 22}$ = 400 Ω.

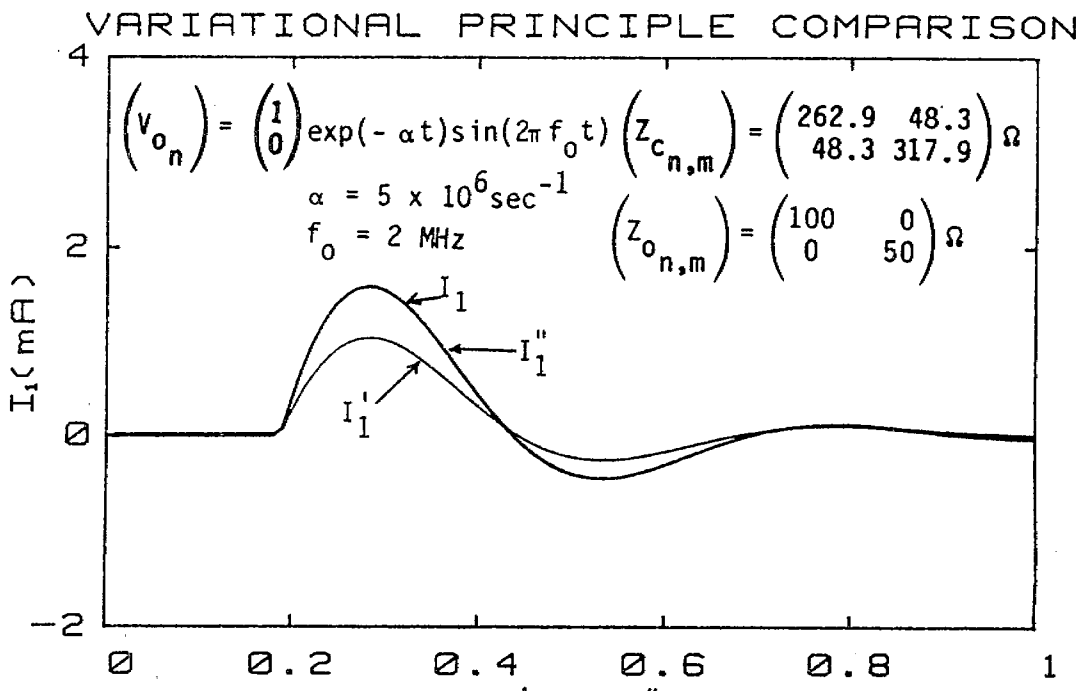

(a) Time history of I_1, I_1', and I_1''.

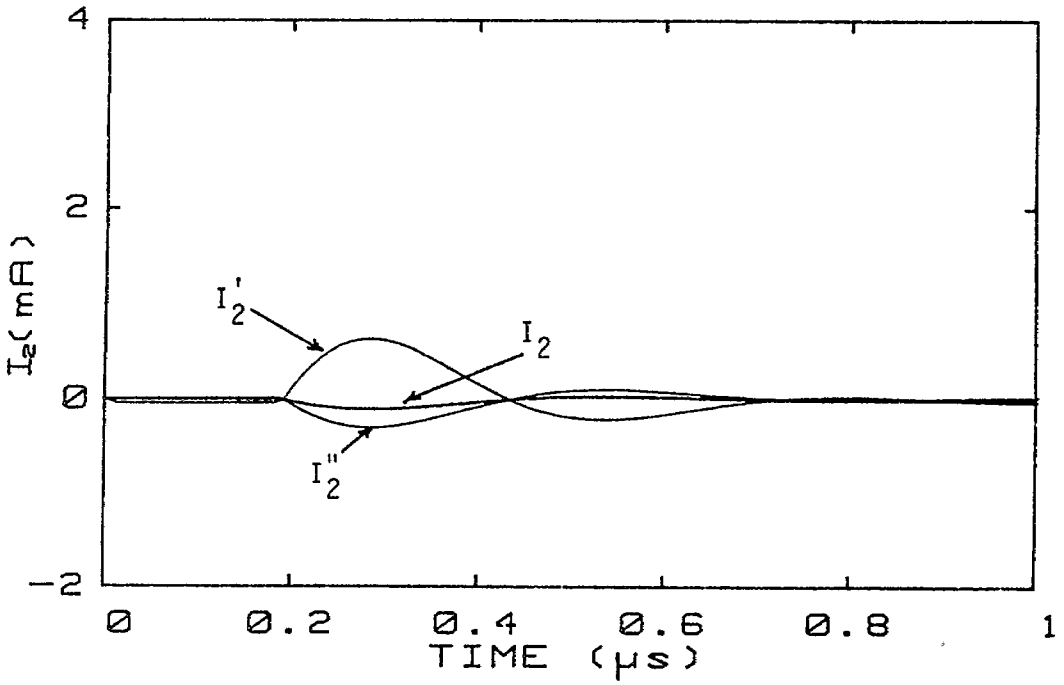

(b) Time history of I_2, I_2', and I_2''.

Figure 13. Exact wire currents (I_1, I_2) and estimated wire currents (I_1', I_2'; I_1'', I_2'') using two variational principle techniques when ℓ = 75 m, x_s = 18.75 m, x_m = 75 m, $Z_{\ell 11}$ = 100 Ω, $Z_{\ell 12} = \infty$, and $Z_{\ell 22}$ = 400 Ω.

In the Appendix, additional curves presenting the comparison of exact wire currents with calculated ones are given.

In an N-wire cable, depending on the measurement sequence, the rate of increase of the accuracy curve will be different. It is possible to obtain an accuracy greater than a certain value from a number of measurements much less that N.

From the above observations, one may make the following conclusions:

- In a multi-wire cable, wire currents can be calculated from a limited number of measurements.
- In a multi-wire cable, if the wires are evenly excited, wire currents calculated from a knowledge of the bulk-cable current have a higher accuracy than that obtained from other kinds of current measurements.
- In a multi-wire cable, if the excitation of one individual wire is dominant over the others, wire currents calculated from a knowledge of the current of that specific wire have a higher accuracy than that obtained from other kinds of current measurements.

The variational technique introduced in this section can be applied to obtain useful information on the wire currents from a limited number of measurements. Although, the technique requires information on the source as well as the load impedance of the cable bundle at the point of interest, the impedance measurements can be performed without the need of bringing the aircraft to the EMP simulator site. Another point is that impedance measurement is relatively easier to perform than stress or susceptibility measurements. Impedance measurements can be performed using network analyzers (Ref. 8).

III. DIRECT-DRIVE TESTING

As stated in the Introduction a "complete" EMP hardness statement for an aircraft requires a knowledge of threat-induced stress or its bound and susceptibility threshold for each pin of each LRU. Direct-drive testing is typically the method by which susceptibility thresholds can be obtained. This type of test can also be used to verify if components and subsystems meet their required specifications. In this section the results obtained in Section II will be applied to the development of two test procedures for direct-drive testing. One is the excitation of the total bundle by a direct-drive. The other is direct driving of a single wire in the bundle.

1. DIRECT DRIVING OF CABLE BUNDLE

Consider a cable bundle with N wires and terminated at one end at an LRU. Figure 14 shows an inverse current probe exciting the entire bundle. It is observed that each wire contained in the bundle is excited by the same amount of source magnetic flux. Consequently, the open-circuit voltages, V_{oc}, induced by the direct-drive excitation are the same (Ref. 9). It was shown in Section II that when the V_{oc}'s of the equivalent circuits were about the same, the bulk cable current I_B would be very informative in evaluating individual wire currents. In fact, if I_B is measured, then the individual wire currents can be found from Equation 31, viz.,

$$I_{L_m} = I_B \frac{Y_{t_{m,n}}}{(1_n)^T \cdot (Y_{t_{n,m}}) \cdot (1_m)} \tag{53}$$

The above equation can be used in verification of an LRU specifications. Consider an LRU in a laboratory. This LRU can be connected by an N-wire cable bundle to another box with an impedance matrix $(Z_{o_{n,m}})$. It is assumed that the impedance matrix $(Z_{o_{n,m}})$ can be changed. Suppose one wants to verify the

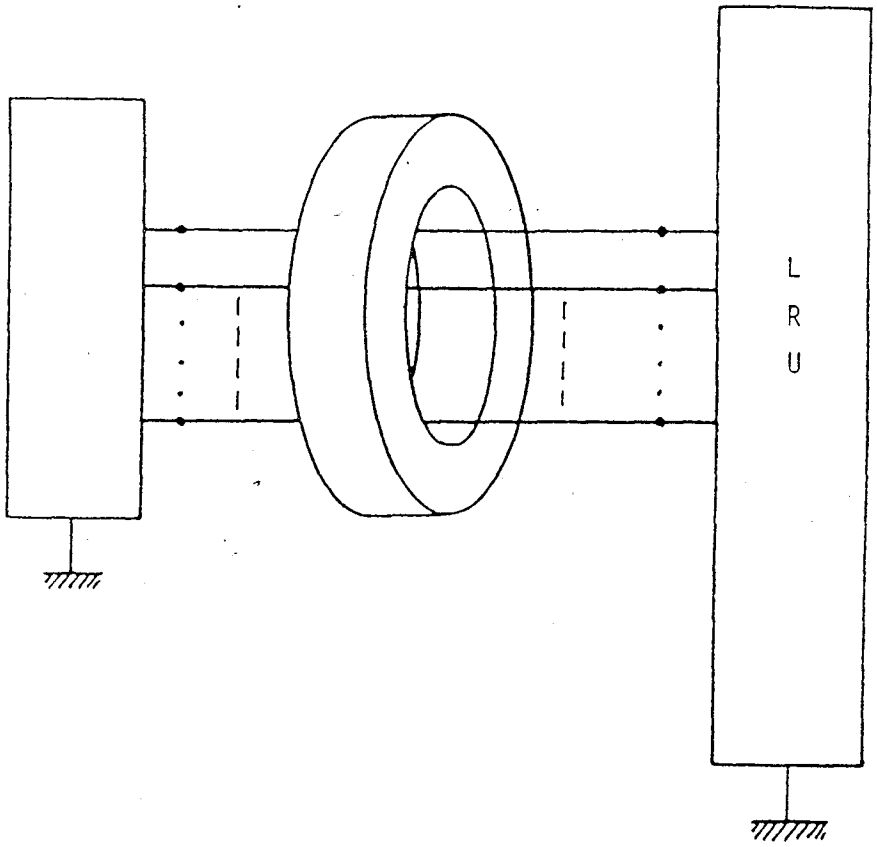

Figure 14. Total cable bundle excitation using an inverse current probe.

pin specifications of a given LRU. One can adjust I_B and the elements of the impedance matrix $Z_{o_{n,m}}$, until the current or voltage of each pin becomes identical to the pin specification. Therefore by using an inverse current probe and a proper impedance matrix ($Z_{o_{n,m}}$), it is possible to verify a pin specification.

It is interesting to note that Equation 53 can also be used in defining the specification of an LRU in terms of I_B. To do so, using Equation 53, one can obtain the specification of LRU from that of the sensitive pin. Therefore, specification can be verified by direct-driving the cable bundle using an inverse current probe.

2. DIRECT DRIVING OF A SINGLE WIRE

In this example only one wire of a cable bundle is directly driven. Therefore, the V_{oc} of this wire is usually dominant over the open-circuit voltages of the other wires. Based on the results obtained in Section II the current in the excited wire can provide information about the other wire currents.

If the current in the excited wire, which is denoted by I_k, is measured we can compute the other wire currents from Equation

$$I_{L_m} = I_k \frac{Y_{t_{m,k}}}{Y_{t_{k,k}}} . \tag{54}$$

This approach can also reduce the number of measurements required to quantify pin susceptibility thresholds. To further illustrate this point, consider an example of a 4-port LRU connected to a driving circuit through a 4-wire cable bundle. The total admittance of the LRU is assumed to be

$$(Y_{t_{m,n}}) = \begin{pmatrix} 1.82 & -1.55 & 1.75 & -0.12 \\ -1.55 & 2.31 & -1.92 & 2.5 \\ 1.75 & -1.92 & 1.65 & -1.3 \\ -0.12 & 2.5 & -1.3 & 2.01 \end{pmatrix} \times 10^{-3} \text{ mho} \quad (55)$$

As can be easily seen only the third column or row has two off-diagonal elements (1.75,-1.92) whose absolute values are greater than the diagonal term (1.65). This implies that if wire #3 is excited, according to Equation 54 wires #1 and #2 will reach their maximum allowable values first before wire #3 will. If the susceptibility thresholds of all the three wires are, say, 100 mA, then one can calculate from Equation 54 and Equation 55 that for I_{L_1} = 100 mA, I_3 should be 94.2 mA, which is less than 100 mA. Similarly for I_{L_2} = 100 mA, I_3 turns out to be 85.9 mA, which is less than 100 mA. Therefore, without changing the experimental setups, i.e., direct driving wire #3 alone, the susceptibility thresholds of the first two pins can be established.

IV. EFFECT OF VARIOUS PARAMETERS ON COMMON- AND DIFFERENTIAL-MODE CURRENTS

To select an optimal measurement approach, the effects of different parameters on wire currents must be studied. In this section, the effects of various parameters (such as the excitation mechanism, bundle configuration, impedances, source and measurement locations, etc.) on wire currents are studied. Before presenting the results, the concept of common and differential modes is introduced.

1. DEFINITION OF COMMON AND DIFFERENTIAL MODES

As mentioned earlier, the sum of wire currents is referred to as the bulk-cable current I_B and it is relatively easy to measure. However, I_B gives only partial information about the individual wire currents. To obtain a complete description of the wire currents, additional information is needed. This additional information can be other combinations of wire currents. For example, for a two-wire cable, I_B is the sum of I_1 and I_2, i.e., $I_B = I_1 + I_2$, and the other combination is the difference between I_1 and I_2, i.e. $I_D = I_1 - I_2$. I_B and I_D may be referred to as the common and differential modes. For the three-wire cable, the common and differential modes are written as:

$$\begin{aligned} I_B &= I_1 + I_2 + I_3 \\ I_{D1} &= I_1 + I_2 - I_3 \\ I_{D2} &= I_1 - I_2 + I_3 \end{aligned} \tag{56}$$

In the analysis that follows, transmission line models are used to study the effects of excitations, configurations, etc. on bulk and differential-mode currents.

2. EFFECT OF LOAD IMPEDANCE

Consider a two-wire line with the terminating impedance matched to the characteristic impedance. For each value of the load impedance, we calculate I_B and I_D. Figures 15 through 17 present these results. From these figures, the following conclusions can be drawn:

- For (two) like pins (i.e. the pin-to-ground impedances of the two pins are the same), I_D is sensitive to pin-pin impedance, whereas I_B is not.
- For (two) unlike pins (i.e., the pin-to-ground impedances of pins are not the same), I_B and I_D do not in general depend appreciably on the pin-pin impedance.

More examples of I_B and I_D for different load impedances are presented in Appendix B.

3. EFFECT OF SOURCE TYPE

In this case, I_B and I_D are calculated for different types of source Figure 18 presents I_B and I_D for different sources. From these figures, we can draw the following conclusions:

- Regardless of the load and source impedances, the I_B/I_D interaction is independent of the type of source, i.e. a voltage or current source. This leads to the following corollaries:
  - If I_B (or I_D) is large compared to I_D (or I_B) with one type of source, it is also large for the other type of source.
  - If one type of source gives rise to zero I_B (or I_D), so does the other.
  - For direct drive tests, either the voltage source or the current source will produce the same wire current distribution.

Additional figures of I_B and I_D for different types of sources are given in Appendix B.

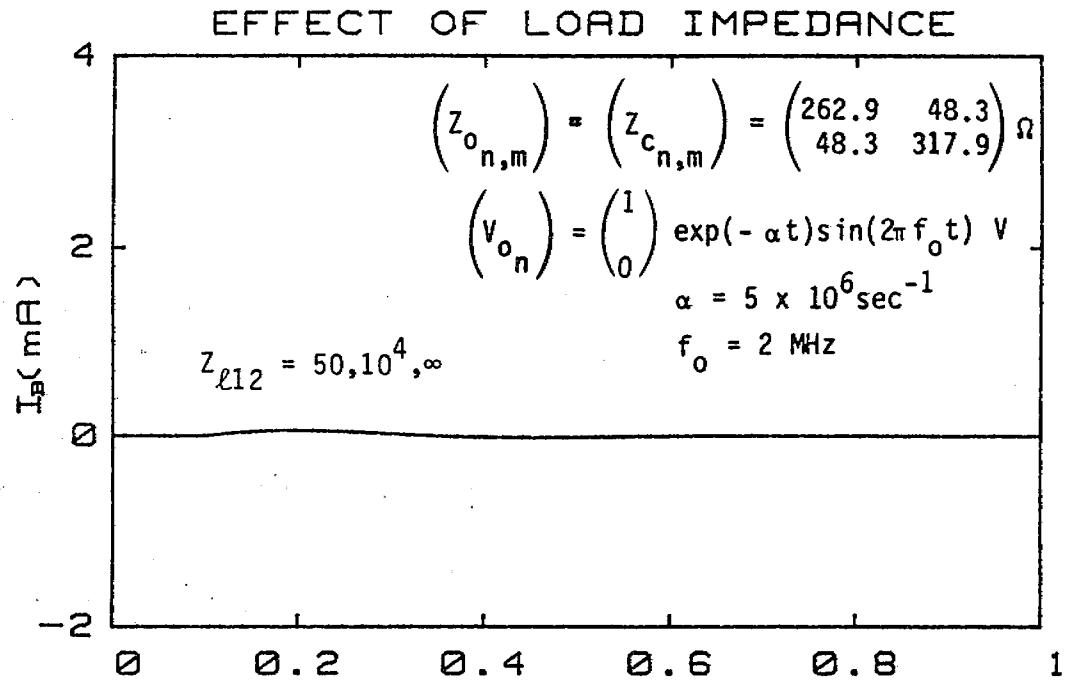

(a) Time history of I_B.

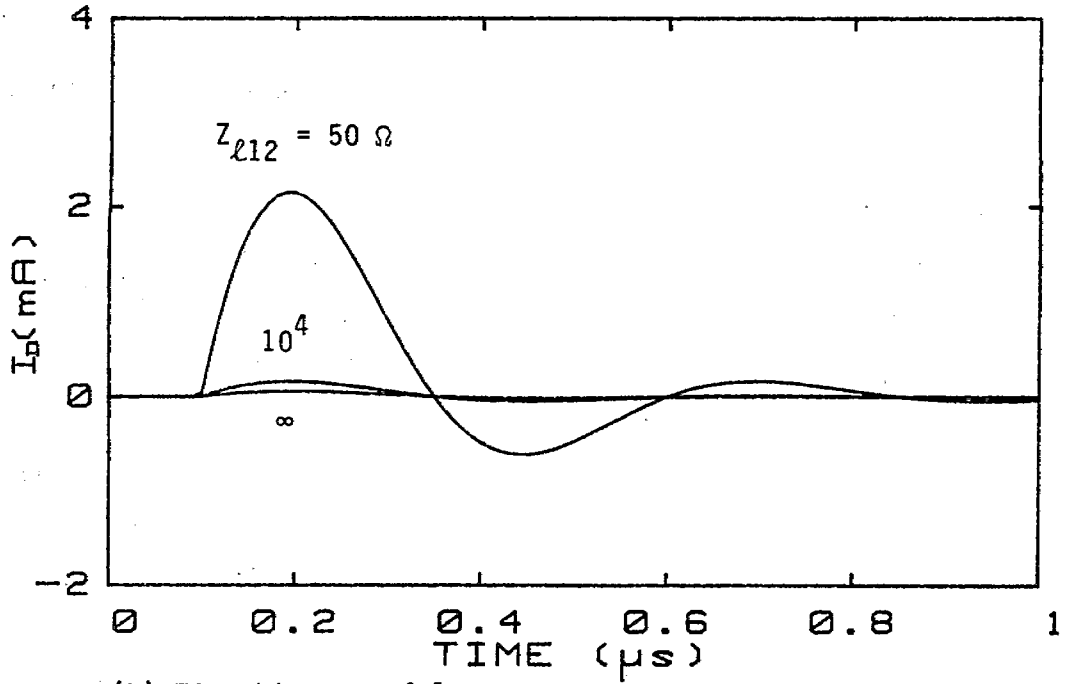

(b) Time history of I_D.

Figure 15. Common and differential mode currents (I_B,I_D) for different $Z_{\ell 12}$ when ℓ = 30 m, x_s = 0.25 m, x_m = 30 m, $Z_{\ell 11} = Z_{\ell 22} = 10^4$ Ω.

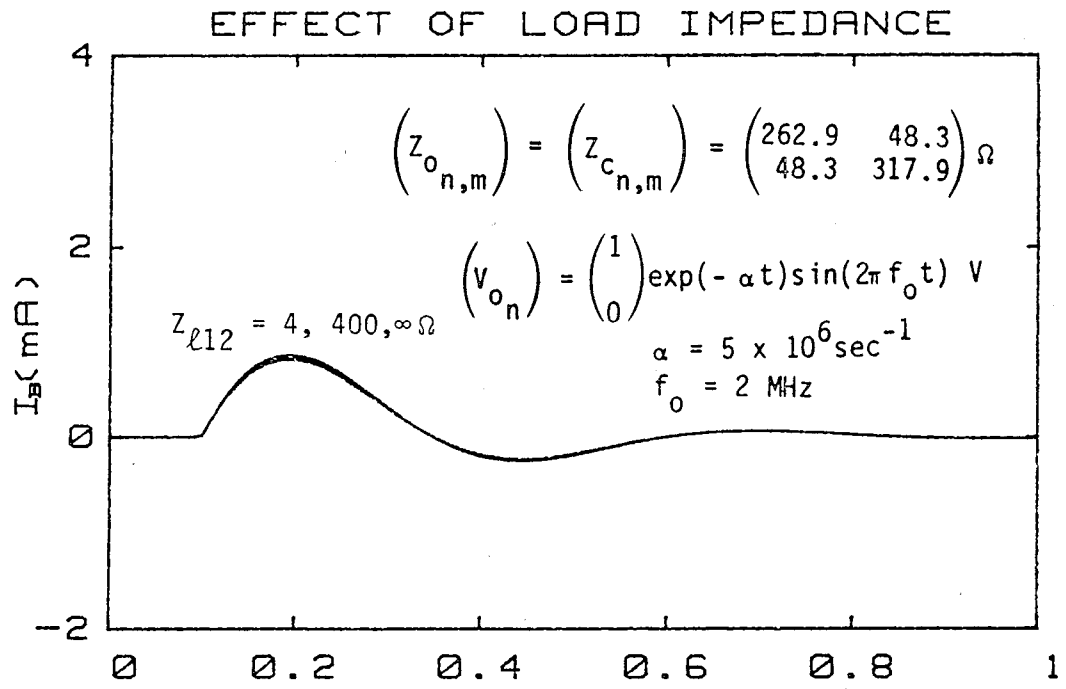

(a) Time history of I_B.

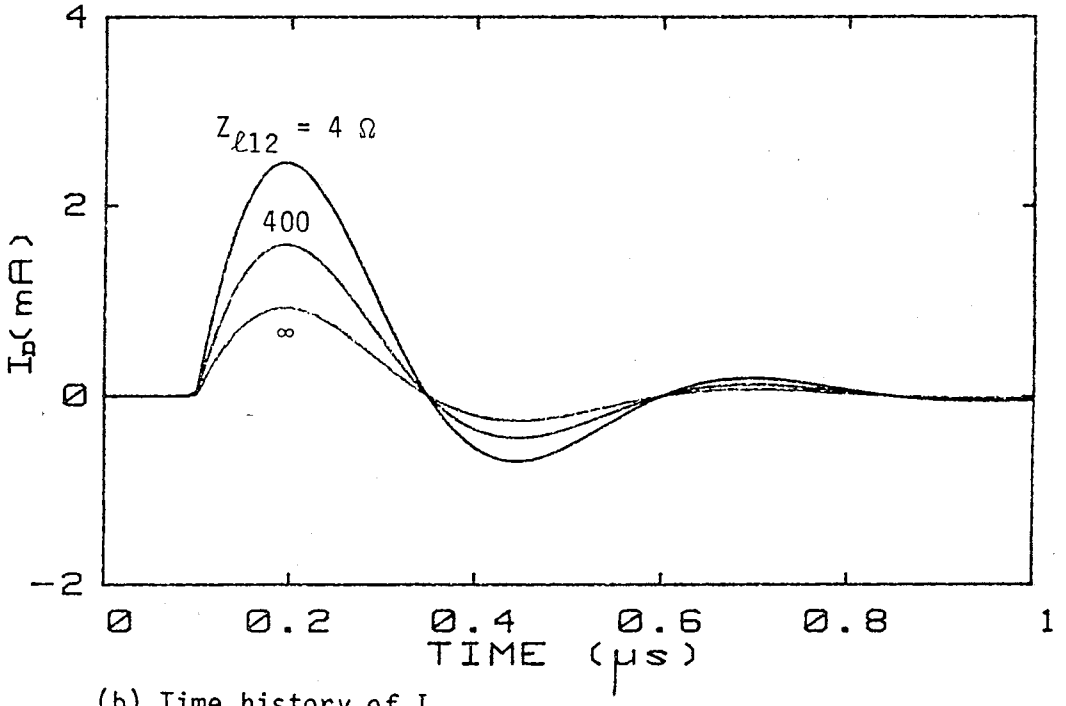

(b) Time history of I_D.

Figure 16. Common and differential mode currents (I_B, I_D) for different $Z_{\ell 12}$ when ℓ = 30 m, x_s = 0.25 m, x_m = 30 m and $Z_{\ell 11} = Z_{\ell 22}$ = 400 Ω.

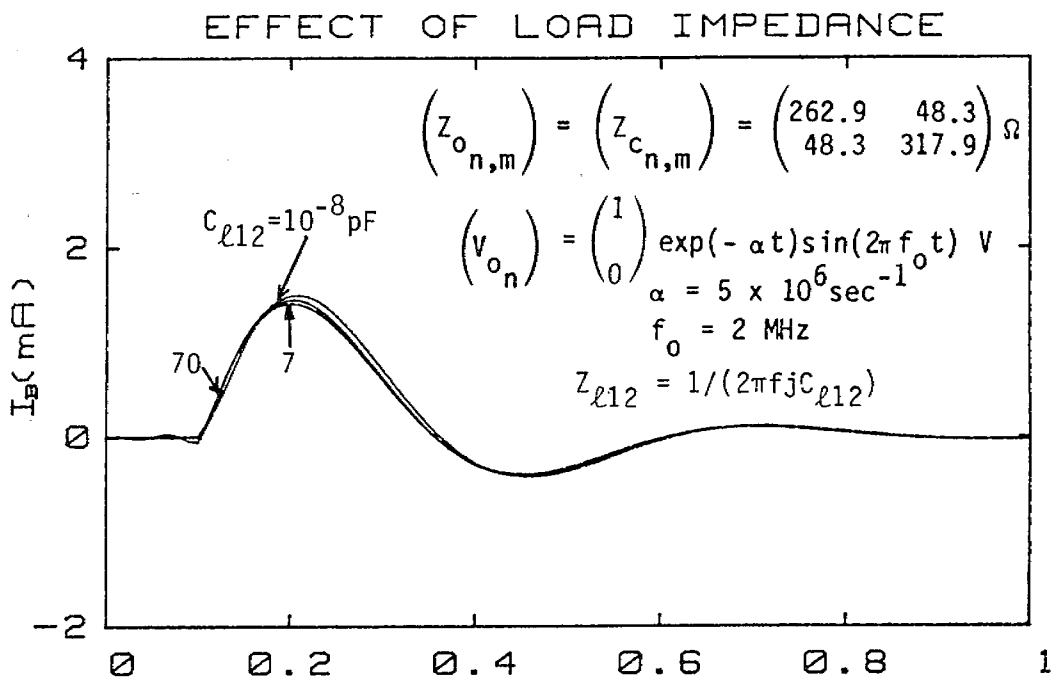

(a) Time history of I_B.

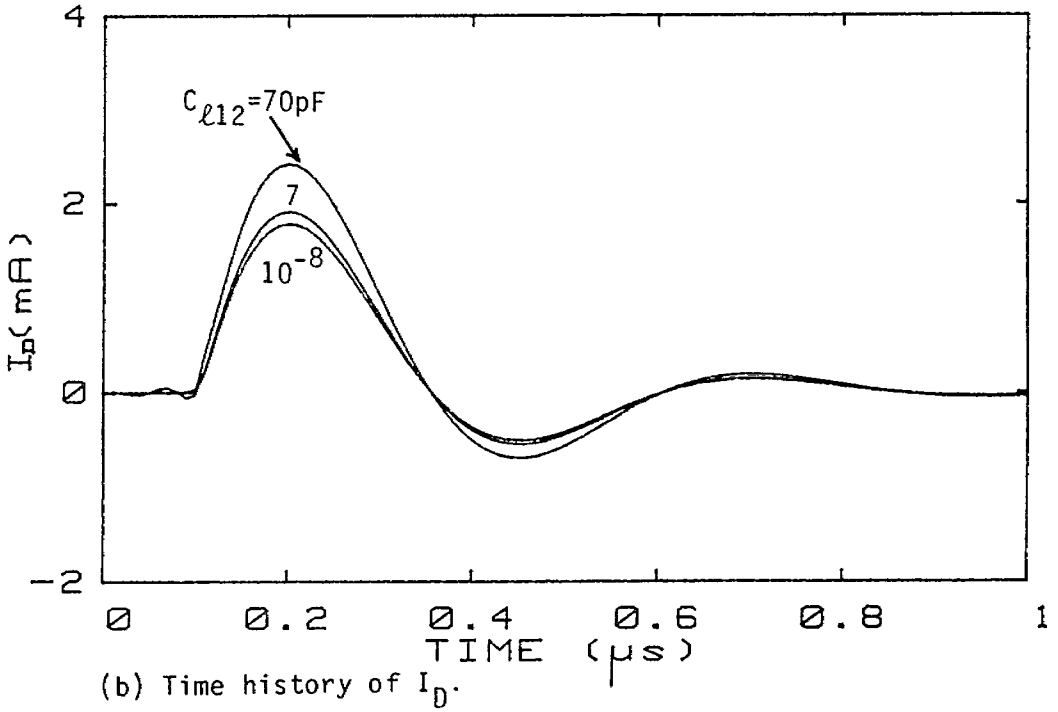

(b) Time history of I_D.

Figure 17. Common and differential mode currents (I_B,I_D) for different values of $C_{\ell 12}$ when ℓ = 30 m, x_s = 0.25 m, x_m = 30 m, $Z_{\ell 11}$ = 100 + $2\pi f j\ (3\times10^{-7})$ + $1/[2\pi f j(7\times10^{-11})]$ Ω, and $Z_{\ell 22}$ = 100 + $2\pi f j\ (2.5\times10^{-6})$ Ω.

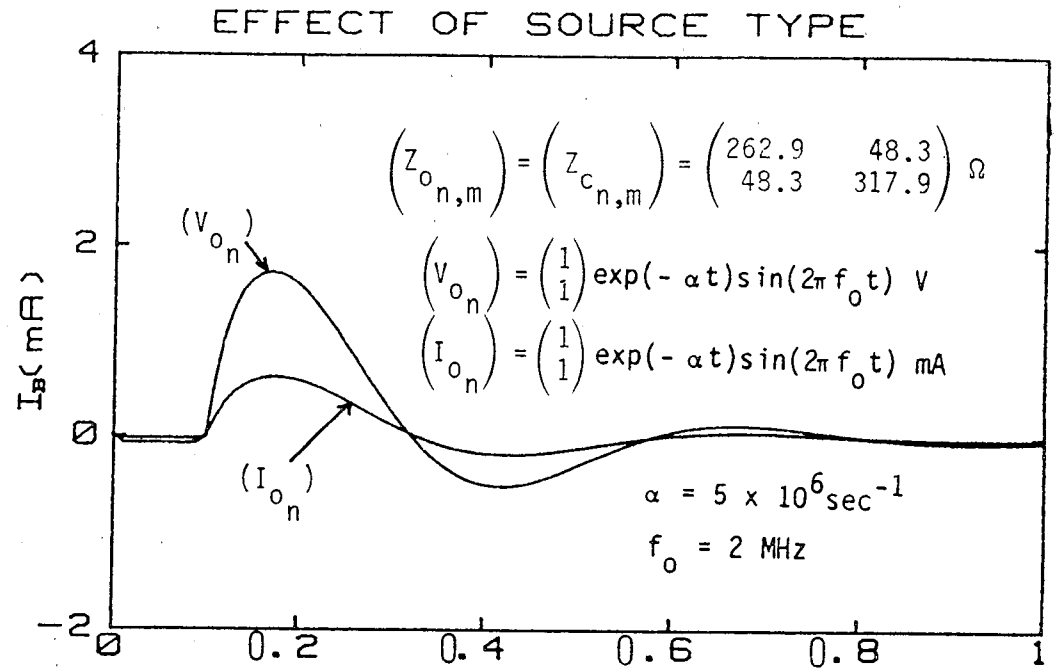

(a) Time history of I_B.

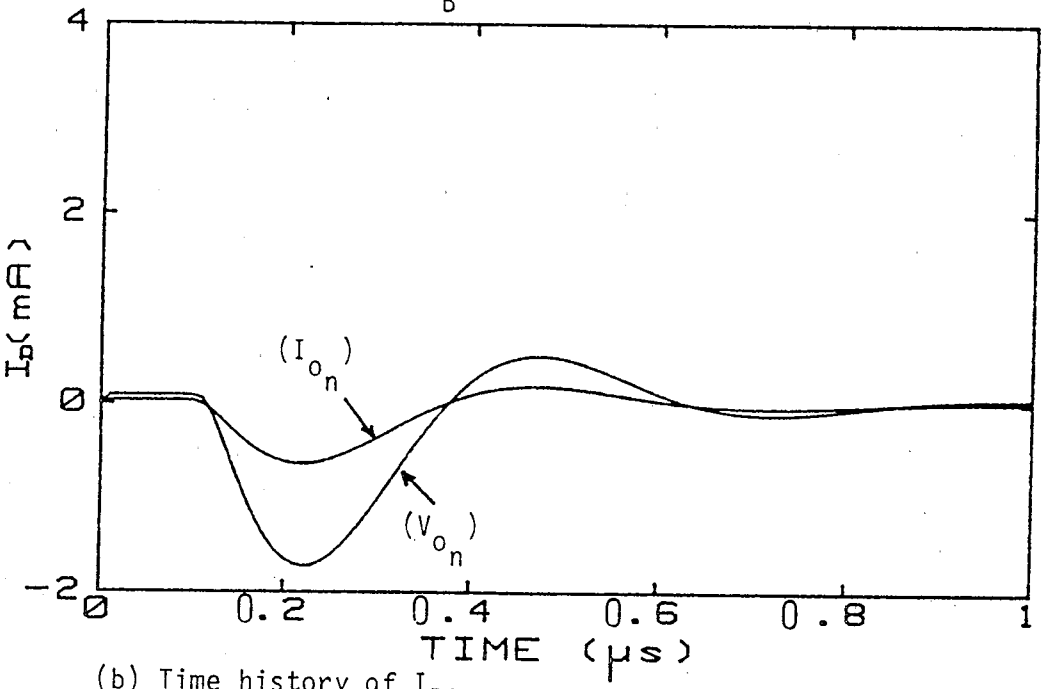

(b) Time history of I_D.

Figure 18. Common and differential mode currents (I_B, I_D) for different types of sources when ℓ = 30 m, x_s = 0.25 m, x_m = 30 m, $Z_{\ell 11} = Z_{\ell 22} = 2\pi fj(3\times10^{-7}) + 1/[2\pi fj(7\times10^{-11})]$ Ω, and $Z_{\ell 12} = 1/[2\pi fj(7\times10^{-12})]$ Ω.

4. EFFECT OF SOURCE POSITION

For this case sources are located at different positions, and for each position I_D and I_B are calculated. Figure 19 shows I_B and I_D for different source positions. From this figure, the following conclusions can be drawn.

- Regardless of load impedance, changing the position of the source merely results in a shift of the waveforms of I_B and I_D. Therefore. the I_B/I_D interaction is, indepedent of source positions. For direct drive test, the location of the drive can be safely assumed to have no effect on the wire current distribution at the load.

In Appendix B, there are additional figures showing I_B and I_D for different source positions.

5. EFFECT OF NUMBER OF EXCITED WIRES

Figures 20 through 22 present the results for I_B and I_D for different numbers of locally excited wires. The conclusions are as follows:

- For (two) like pins, changing the number of excited wires from one to two generally causes I_B to increase and I_D to drop to zero, regardless of the load and source impedances.
- For (two) unlike pins, changing the number of excited wires, from one to two causes I_B to increase and I_D to decrease regardless of load and source impedances.

In Appendix B, there are additional figures presenting I_B and I_D for different numbers of excited wires.

6. EFFECT OF LINE CONFIGURATION

The effect of line parameters on I_D and I_B, can be studied by varying the elements in the characteristic impedance matrix. Figure 23 presents I_B and I_D for different characteristic impedances. From these figures the following important conclusion is reached:

- The line parameters do not have any significant effect on I_B and I_D.

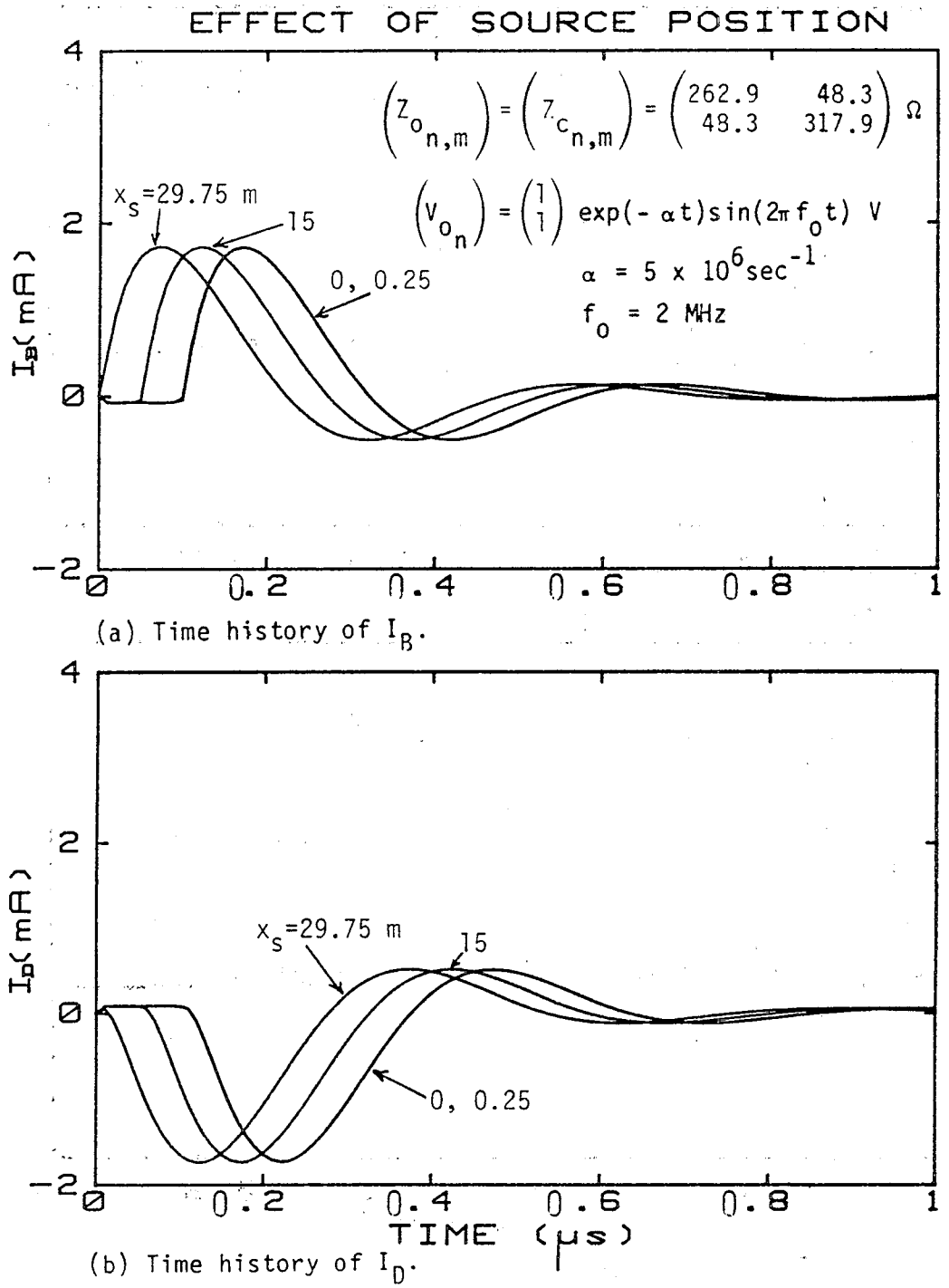

(a) Time history of I_B.

(b) Time history of I_D.

Figure 19. Common and differential mode currents (I_B, I_D) for different source locations when ℓ = 30 m, x_m = 30 m, $Z_{\ell 11} = Z_{\ell 22} = 2\pi fj(3\times10^{-7}) + 1/[2\pi fj(7\times10^{-11})]$ Ω, and $Z_{\ell 12} = 1/[2\pi fj(7\times10^{-12})]$ Ω.

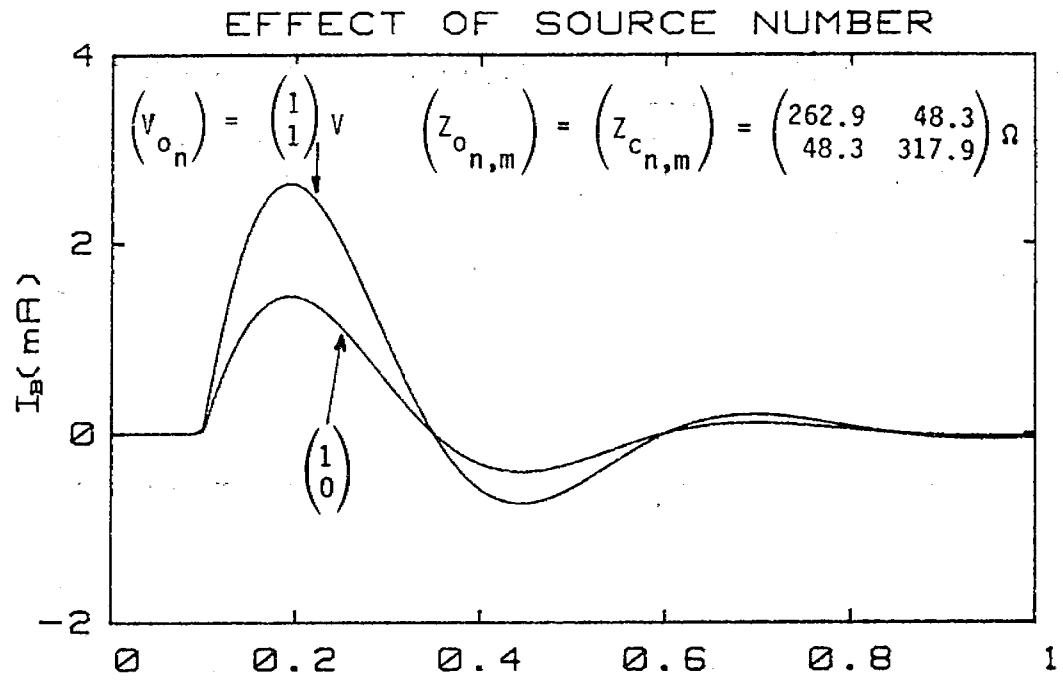

(a) Time history of I_B.

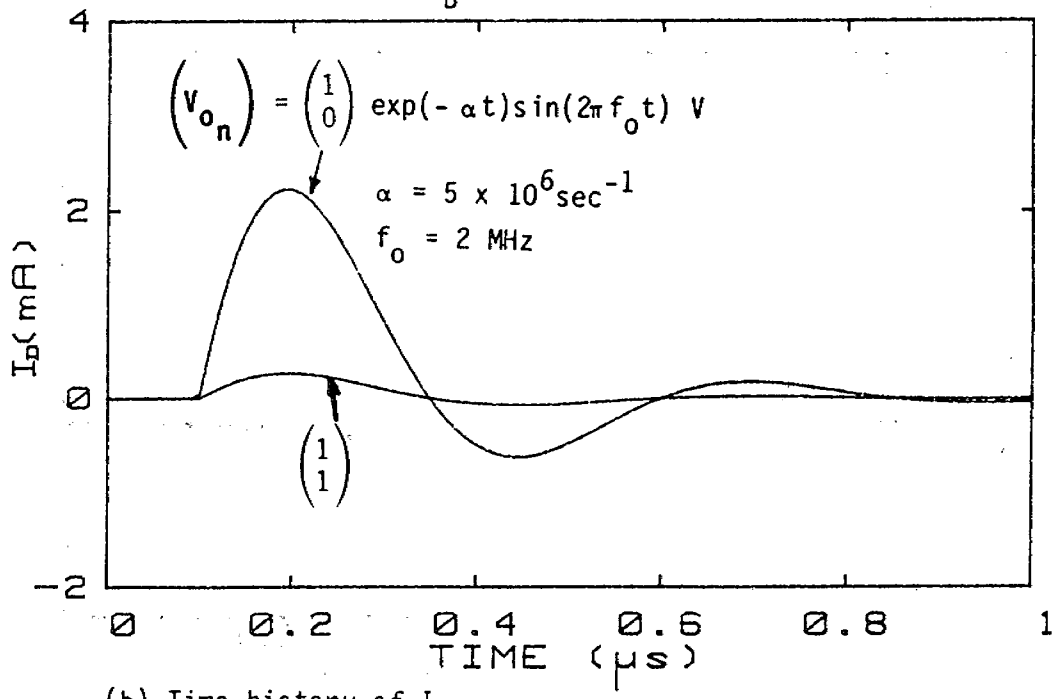

(b) Time history of I_D.

Figure 20. Common and differential mode currents (I_B, I_D) for different numbers of sources when ℓ = 30 m, x_s = 0.25 m, x_m = 30 m, $Z_{\ell 11} = Z_{\ell 12} = Z_{\ell 22}$ = 100 Ω.

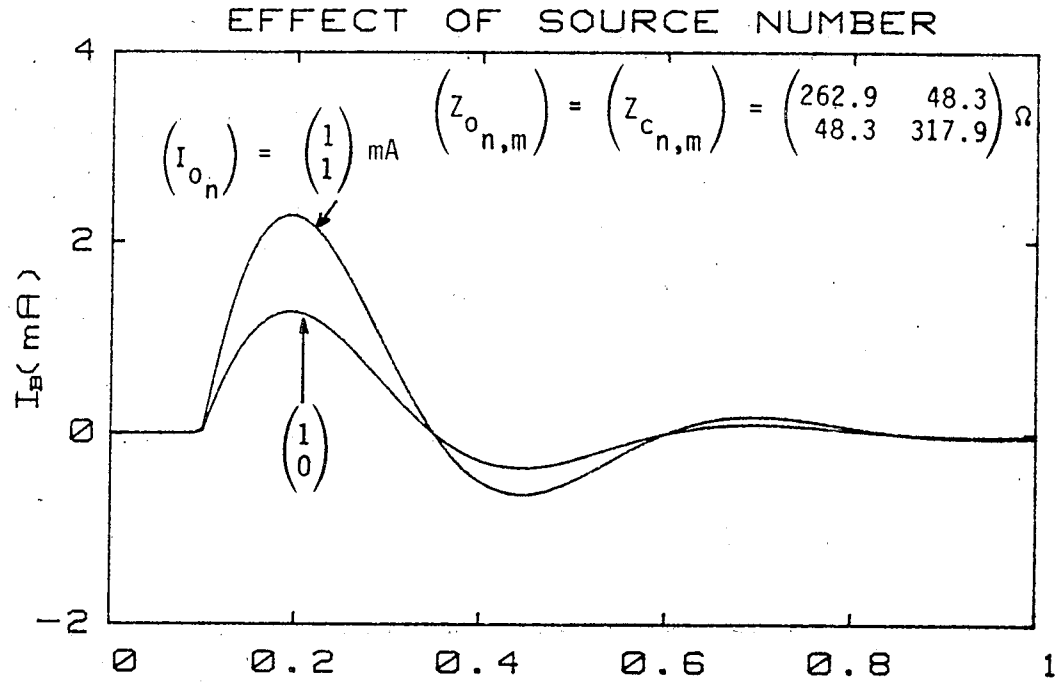

(a) Time history of I_B.

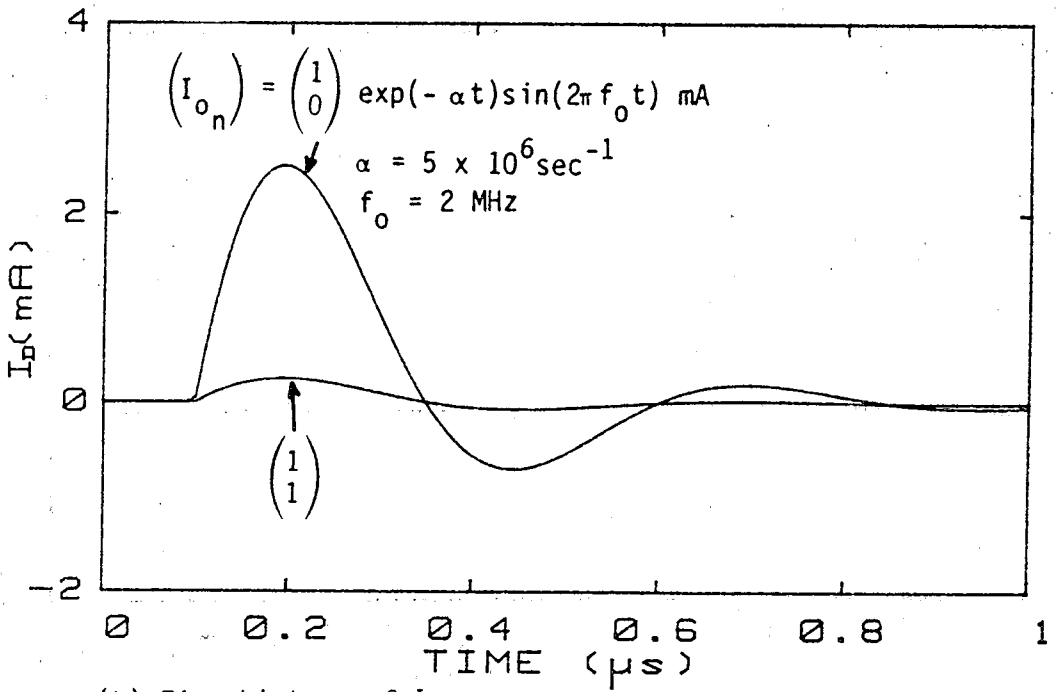

(b) Time history of I_D.

Figure 21. Common and differential mode currents (I_B, I_D) for different numbers of sources when ℓ = 30 m, x_s = 0.25 m, x_m = 30 m, $Z_{\ell 11}$ = 500 Ω, $Z_{\ell 12}$ = 1 Ω, and $Z_{\ell 22}$ = 100 Ω.

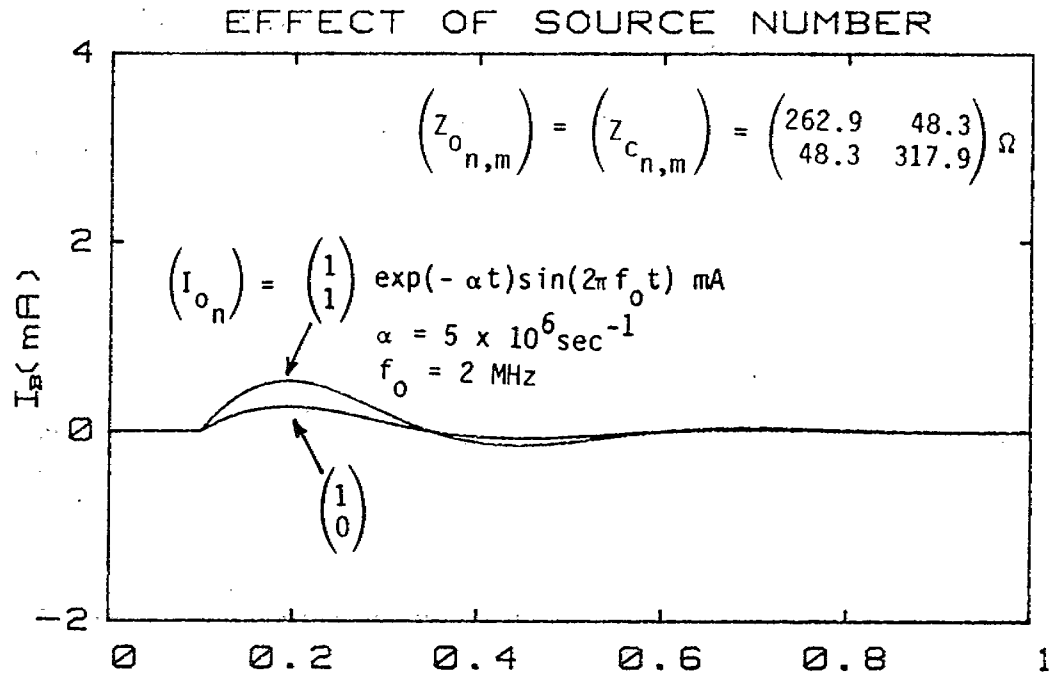

(a) Time history of I_B.

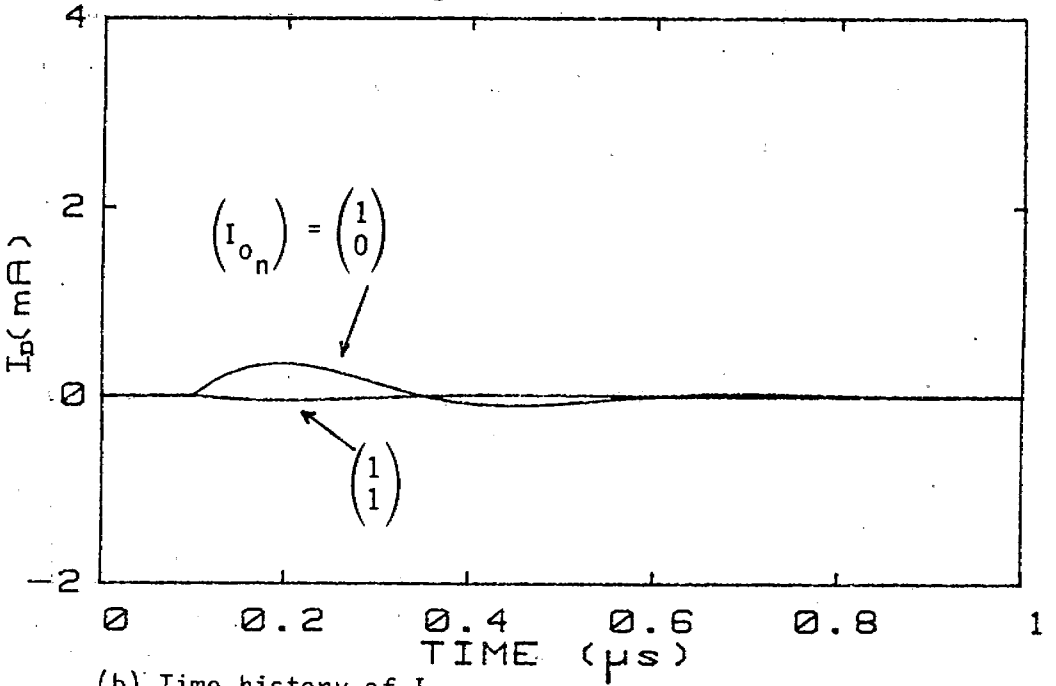

(b) Time history of I_D.

Figure 22. Common and differential mode currents (I_B, I_D) for different numbers of sources when ℓ = 30 m, x_s = 0.25 m, x_m = 30 m, $Z_{\ell 11}$ = $Z_{\ell 12}$ = $Z_{\ell 22}$ = 400 Ω.

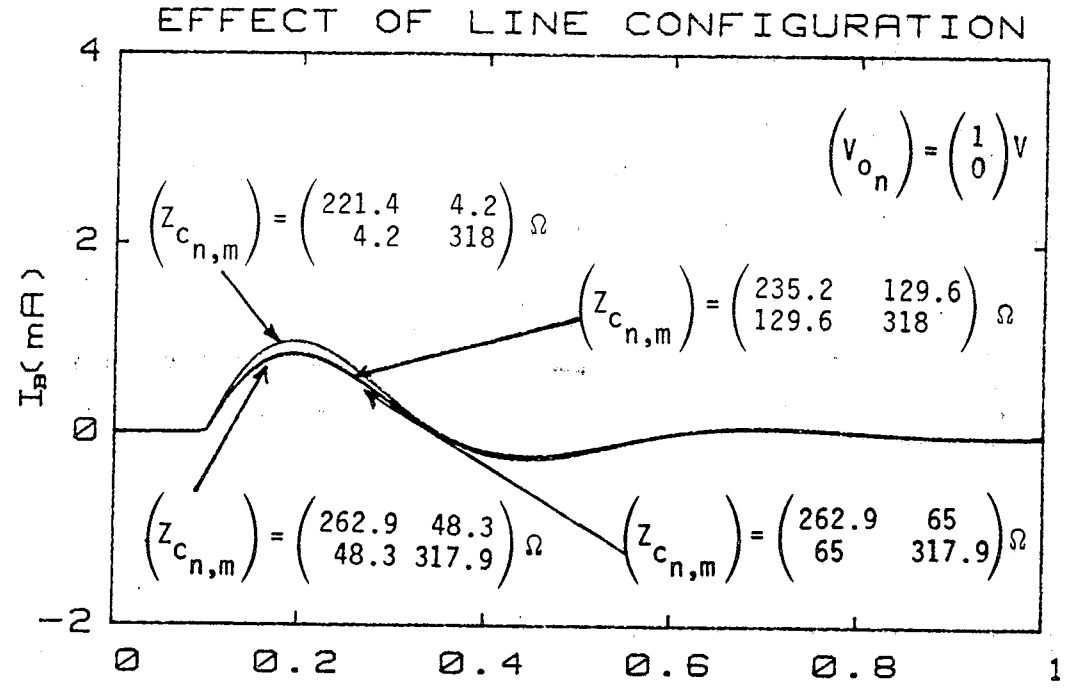

(a) Time history of I_B.

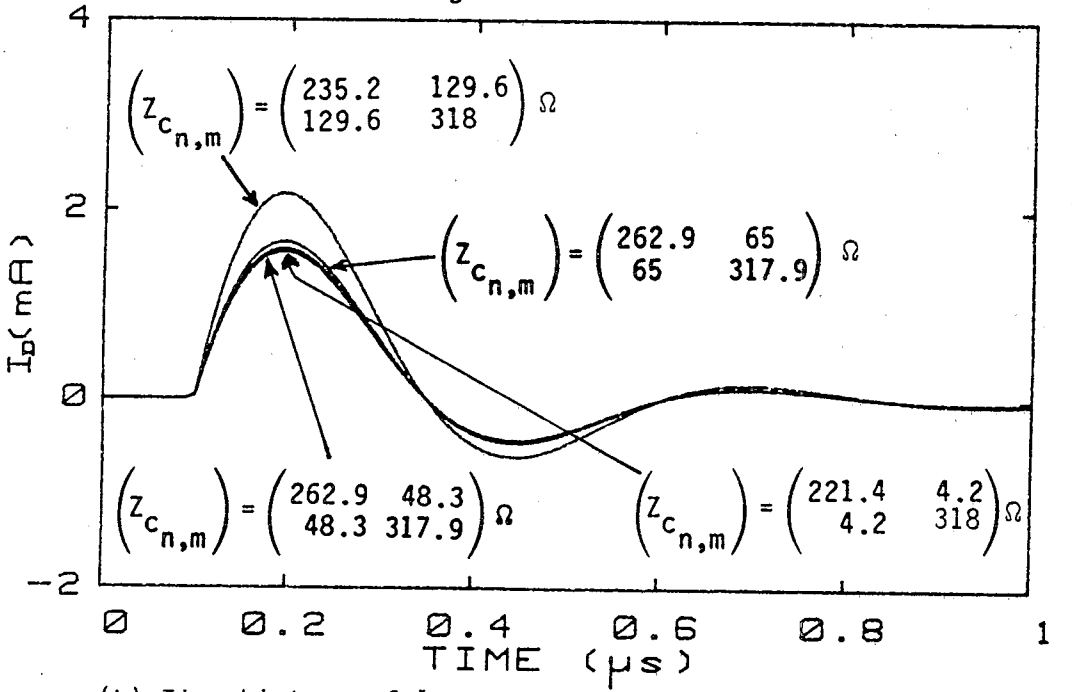

(b) Time history of I_D.

Figure 23. Common and differential mode currents (I_B, I_D) for different characteristic impedances when ℓ = 30 m, x_s = 0.25 m, x_m =30 m, $Z_{\ell 11} = Z_{\ell 12} = Z_{\ell 22}$ = 400 Ω, and $(Z_{o_{n,m}}) = (Z_{c_{n,m}})$.

An additional figure of I_B and I_D for different characteristic impedances is given in Appendix B.

7. EFFECT OF MEASUREMENT LOCATION

In this case, I_B and I_D are calculated at different locations of the line. Figure 24 shows these results. From these figures we can draw the following conclusions:

- Regardless of the load impedance, changing the measurement point produces only a shift of the waveforms of I_B and I_D.

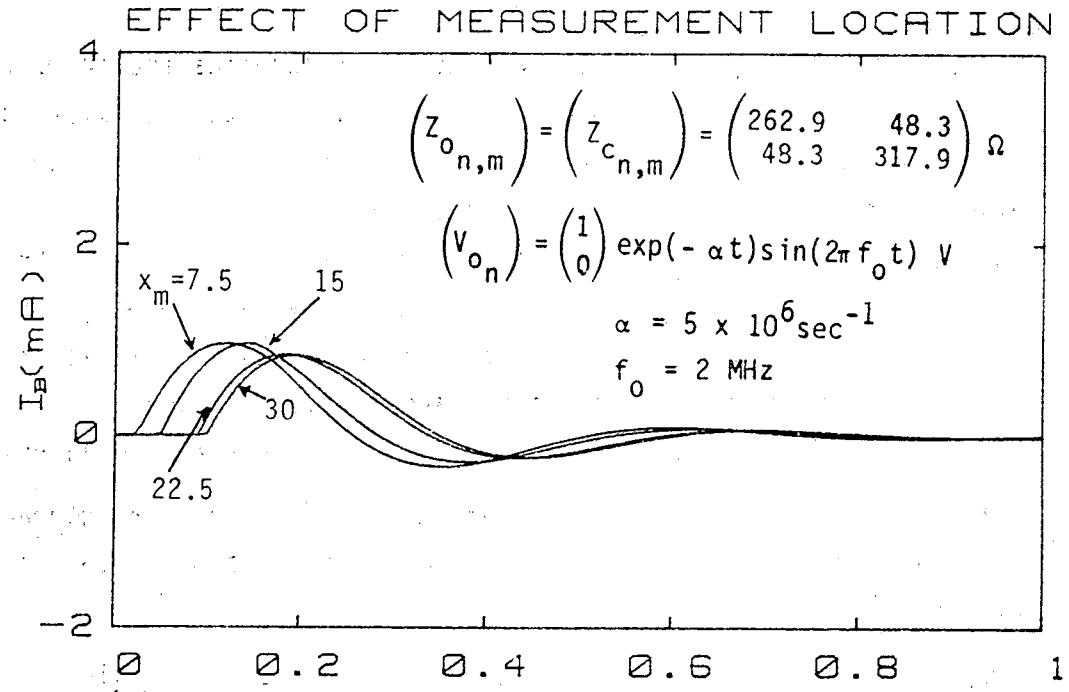

(a) Time history of I_B.

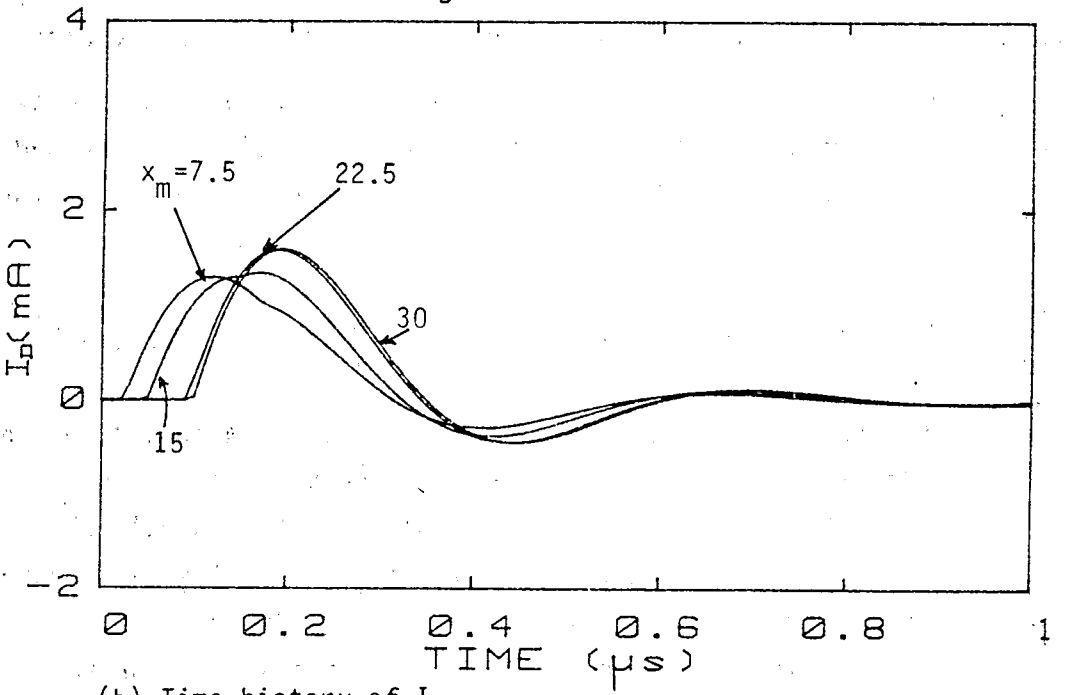

(b) Time history of I_D.

Figure 24. Common and differential mode currents (I_B, I_D) for different measurement locations when ℓ = 30 m, x_s = 0.25 m, $Z_{\ell 11} = Z_{\ell 12} = Z_{\ell 12}$ = 400 Ω.

V. SUGGESTED EXPERIEMENT

The variational technique introduced in Section II requires the information on the impedances of the cable bundle at the pins. Since the existing data base does not provide such information, new experiments are necessary for the verification of the rules established in previous sections. By using an accuracy gauge such as that defined in Equation 52, the verification of the rules can be accomplished. For example, take an accuracy measure of greater than 80% to be a satisfactory criterion. Then, if the results obtained from the rules give such an accuracy measure, the rules can be considered to be valid. Two examplary experiments are suggested to verify the following rules·

- In a multi-wire cable, if the wires are evenly excited, wire currents calculated from a knowledge of the bulk-cable current alone can have a satisfactory accuracy.
- In a multi-wire cable, if the excitation of one individual wire is dominant over the others, wire currents calculated from a knowledge of the current of that specific wire can have a satisfactory accuracy.

If the rules do not provide satisfactory results when compared with the experimental results, it generally means that additional constraints are needed. To demonstrate this point, a third experiment is suggested which allows for two contraints.

1. EXPERIMENT TO VERIFY THE RULE OF USING THE VARIATIONAL TECHNIQUE AND ONLY I_B MEASUREMENT

In an aircraft under a simulator environment select a cable bundle whose wires all lead to Points of Entry (POE) of similar penetration strength. One then measures I_B and load and source impedances and uses the formula obtained in Section II (Equation 31) to calculate the wire currents. The calculated wire currents are then compared with the measured ones. The degree of accuracy can then be calculated and the verification of the rule for the selected cable can then be accomplished. If it is impossible to locate such a cable inside an aircraft, a laboratory set-up should be used as an alternative.

2 EXPERIMENT TO VERIFY THE RULE OF USING THE VARIATIONAL TECHNIQUE AND ONLY A MEASUREMENT OF ONE INDIVIDUAL WIRE CURRENT

In an aircraft under a simulator environment, select a cable bundle in which only one wire is strongly excited by a POE. One then measures the current on that wire and load and source impedances and uses Equation 47 to calculate each individual wire current. The calculated wire currents are then compared with the measured ones to obtain the accuracy measure (Equation 52). The verification of the rule can then be accomplished. Again, if one cannot find such a cable inside an aircraft, a laboratory setup must be used as an alternative.

3. EXPERIMENT TO VERIFY THE RULE OF USING THE VARIATIONAL TECHNIQUE AND TWO WIRE CURRENT MEASUREMENTS

For the cable bundles selected in the above two experiments. it is possible that the accuracy measures obtained are too low to be satisfactory. Under this situation, one should perform another measurement (in experiment 1 current measurement of a relatively strongly excited wire; in experiment 2, measurement of I_B) and apply Equation 49 to calculate the individual wire currents. These calculated currents are compared with the measured currents for accuracy measure.

4. EXTENDED EXPERIMENT TO IDENTIFY BEST MEASUREMENT COMBINATION

The previous experiments can be extended to determine the best combination of current measurements which provides a satisfactory accuracy measure. One takes a cable bundle in the aircraft. For the selected cable bundle, one first determines whether the rules identified in the previous experiments can be used and performs the corresponding experiments. If the accuracy measure obtained therefrom is satisfactory, the search for the best measurement combination is completed. If the accuracy measure shows otherwise, one should take another measurement and apply the variational technique to calculate the wire currents. Different measurements will give different accuracy measures. The measurement which gives the highest accuracy measure shall be taken. This process shall be continued until a satisfactory accuracy measure is reached. Once this is reached, one essentially has a best measurement combination which can be used for future stress and susceptibility threshold calculation and for determination and verification of LRU specification.

VI. SUMMARY

In this report, analytical procedures have been developed for reducing the number of measurements required for a reliable aircraft LRU hardness assessment. A deterministic approach via a variational technique has been undertaken to find the relationships among the bulk cable current and the individual wire currents. A measure of accuracy has also been defined. For a given accuracy imposed on each individual wire current, optimal measurement approaches can be developed, which strongly depend on the excitation mechanism. For example, under two simple excitation conditions, the optimal measurement approaches are given below:

- If the wires in a cable bundle are evenly excited, the bulk cable current should be the first quantity to be measured
- If the excitation of one individual wire is dominant over the others, the current on that specific wire should be the first quantity to be measured.

From the measured quantities, the individual wire currents in the cable bundle can then be calculated from Equations 31 and 47 in Section II.

To support these conclusions, a 2-wire cable over a ground plane is studied in detail to find the effects on the wire currents of various parameters such as the excitation mechanism, bundle configuration, load impedance, source and measurement locations, etc.

The results derived from the variational technique can be applied to the direct-drive testing for the determination of susceptibility thresholds and for the development and verification of specifications of an LRU. For example, it is possible that a proper excitation of one wire enables one to determine and verify the specifications of other wires in the same bundle. In some cases, the bulk cable current alone can be considered a candidate for specification of an LRU.

New experiments have been suggested for verifying and improving the simple engineering rules on multi-wire cables, which have been derived by the variational techniques in this report.

REFERENCES

1. Agrawal, A.K., and C.E. Baum, "Bounding of Signal Levels at Terminations of a Multiconductor Transmission-Line Network," Interaction Note No. 419. Air Force Weapons Laboratory, Kirtland AFB, New Mexico, April 1983.

2. Scott, L., H. Price, and A. Agrawal, "Bounding of EMP-Induced Cable Currents in Aircraft," AFWL-TR-82-41, Air Force Weapons Laboratory, Kirtland AFB, New Mexico, January 1983.

3. Guillemin, E.A., Introductory Circuit Theory, John Wiley & Sons, Inc., New York, 1953.

4. Caratheodory, C., Calculus of Variations and Partial Differential Equations of the First Order, Part II: Calculus of Variations, Holden-Day, Inc., San Francisco, 1967.

5. Hildebrand, F.B., Advanced Calculus for Applications, Prentice-Hall, Inc., Englewood Cliffs, New Jersey, 1976.

6. Wylie, C.R., Advanced Engineering Mathematics, McGraw-Hill, New York. 1975.

7. Baum, C.E., "On the Singularity Expansion Method for the Solution of Electromagnetic Interaction Problems," Interaction Note 88, Air Force Weapons Laboratory, Kirtland AFB, NM, 1971.

8. Gurbaxani, S.H., and A.K. Agrawal, "Further Experimental Verification of Frequency-Domain Multiconductor-Transmission-Line Characterization," IEEE, Trans. Electromagnetic Compat. Vol. EMC-25, No. 3, August 1983.

9. Lee, K.S.H. editor, "EMP Interaction: Principles, Techniques and Reference Data," PP. 103 - 119, EMP Interaction 2-1, Air Force Weapons Laboratory, Kirtland AFB, December 1980.

APPENDIX A

RELATIONSHIPS AMONG WIRE CURRENTS WHEN ONLY BULK CABLE CURRENT AND CURRENT ON ONE STRONGLY EXCITED WIRE ARE MEASURED

There are two constraints that are imposed in this case. One is the sum of individual wire currents. I_B, and the other one is the current of the most strongly excited individual wire, I_k. Thus, the two constraints can be written as follows:

$$\sum_{m=1}^{N} I_{L_m} = I_B \tag{1A}$$

$$I_{L_k} = I_k \tag{2A}$$

Substituting

$$I_{L_m} = a_m + jb_m \tag{3A}$$

$$I_B = I_{Br} + jI_{Bi} \tag{4A}$$

$$I_k = I_{kr} + jI_{ki} \tag{5A}$$

into Equations 1A and 2A, we obtain

$$\sum_{m=1}^{N} a_m = I_{Br} \tag{6A}$$

$$\sum_{m=1}^{N} b_m = I_{Bi} \tag{7A}$$

$$a_k = I_{kr} \tag{8A}$$

$$b_k = I_{ki} \tag{9A}$$

The energy function of the Thevenin equivalent circuit is given by

$$P = \sum_{n=1}^{N} \sum_{m=1}^{N} I_{L_n}^{*} Z_{t_{n,m}} I_{L_m} \tag{10A}$$

where $(Z_{t_{n,m}}) = (Z_{L_{n,m}}) + (Z_{s_{n,m}})$. Substituting Equation 3A into Equation 10A, we obtain

$$P = \sum_{n=1}^{N} \sum_{m=1}^{N} (a_n - jb_n)\, Z_{t_{n,m}}\, (a_m + jb_m) \tag{11A}$$

Now, we must find the stationary points of the expression

$$f = \sum_{n=1}^{N} \sum_{m=1}^{N} (a_n - jb_n)\, Z_{t_{n,m}}\, (a_m + jb_m) +$$

$$+ \lambda_1 (I_{Br} - \sum_{m=1}^{N} a_m) + \lambda_2 (I_{Bi} - \sum_{m=1}^{N} b_m) \tag{12A}$$

$$+ \lambda_3 (I_{kr} - a_k) + \lambda_4 (I_{ki} - b_k)$$

where λ_1, λ_2, λ_3, and λ_4 are Lagrange Multipliers. Accordingly, we should have

$$\frac{\partial f}{\partial a_n} = 0 \ , \ n = 1, 2, \ldots , N \tag{13A}$$

$$\frac{\partial f}{\partial b_n} = 0 \ , \ n = 1, 2, \ldots , N \tag{14A}$$

Consequently, we get

$$\sum_{m=1}^{N} Z_{t_{n,m}} (a_m + jb_m) + \sum_{m=1}^{N} (a_m - jb_m) Z_{t_{m,n}} - \lambda_1 - \lambda_3 \delta_{nk} = 0 \tag{15A}$$

$$-j \sum_{m=1}^{N} Z_{t_{n,m}} (a_m + jb_m) + j \sum_{m=1}^{N} (a_m - jb_m)\, Z_{t_{m,n}} - \lambda_2 - \lambda_4 \delta_{nk} = 0 \tag{16A}$$

Assuming that $(Z_{t_{n,m}})$ is a symmetric matrix, one can rewrite Equations 15A and 16A as

$$2(Z_{t_{n,m}}) \cdot (a_m) = \lambda_1 (1_n) + \lambda_3 \delta_{nk} \tag{17A}$$

$$2(Z_{t_{n,m}}) \cdot (b_m) = \lambda_2(1_n) + \lambda_4 \delta_{nk} \tag{18A}$$

where

$$(a_m)^T = (a_1, a_2, \ldots, a_N),\ (b_m)^T = (b_1, b_2, \ldots, b_N),\ \text{and}$$

$$(1_n)^T = (1, 1, \ldots, 1)$$

(a_m) and (b_m) can thus be written as follows

$$(a_m) = 1/2\ \lambda_1(Y_{t_{m,n}}) \cdot (1_n) + 1/2\ \lambda_3\ Y_{t_{m,k}} \tag{19A}$$

$$(b_m) = 1/2\ \lambda_2(Y_{t_{m,n}}) \cdot (1_n) + 1/2\ \lambda_4\ Y_{t_{m,k}} \tag{20A}$$

where $(Y_{t_{m,n}}) = (Z_{t_{m,n}})^{-1}$. Substituting Equations 19A and 20A into Equations 6A through 9A, and solving for λ_1, λ_2, λ_3 and λ_4 we find

$$\lambda_1 = 2\ \frac{I_{Br}\ Y_{t_{k,k}} - I_{kr}\ \left(\sum_{m=1}^{N} Y_{t_{m,k}}\right)}{Y_{t_{k,k}} \left(\sum_{m=1}^{N}\sum_{n=1}^{N} Y_{t_{m,n}}\right) - \left(\sum_{m=1}^{N} Y_{t_{m,k}}\right)\left(\sum_{m=1}^{N} Y_{t_{k,m}}\right)} \tag{21A}$$

$$\lambda_2 = 2\ \frac{I_{kr}\ \left(\sum_{m=1}^{N}\sum_{n=1}^{N} Y_{t_{m,n}}\right) - I_{Br}\ \left(\sum_{m=1}^{N} Y_{t_{k,m}}\right)}{Y_{t_{k,k}} \left(\sum_{m=1}^{N}\sum_{n=1}^{N} Y_{t_{m,n}}\right) - \left(\sum_{m=1}^{N} Y_{t_{m,k}}\right)\left(\sum_{m=1}^{N} Y_{t_{k,m}}\right)} \tag{22A}$$

$$= 2 \frac{I_{Bi} Y_{t_{k,k}} - I_{ki} \left(\sum_{m=1}^{N} Y_{t_{m,k}} \right)}{Y_{t_{k,k}} \left(\sum_{m=1}^{N} \sum_{n=1}^{N} Y_{t_{m,n}} \right) - \left(\sum_{m=1}^{N} Y_{t_{m,k}} \right) \left(\sum_{m=1}^{N} Y_{t_{k,m}} \right)} \quad (23A)$$

$$\lambda_4 = 2 \frac{I_{ki} \left(\sum_{m=1}^{N} \sum_{n=1}^{N} Y_{t_{m,n}} \right) - I_{Bi} \left(\sum_{m=1}^{N} Y_{t_{k,m}} \right)}{Y_{t_{k,k}} \left(\sum_{m=1}^{N} \sum_{n=1}^{N} Y_{t_{m,n}} \right) - \left(\sum_{m=1}^{N} Y_{t_{m,k}} \right) \left(\sum_{m=1}^{N} Y_{t_{k,m}} \right)} \quad (24A)$$

Substituting Equations 21A through 24A into Equations 19A and 20A, and then using Equation 3A, one finally obtains

$$I_{L_n} = I_B \frac{Y_{t_{k,k}} \left(\sum_{m=1}^{N} Y_{t_{n,m}} \right) - Y_{t_{n,k}} \left(\sum_{m=1}^{N} Y_{t_{k,m}} \right)}{Y_{t_{k,k}} \left(\sum_{m=1}^{N} \sum_{p=1}^{N} Y_{t_{m,p}} \right) - \left(\sum_{m=1}^{N} Y_{t_{m,k}} \right) \left(\sum_{m=1}^{N} Y_{t_{k,m}} \right)} \quad (25A)$$

$$+ I_k \frac{Y_{t_{n,k}} \left(\sum_{m=1}^{N} \sum_{p=1}^{N} Y_{t_{m,p}} \right) - \left(\sum_{m=1}^{N} Y_{t_{m,k}} \right) \left(\sum_{m=1}^{N} Y_{t_{n,m}} \right)}{Y_{t_{k,k}} \left(\sum_{m=1}^{N} \sum_{p=1}^{N} Y_{t_{m,p}} \right) - \left(\sum_{m=1}^{N} Y_{t_{m,k}} \right) \left(\sum_{m=1}^{N} Y_{t_{k,m}} \right)}$$

where I_B and I_k are the measured bulk cable and the k-th wire current, respectively.

APPENDIX B

ADDITIONAL FIGURES

This appendix presents additional figures to show the comparison of exact wire currents with those obtained from the variational technique, and also curves to demonstrate the effects of load impedances, source types and locations, number of excited wires, line configurations and measurement locations on common- and differential-mode currents.

1. COMPARISON OF EXACT WIRE CURRENTS WITH THOSE OBTAINED FROM VARIATIONAL TECHNIQUES

Figures B1 through B11 illustrate the comparison of exact wire currents (I_1, I_2) with those obtained from variational techniques. I_1' and I_2' are the wire currents obtained from a knowledge of I_B which is $I_1 + I_2$. I_1'' and I_2'' are the wire currents obtained from a knowledge of one individual wire current which is taken to be I_1.

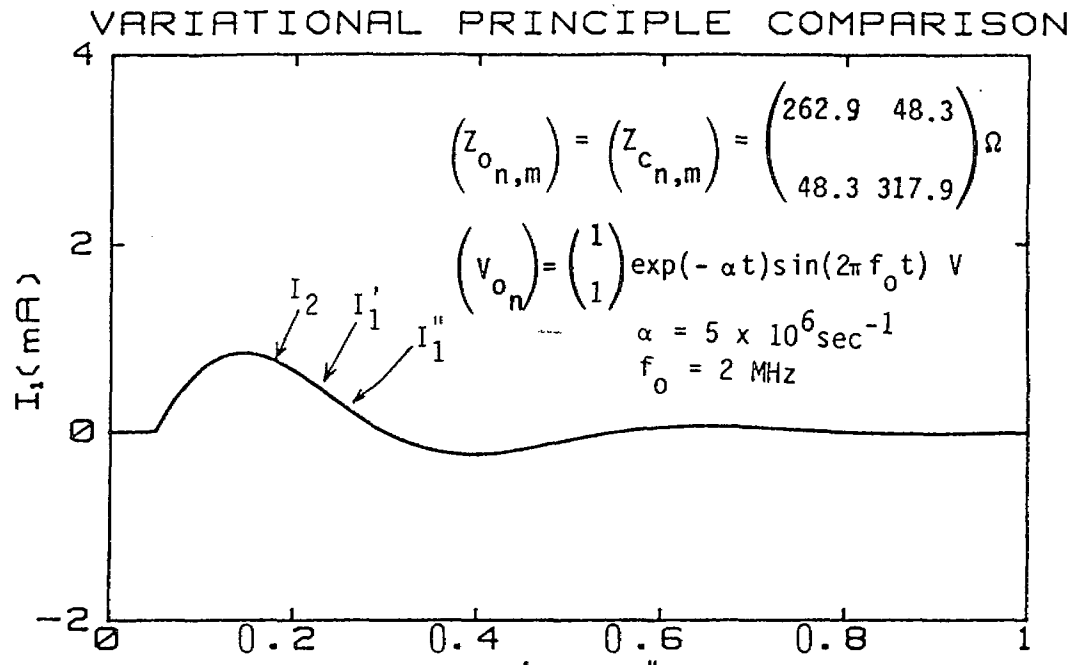

(a) Time history of I_1, I_1', and I_1''.

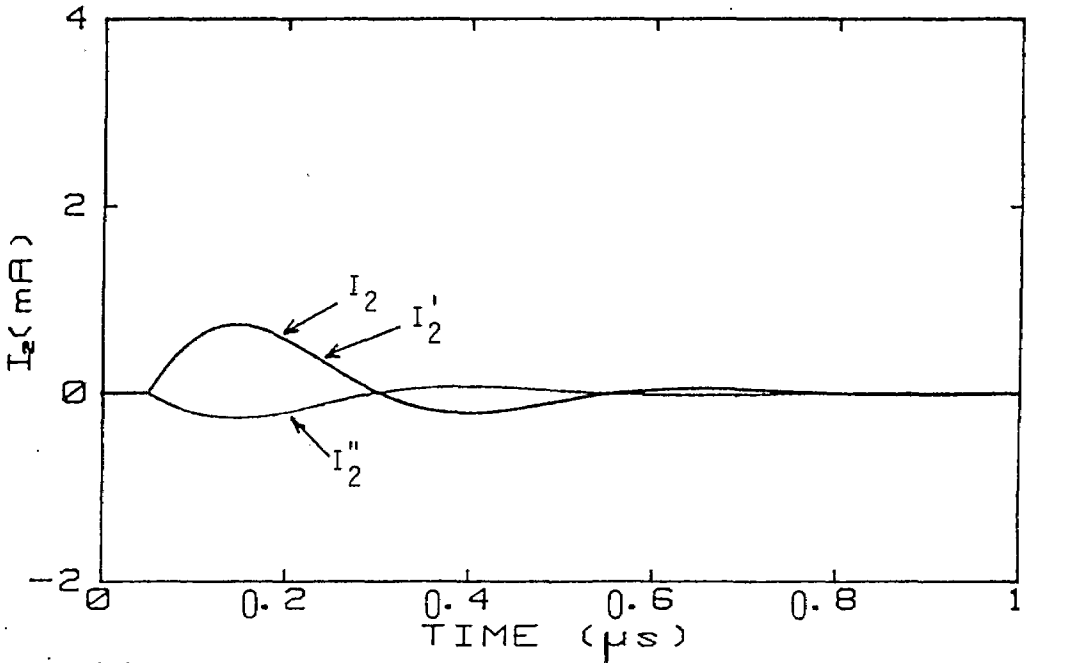

(b) Time history of I_2, I_2', and I_2''.

Figure B1. Exact wire currents (I_1, I_2) and estimated wire currents (I_1', I_2'; I_1'',I_2'') using two variational principle techniques when ℓ = 30 m, x_s = 15 m , x_m = 30 m , $Z_{\ell 11} = Z_{\ell 12} = Z_{\ell 22}$ = 400 Ω.

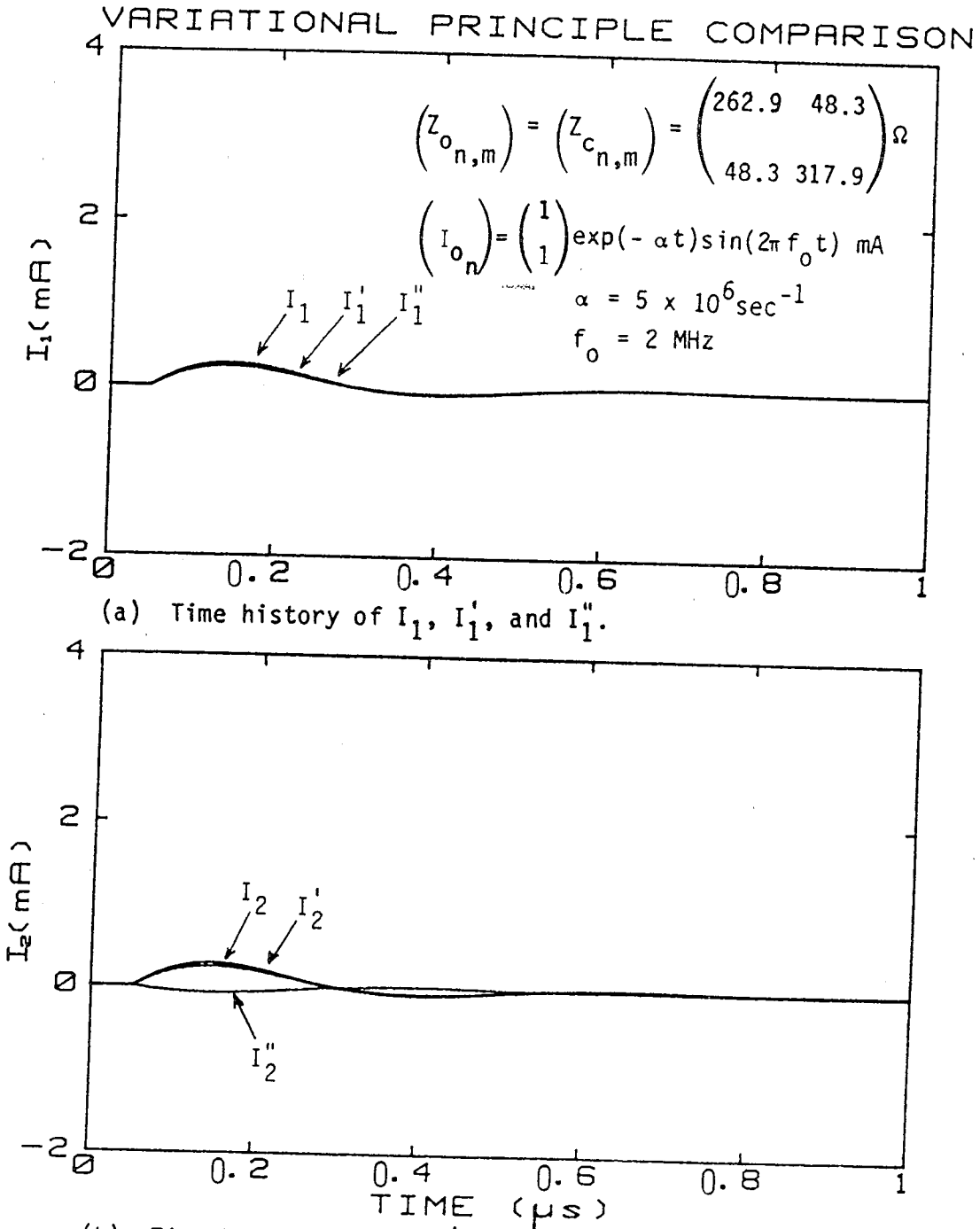

Figure B2. Exact wire currents (I_1, I_2) and estimated wire currents (I_1', I_2'; I_1'',I_2'') using two variational principle techniques when ℓ = 30 m, x_s = 15 m , x_m = 30 m, $Z_{\ell 11} = Z_{\ell 12} = Z_{\ell 22}$ = 400 Ω.

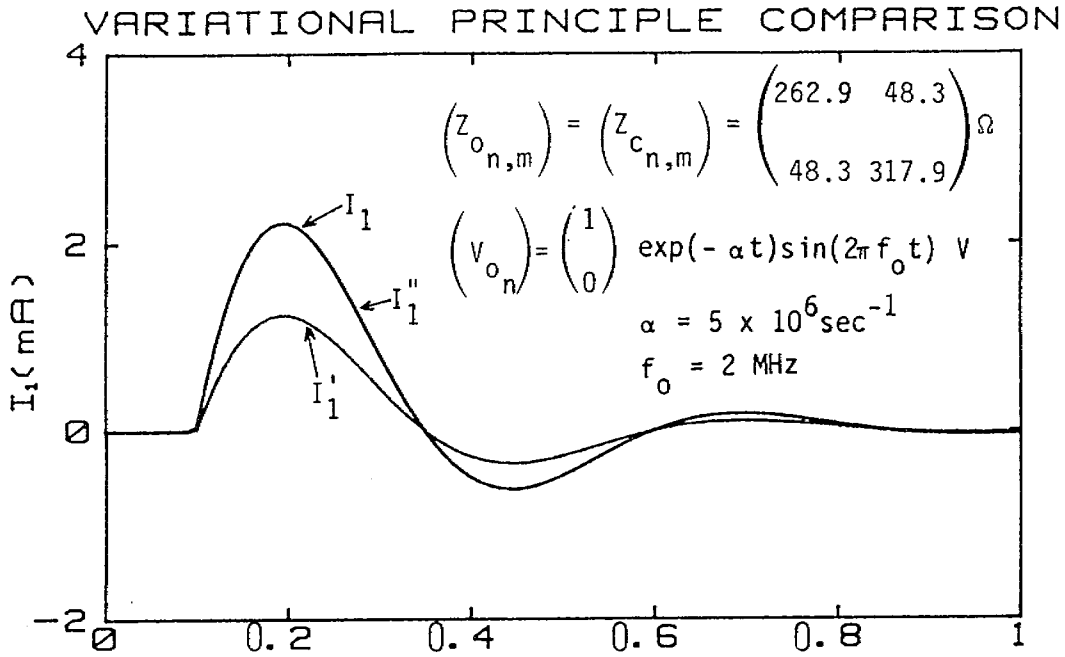

(a) Time history of I_1, I_1', and I_1''.

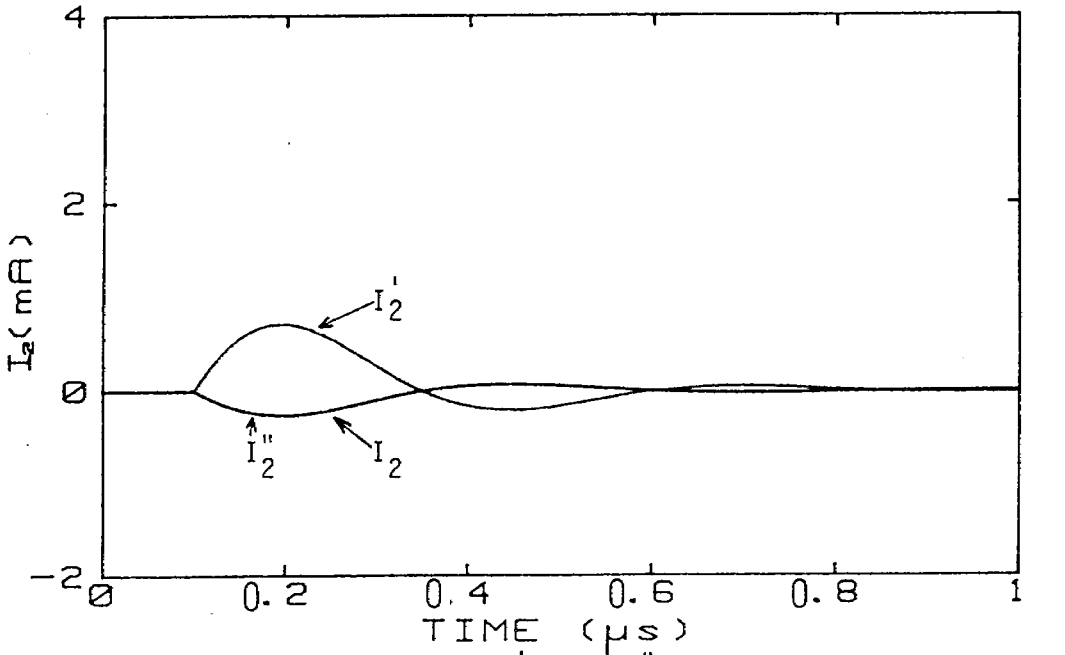

(b) Time history of I_2, I_2', and I_2''.

Figure B3. Exact wire currents (I_1, I_2) and estimated wire currents (I_1', I_2'; I_1'',I_2'') using two variational principle techniques when ℓ = 30 m, x_s = 0.25 m, x_m = 30 m, $Z_{\ell 11}$ = 1 Ω, $Z_{\ell 12}$ = 100 Ω, and $Z_{\ell 22}$ = 10^4 Ω.

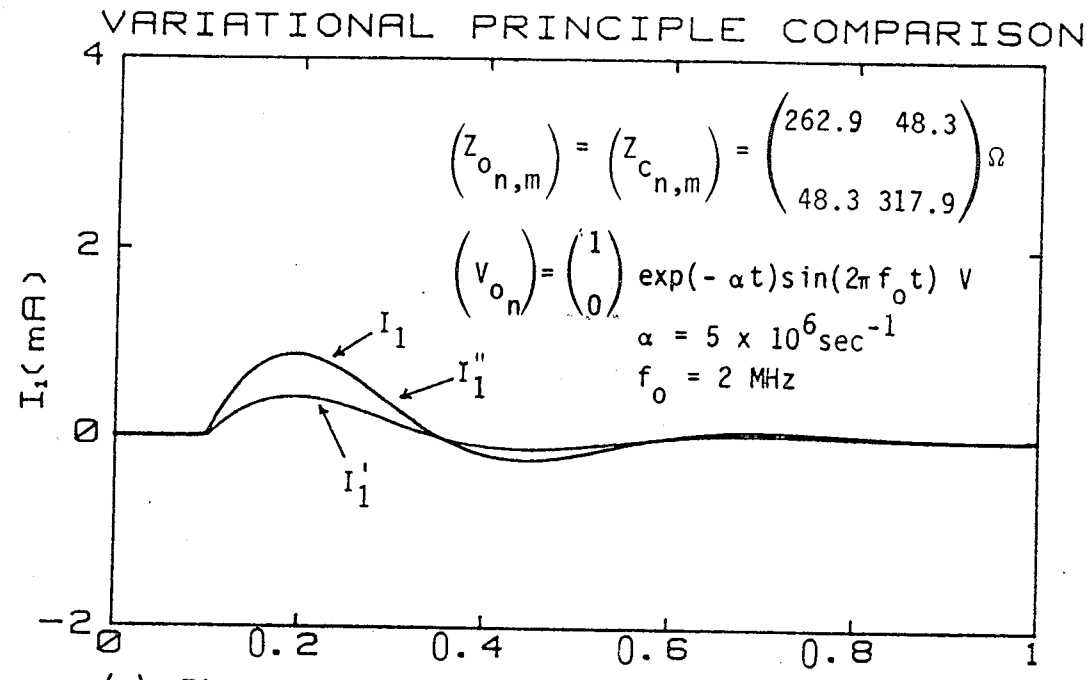

(a) Time history of I_1, I_1', and I_1''.

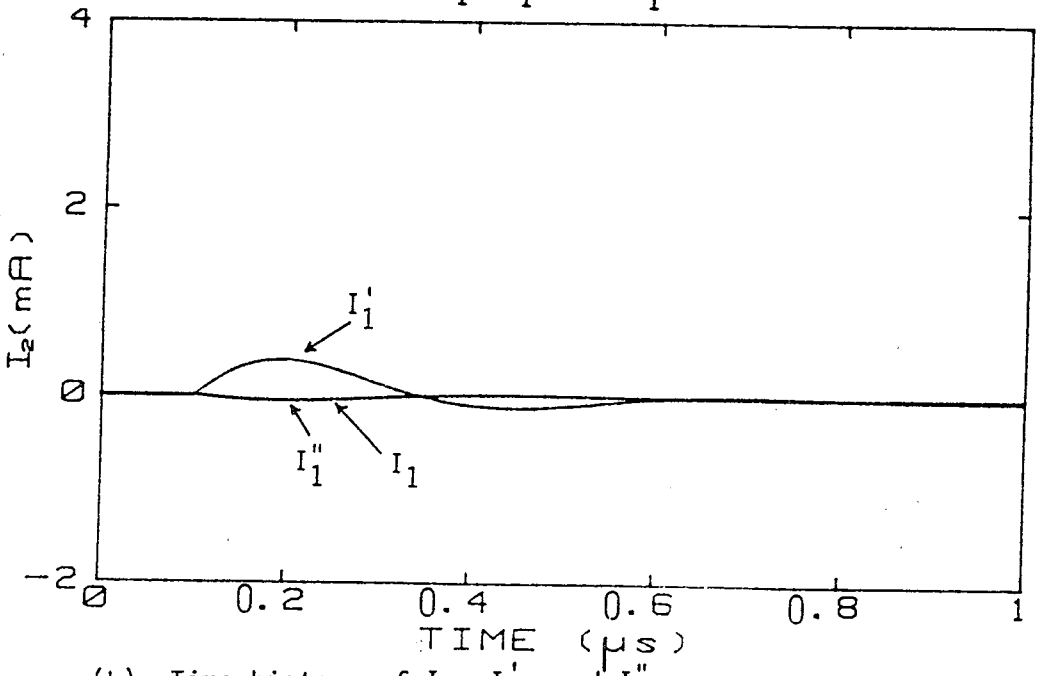

(b) Time history of I_2, I_2', and I_2''.

Figure B4. Exact wire currents (I_1, I_2) and estimated wire currents (I_1', I_2'; I_1'',I_2'') using two variational principle techniques when ℓ = 30 m, x_s = 0.25 m, x_m = 30 m, $Z_{\ell 11}$ = 400 Ω, $Z_{\ell 12} = \infty$ and $Z_{\ell 22}$ = 400 Ω.

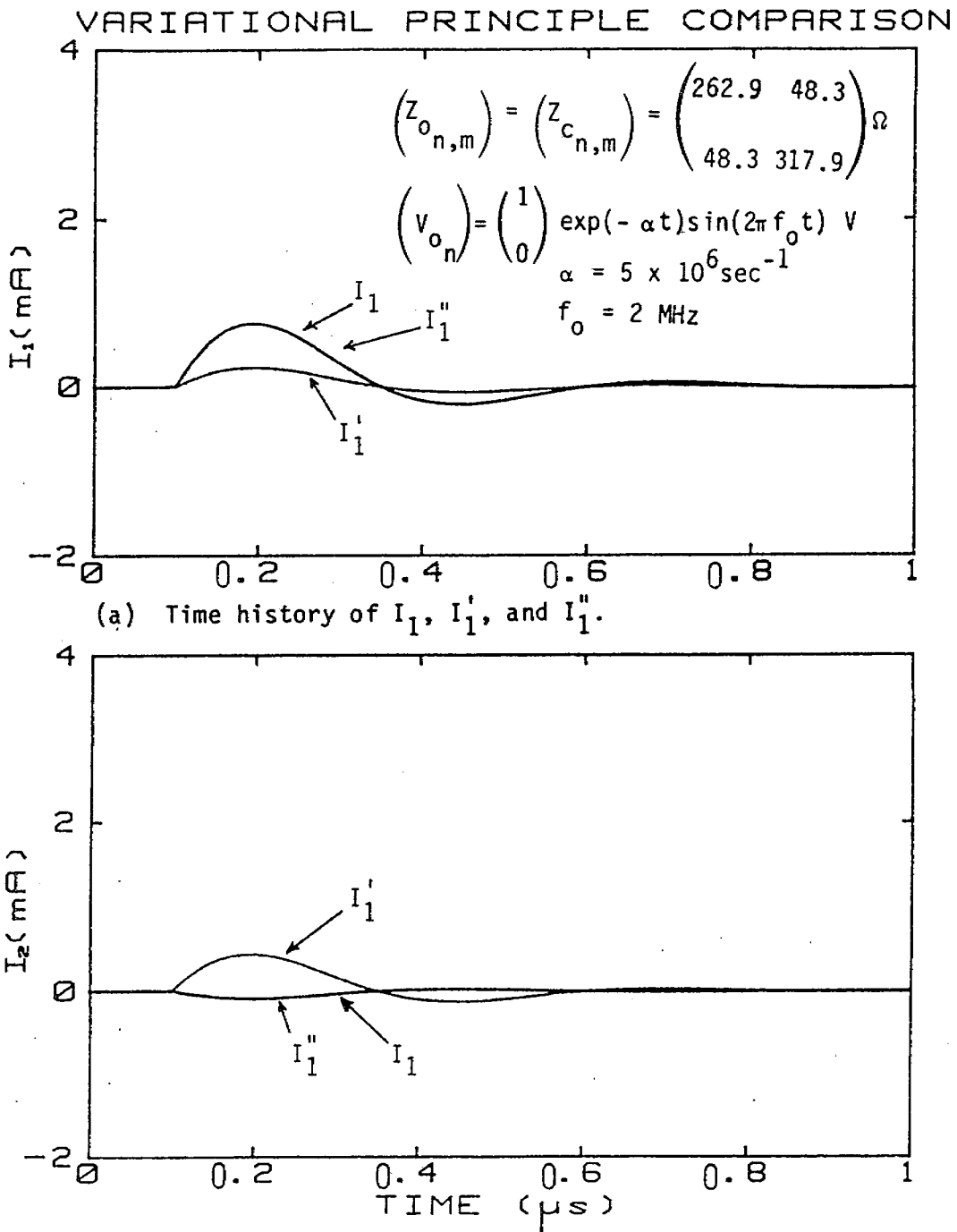

(a) Time history of I_1, I_1', and I_1''.

(b) Time history of I_2, I_2', and I_2''.

Figure B5. Exact wire currents (I_1, I_2) and estimated wire currents (I_1', I_2'; I_1'',I_2'') using two variational principle techniques when ℓ = 30 m, x_s = 0.25 m, x_m = 30 m, $Z_{\ell 11}$ = 500 Ω $Z_{\ell 12}$ = ∞, and $Z_{\ell 22}$ = 100 Ω.

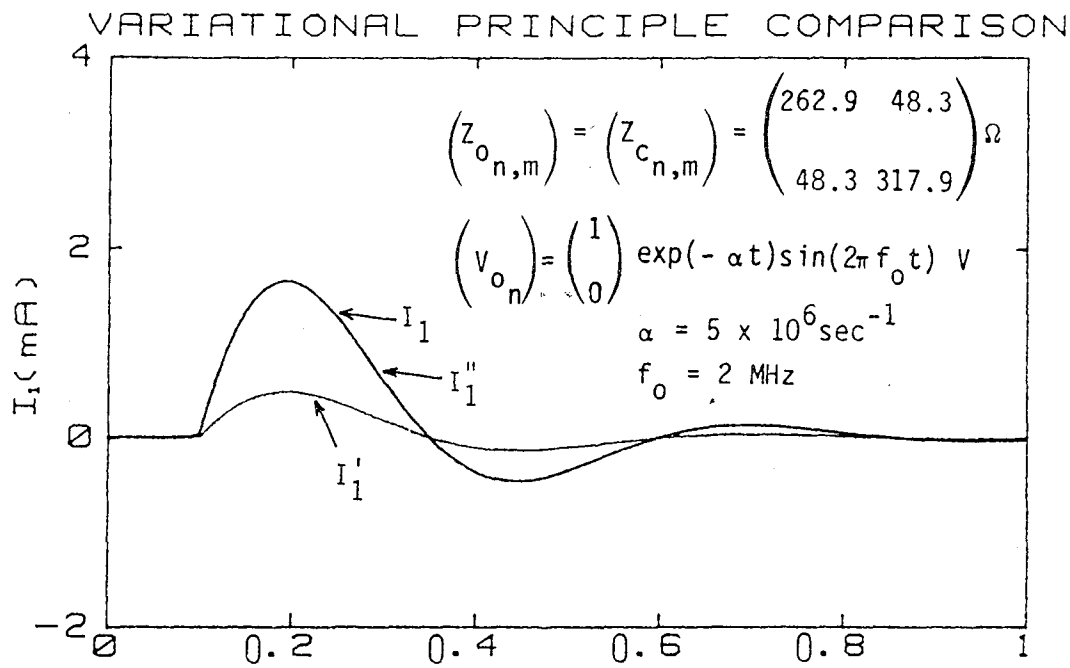

(a) Time history of I_1, I_1', and I_1''.

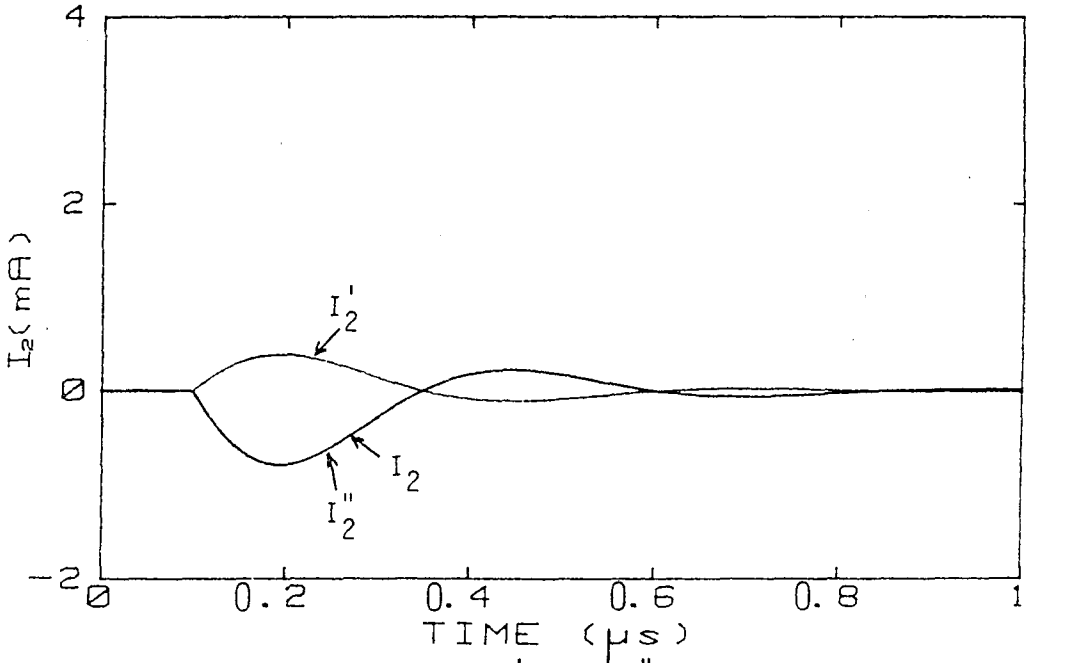

(b) Time history of I_2, I_2', and I_2''.

Figure B6. Exact wire currents (I_1, I_2) and estimated wire currents (I_1', I_2'; I_1'',I_2'') using two variational principle techniques when $\ell = 30$ m, $x_s = 0.25$ m, $x_m = 30$ m, $Z_{\ell 11} = 400\ \Omega$, $Z_{\ell 12} = 4\ \Omega$, and $Z_{\ell 22} = 400\ \Omega$.

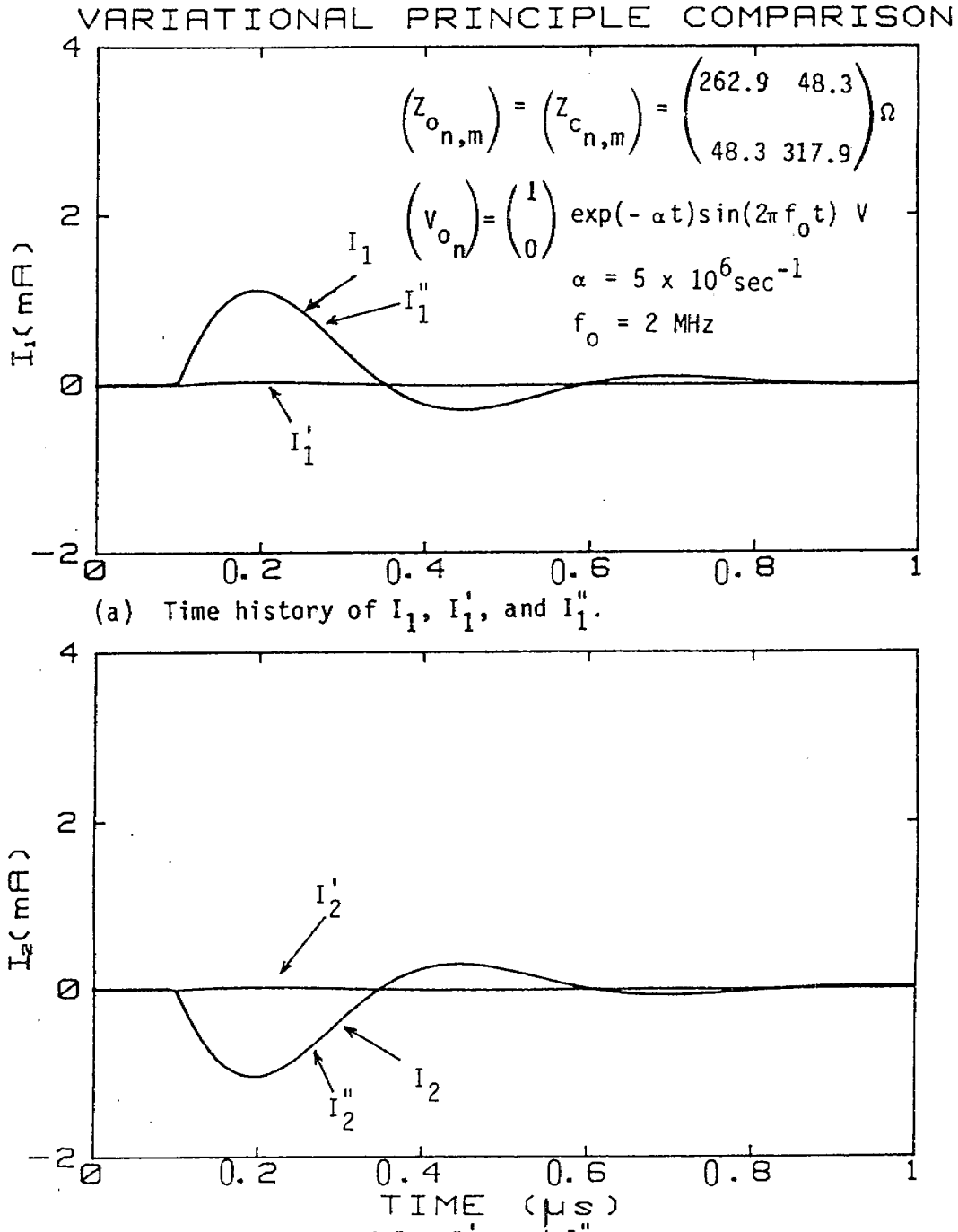

(a) Time history of I_1, I_1', and I_1''.

(b) Time history of I_2, I_2', and I_2''.

Figure B7. Exact wire currents (I_1, I_2) and estimated wire currents (I_1', I_2'; I_1'',I_2'') using two variational principle techniques when ℓ = 30 m, x_s = 0.25 m, x_m = 30 m, $Z_{\ell 11} = 10^4 \Omega$, $Z_{\ell 12} = 50\ \Omega$, and $Z_{\ell 22} = 10^4\ \Omega$.

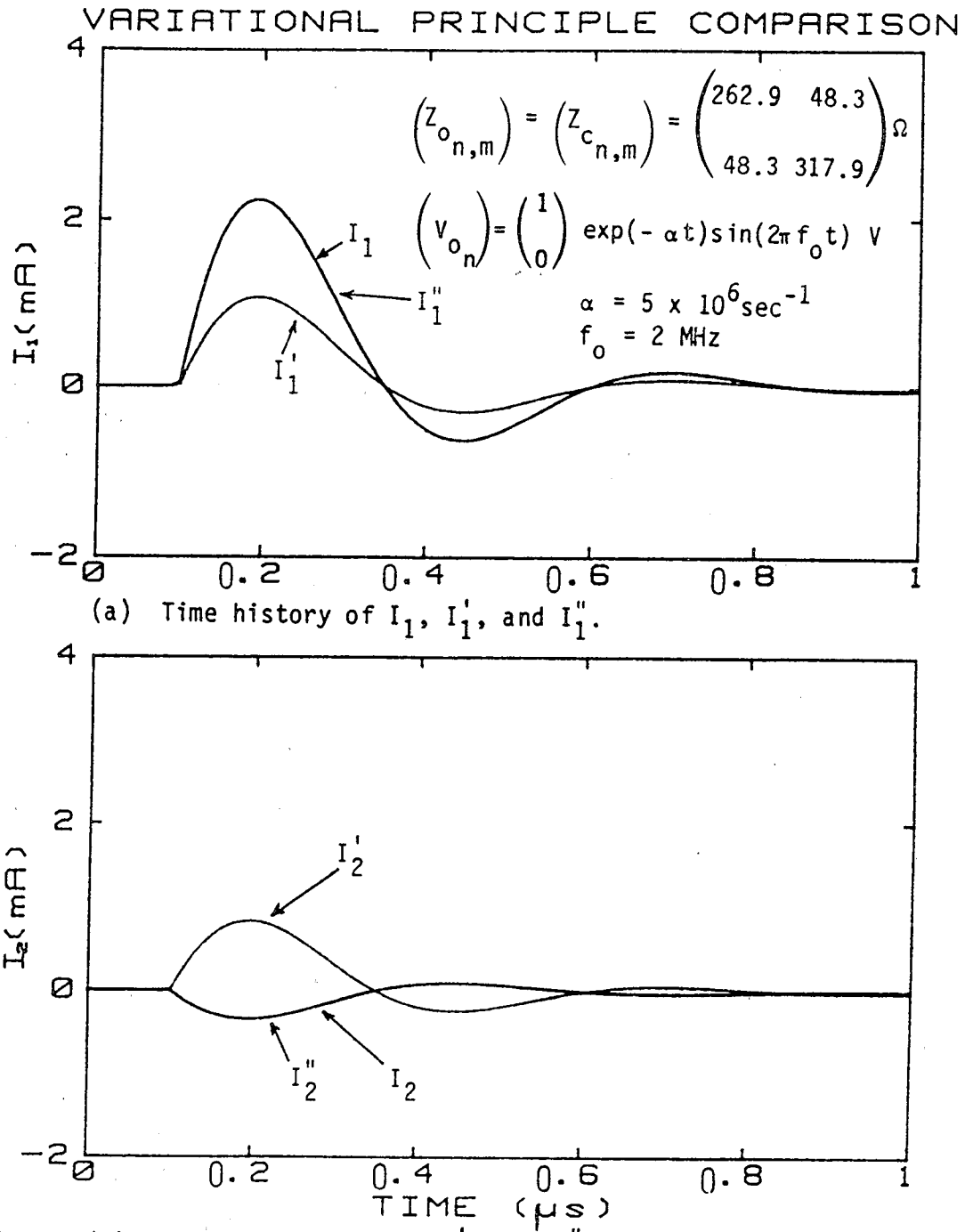

(a) Time history of I_1, I_1', and I_1''.

(b) Time history of I_2, I_2', and I_2''.

Figure B8. Exact wire currents (I_1, I_2) and estimated wire currents (I_1', I_2'; I_1'',I_2'') using two variational principle techniques when ℓ = 30 m, x_s = 0.25 m, x_m = 30 m, $Z_{\ell 11}$ = 1 Ω, $Z_{\ell 12}$ = 1 Ω and $Z_{\ell 22} = 10^4 \Omega$.

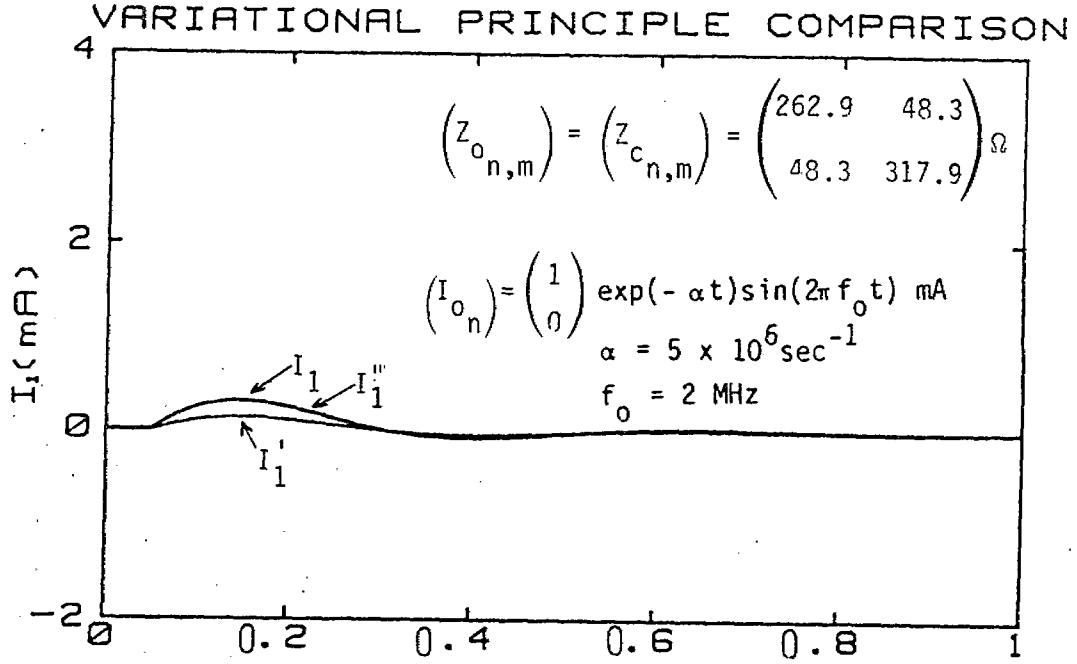

(a) Time history of I_1, I_1', and I_1''.

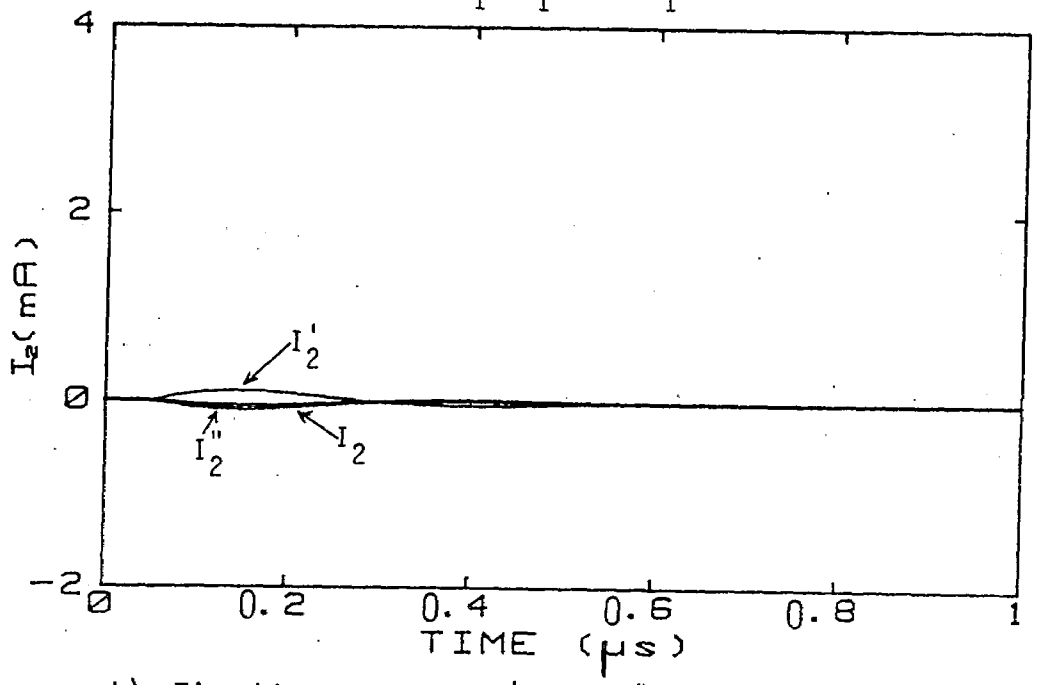

b) Time history of I_2, I_2', and I_2''.

Figure B9. Exact wire currents (I_1,I_2) and estimated wire currents (I_1', I_2'; I_1'' I_2'') using two variational principle techniques when ℓ = 30 m, x_s = 15 m, x_m = 30 m, and $Z_{\ell 11} = Z_{\ell 12} = Z_{\ell 22}$ = 400 Ω.

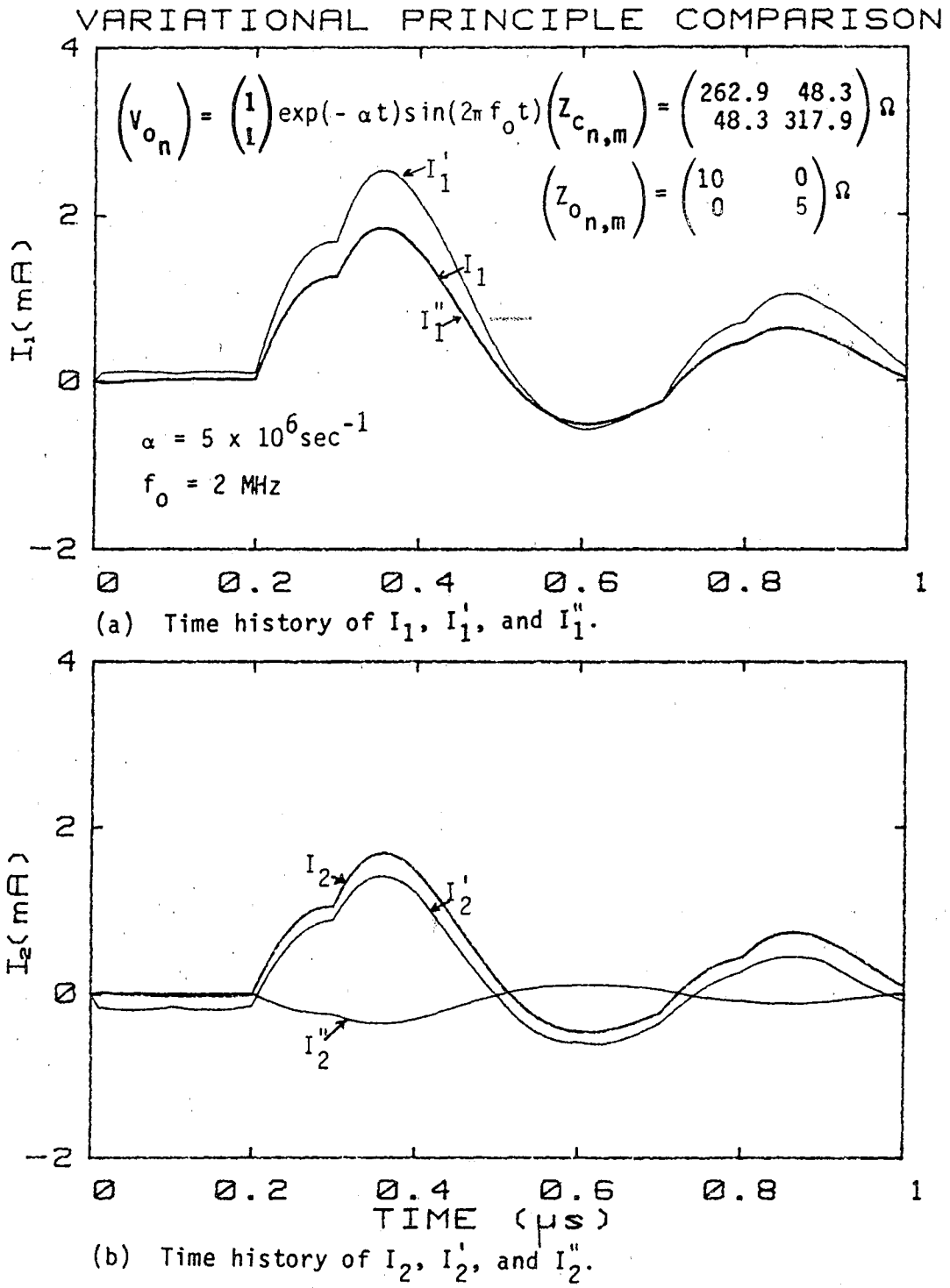

(a) Time history of I_1, I_1', and I_1''.

(b) Time history of I_2, I_2', and I_2''.

Figure B10. Exact wire currents (I_1, I_2) and estimated wire currents (I_1', I_2'; I_1'', I_2'') using two variational principle techniques when ℓ = 75 m, x_s = 15 m, x_m = 75 m, $Z_{\ell 11}$ = 100 Ω, $Z_{\ell 12}$=1 Ω, and $Z_{\ell 22}$ = 400 Ω.

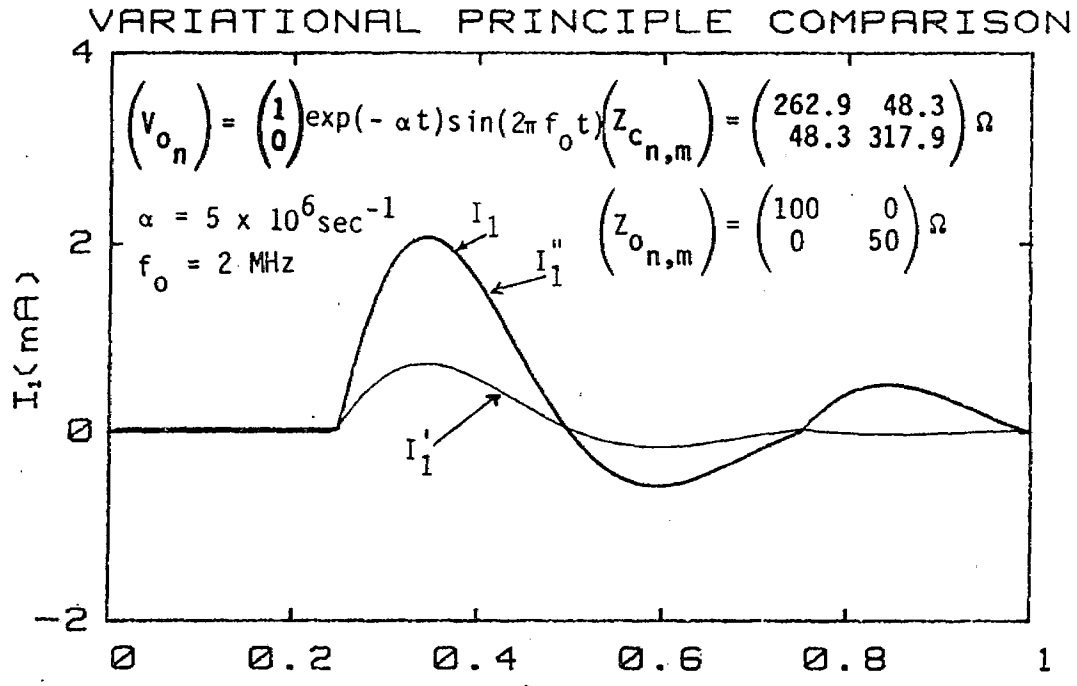

(a) Time history of I_1, I_1', and I_1''.

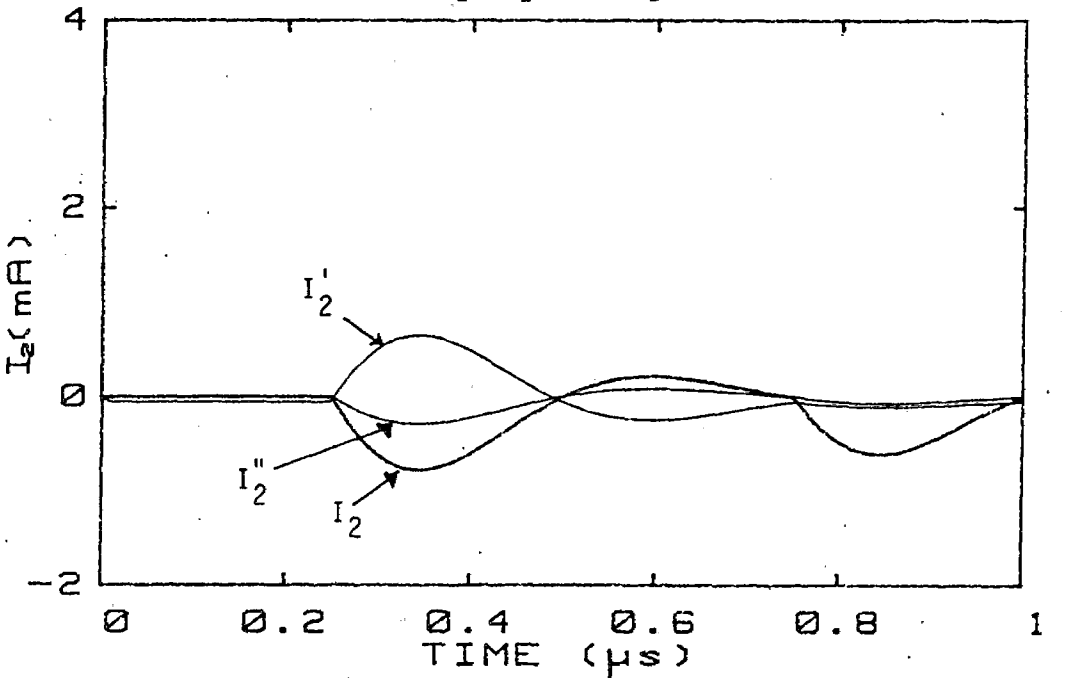

(b) Time history of I_2, I_2, and I_2''.

Figure B11. Exact wire currents (I_1, I_2) and estimated wire currents (I_1', I_2'; I_1'', I_2'') using two variational principle techniques when ℓ = 75 m, x_s = 0.25 m, x_m = 75 m, $Z_{\ell 11}$ = 500 Ω, $Z_{\ell 12}$ = 250 Ω, and $Z_{\ell 22}$ = 100 Ω.

2. EFFECT OF LOAD IMPEDANCE

Figures B12 through B17 illustrate effects of pin-to-pin impedance ($Z_{\ell_{12}}$) on common and differential mode currents (I_B, I_D)

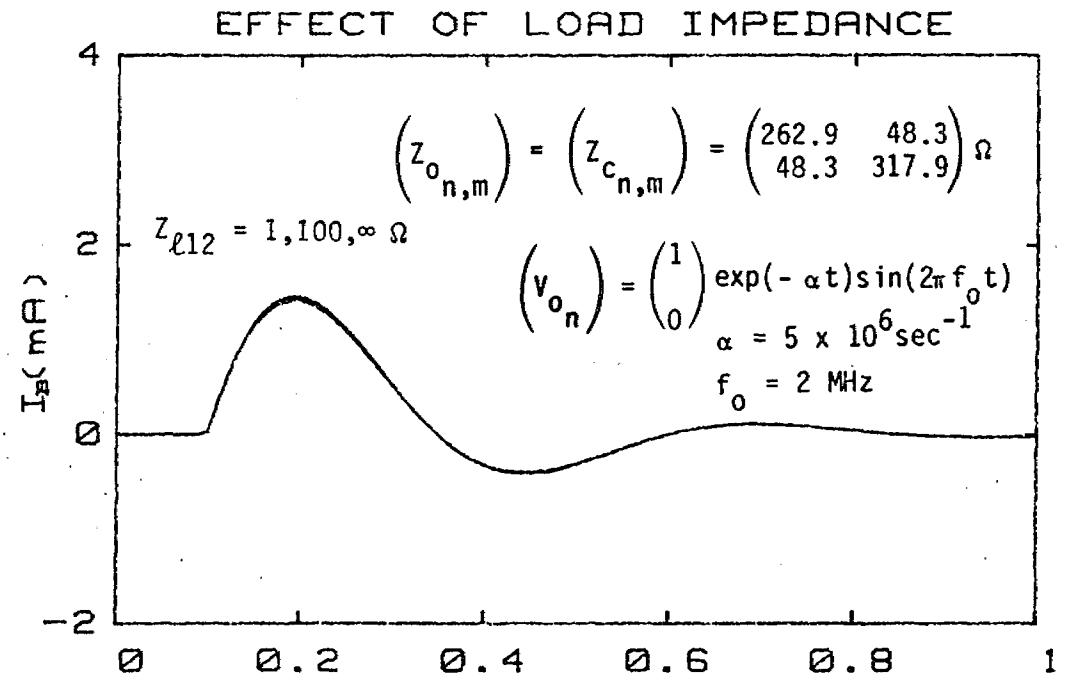

(a) Time history of I_B.

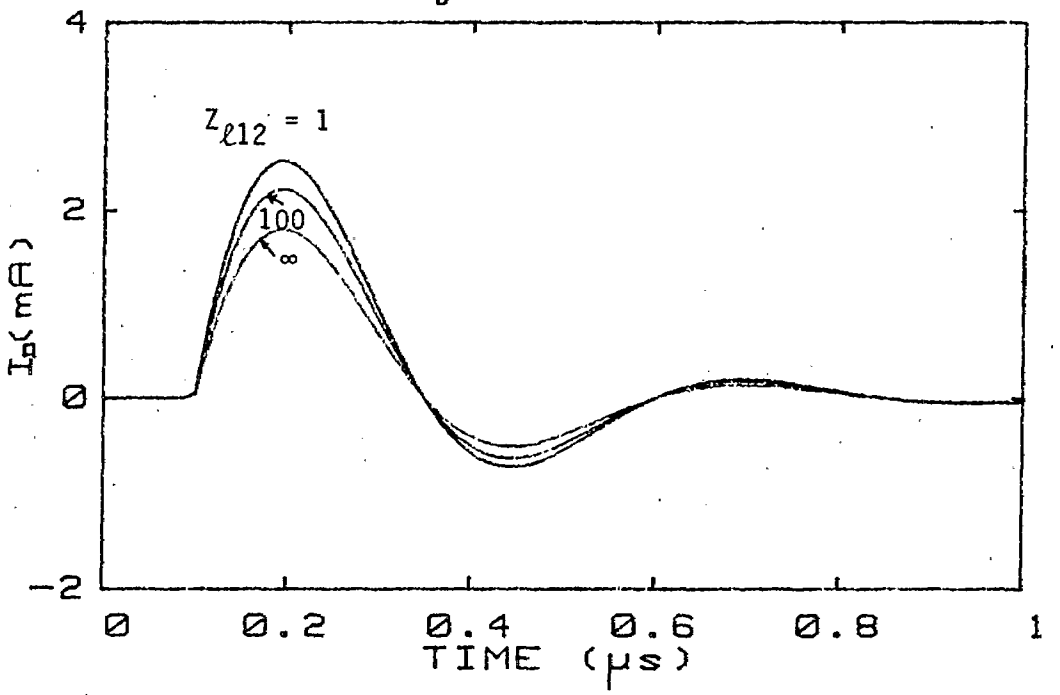

(b) Time history of I_D.

Figure B12. Common and differential mode currents (I_B, I_D) for different $Z_{\ell 12}$ when ℓ = 30 m, x_s = 0.25 m, x_m = 30 m and $Z_{\ell 11} = Z_{\ell 22}$ = 100 Ω.

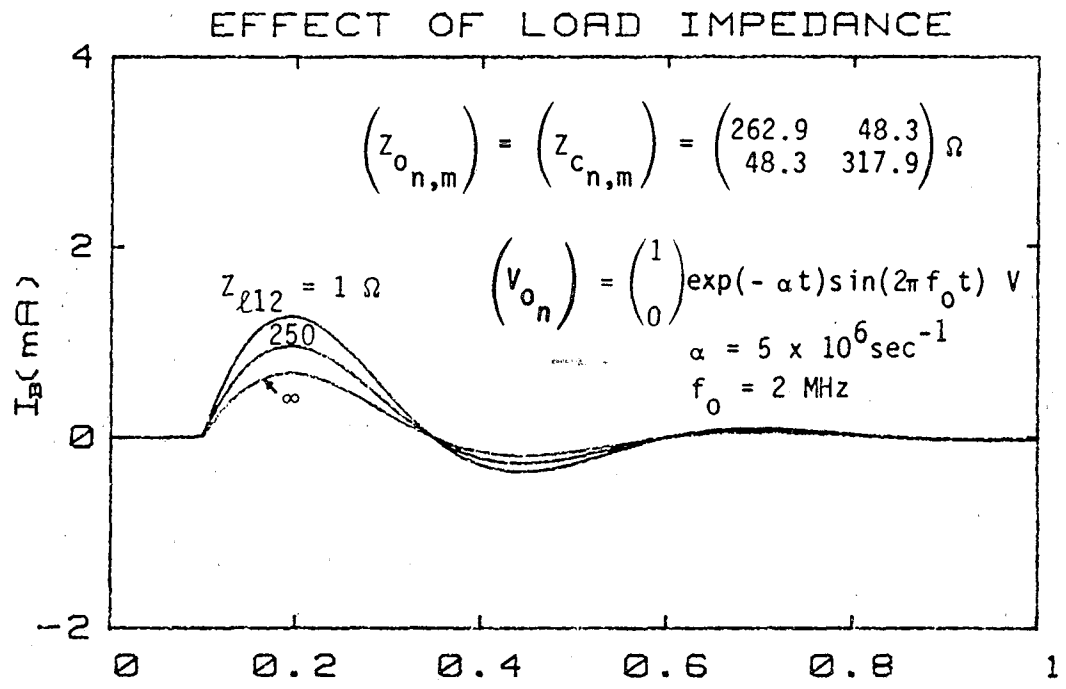

(a) Time history of I_B.

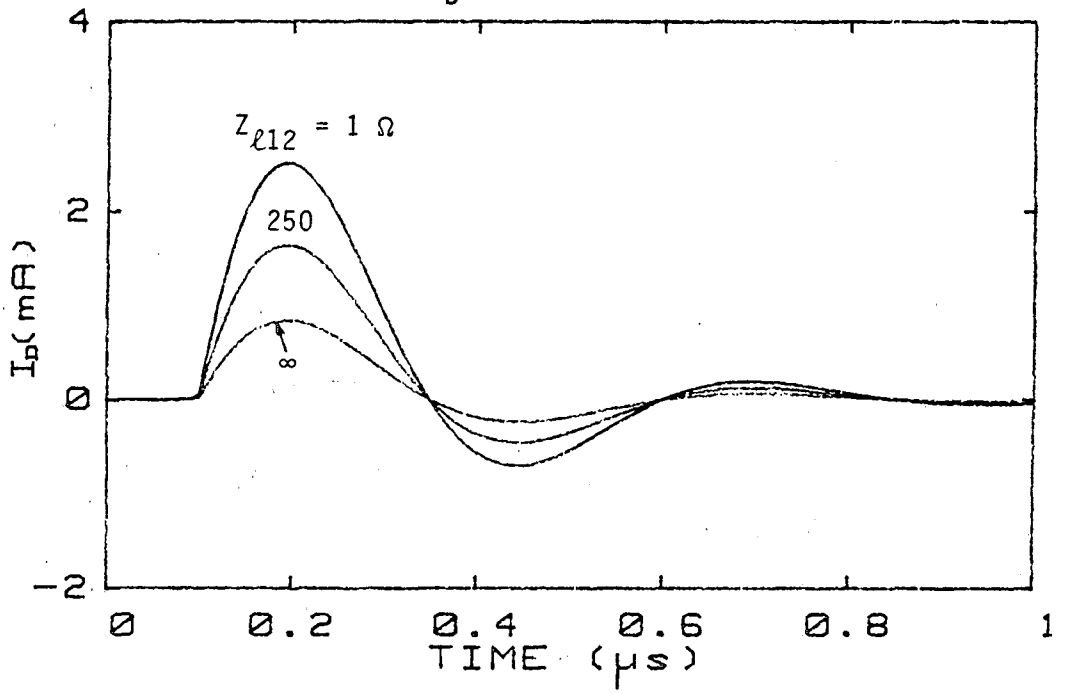

(b) Time history of I_D.

Figure B13. Common and differential mode currents (I_B, I_D) for different $Z_{\ell 12}$ when ℓ = 30 m, x_s = 0.25 m, x_m = 30 m, $Z_{\ell 11}$ = 500 Ω, and $Z_{\ell 22}$ = 100 Ω.

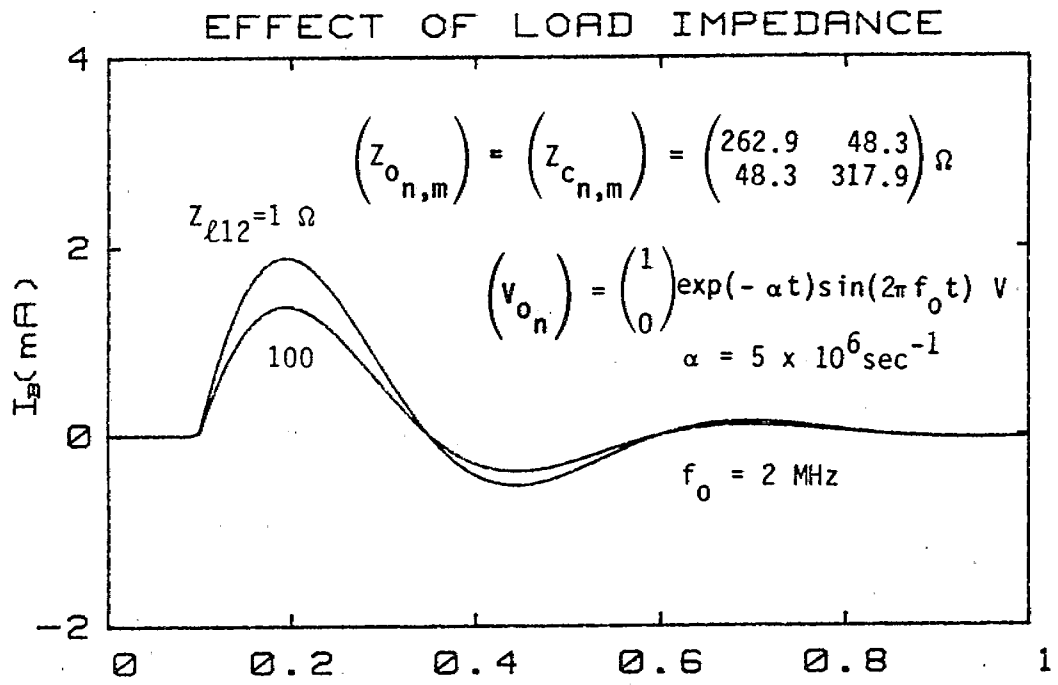

(a) Time history of I_B.

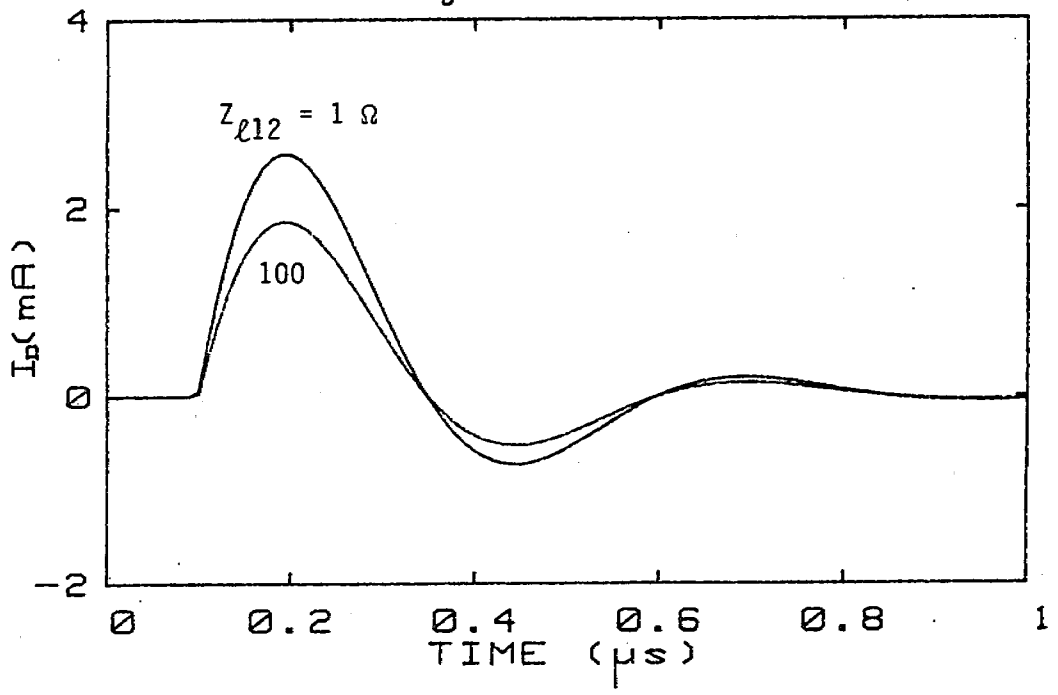

(b) Time history of I_D.

Figure B14. Common and differential mode currents (I_B, I_D) for different $Z_{\ell 12}$ when ℓ = 30 m, x_s = 0.25 m, x_m = 30 m, $Z_{\ell 11}$ = $10^4\Omega$. and $Z_{\ell 22}$ = 1 Ω.

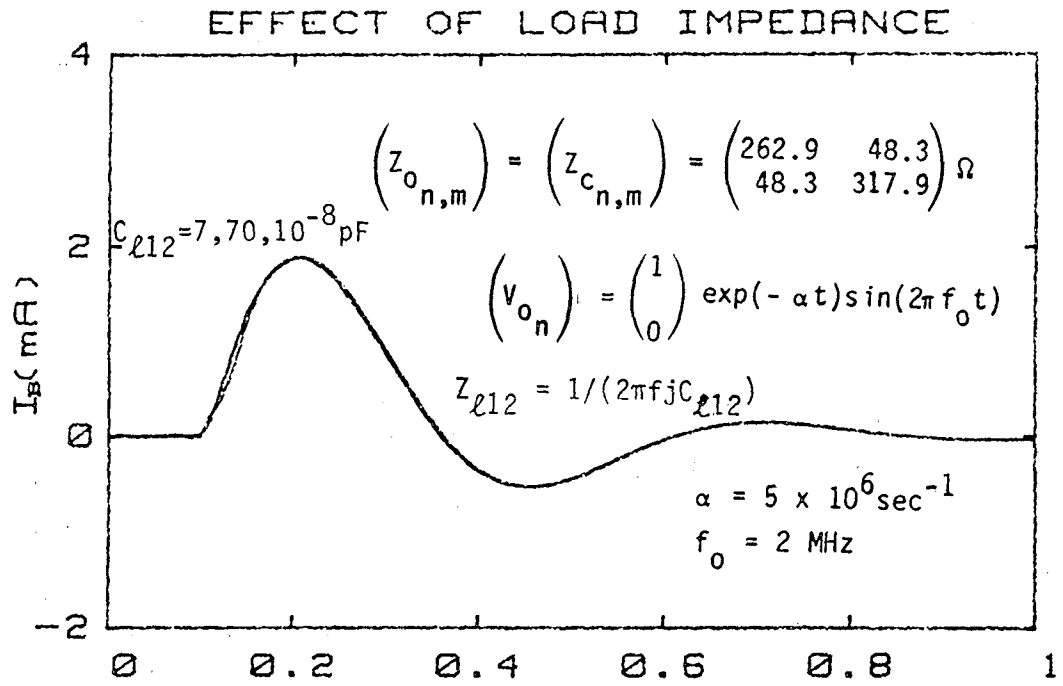

(a) Time history of I_B.

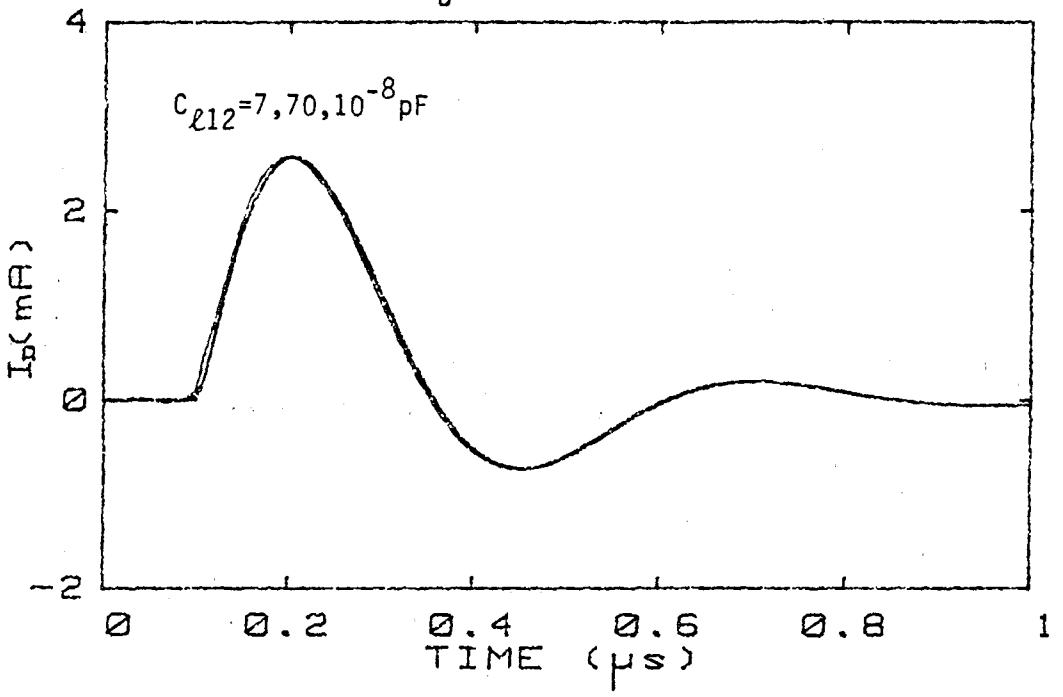

(b) Time history of I_D.

Figure B15. Common and differential mode currents (I_B, I_D) for different $Z_{\ell 12}$ when ℓ = 30 m, x_s = 0.25 m, x_m = 30 m, $Z_{\ell 11} = 2\pi fj(3x10^{-7}) + 1/[2\pi fj(7x10^{-11})]\Omega$, and $Z_{\ell 22} = 2\pi fj(2.5x10^{-7})$.

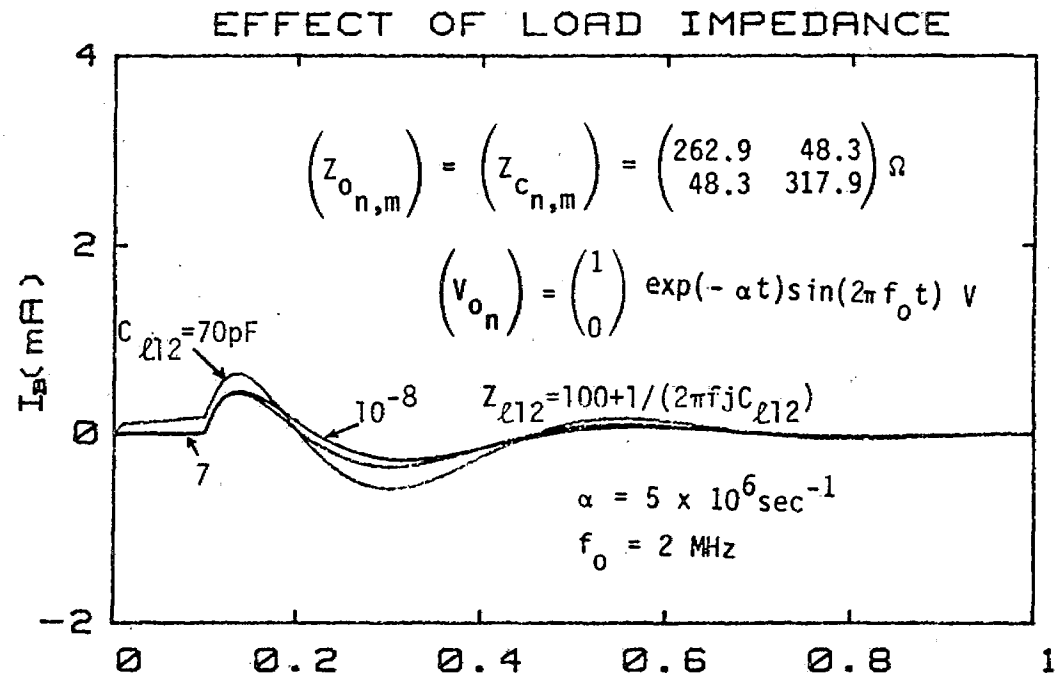

(a) Time history of I_B.

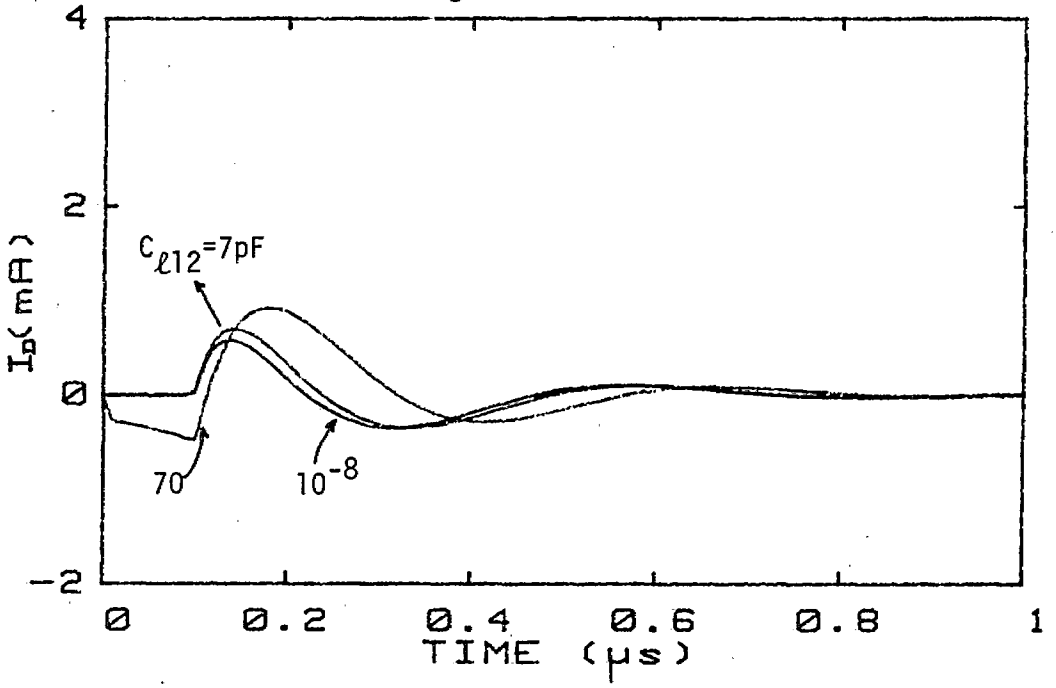

(b) Time history of I_D.

Figure B16. Common and differential mode currents (I_B, I_D) for different $Z_{\ell 12}$ when ℓ = 30 m, x_s = 0.25 m, x_m = 30 m, $Z_{\ell 11} = Z_{\ell 22} = 100 + 2\pi fj(3\text{x}10^{-7}) + 1/[2\pi fj(7\text{x}10^{-11})]$ Ω.

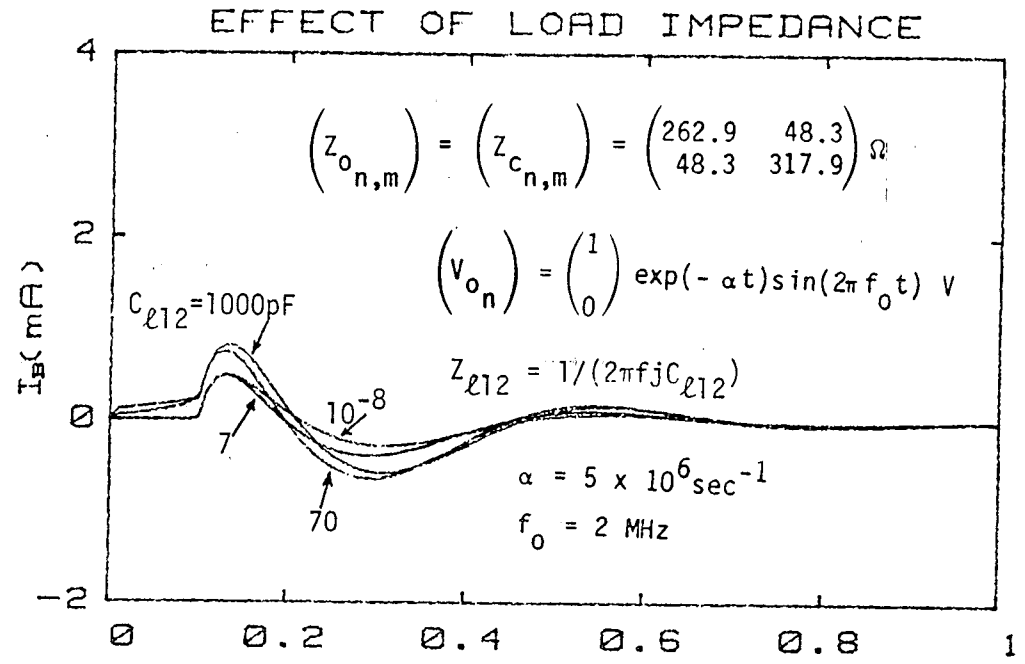

(a) Time history of I_B.

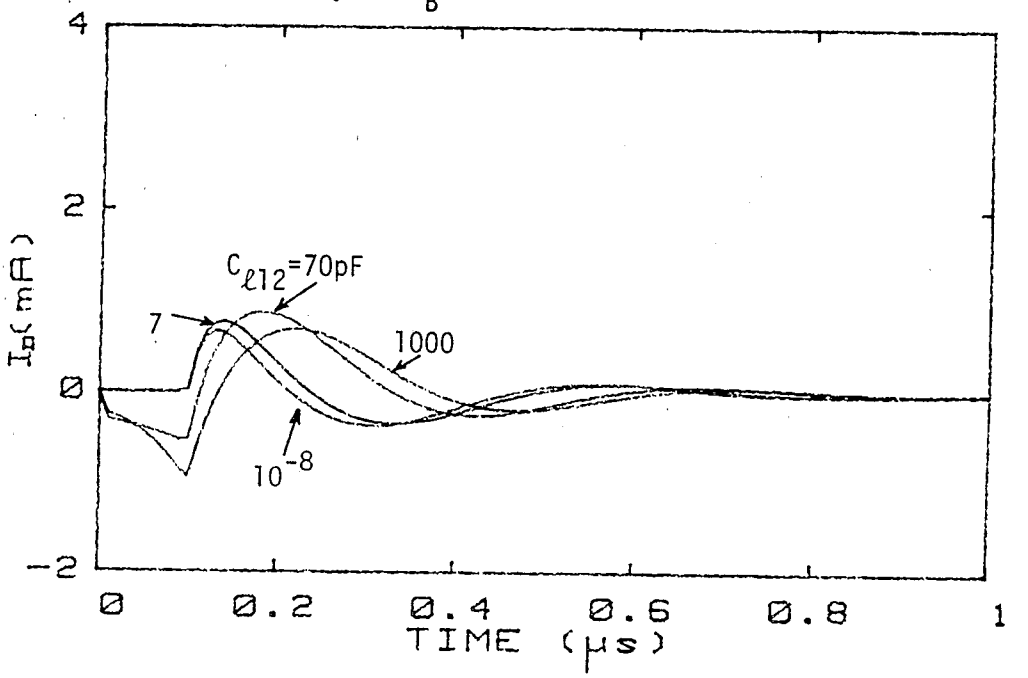

(b) Time history of I_D.

Figure B17. Common and differential mode currents (I_B, I_D) for different $Z_{\ell 12}$ when ℓ = 30 m, x_s = 0.25 m, x_m = 30 m, and $Z_{\ell 11} = Z_{\ell 22} = 2\pi f j(3\times10^{-7}) + 1/[2\pi f j(7\times10^{-11})]\ \Omega$.

3. EFFECT OF SOURCE TYPE

Figures B19 and B20 illustrate the effects of source type on common- and differential-mode currents (I_B, I_D).

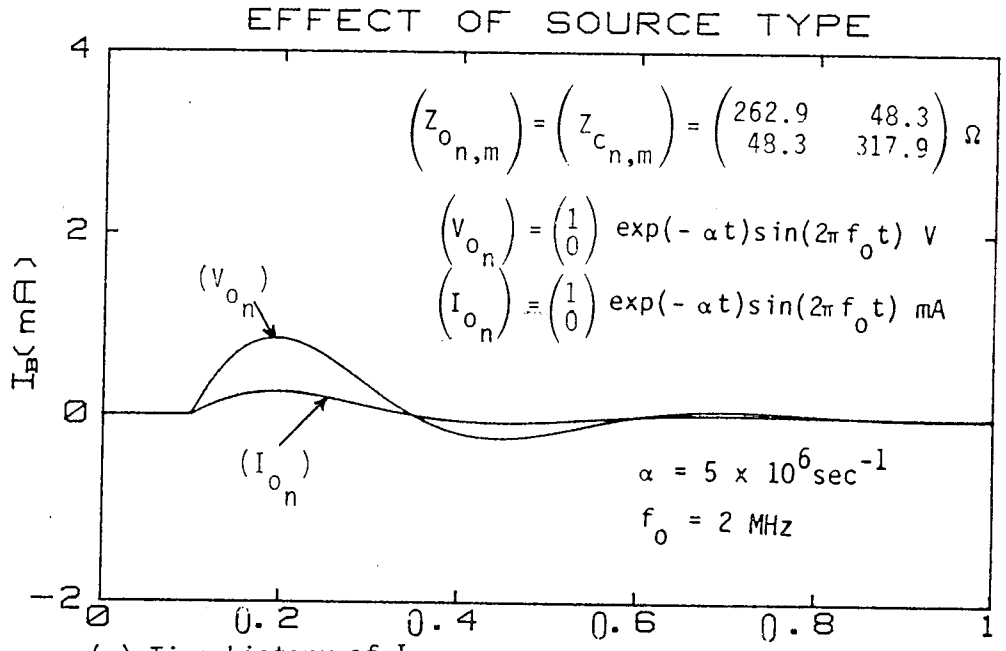

(a) Time history of I_B.

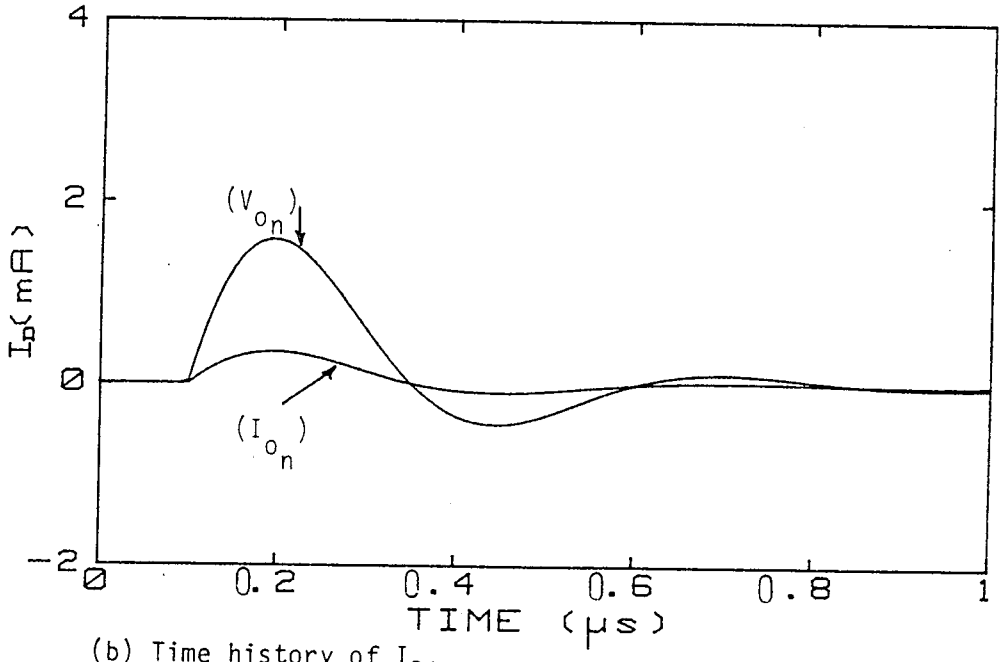

(b) Time history of I_D.

Figure B18. Common and differential mode currents (I_B, I_D) for different types of source when ℓ = 30 m, x_s = 0.25 m, x_m = 30 m, $Z_{\ell 11}$ = $Z_{\ell 12}$ = $Z_{\ell 22}$ = 400 Ω.

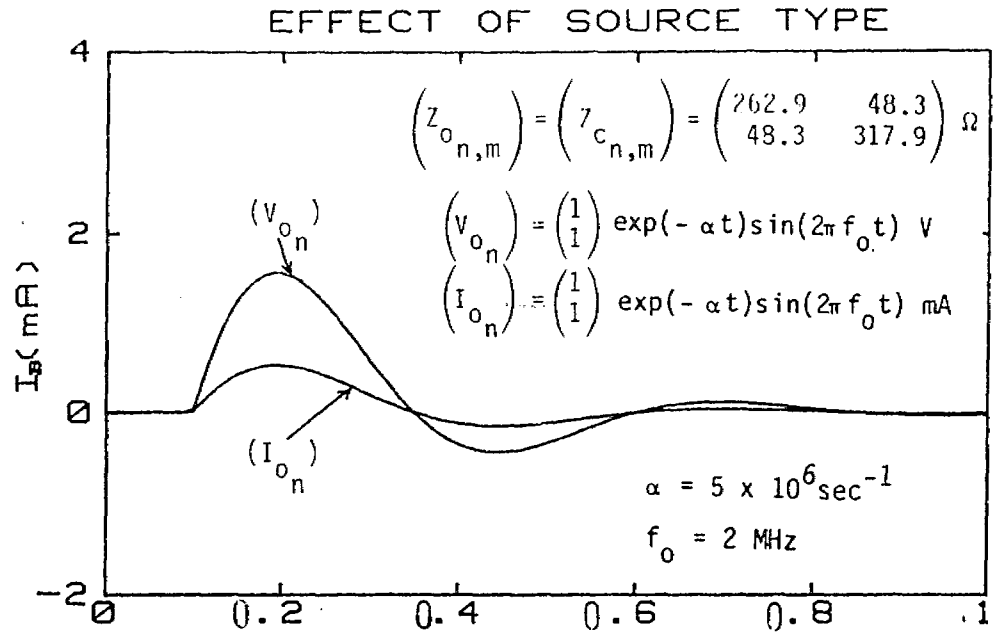

(a) Time history of I_B.

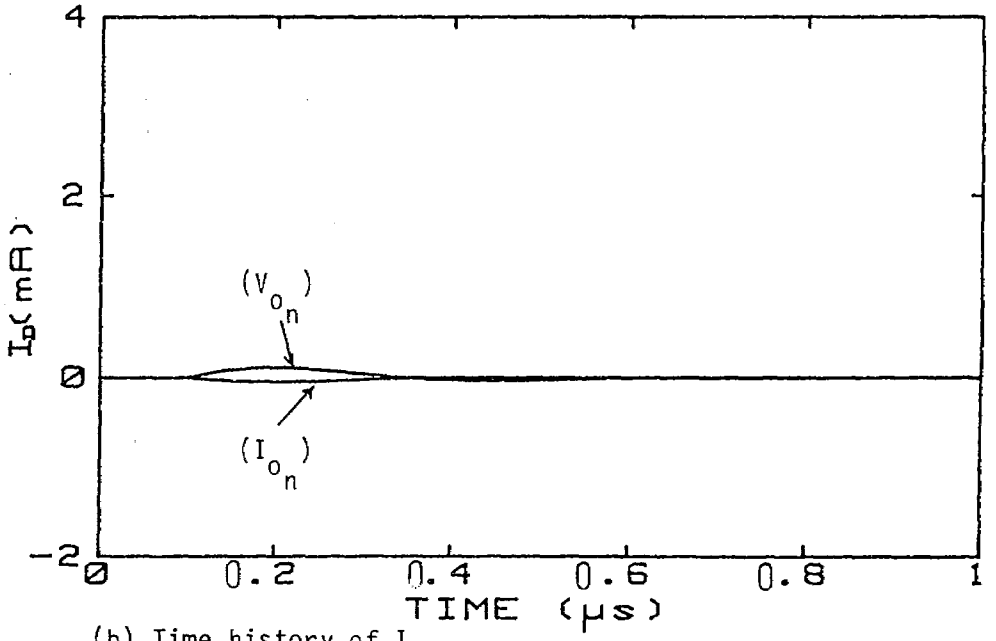

(b) Time history of I_D.

Figure B19. Common and differential mode currents (I_B, I_D) for different types of source when ℓ = 30 m, x_s = 0.25 m, x_m = 30 m, $Z_{\ell 11}$ = $Z_{\ell 12}$ = $Z_{\ell 22}$ = 400 Ω.

4. EFFECT OF SOURCE LOCATION

Figures B20 and B21 illustrate effects of source location on common- and differential-mode currents (I_B, I_D).

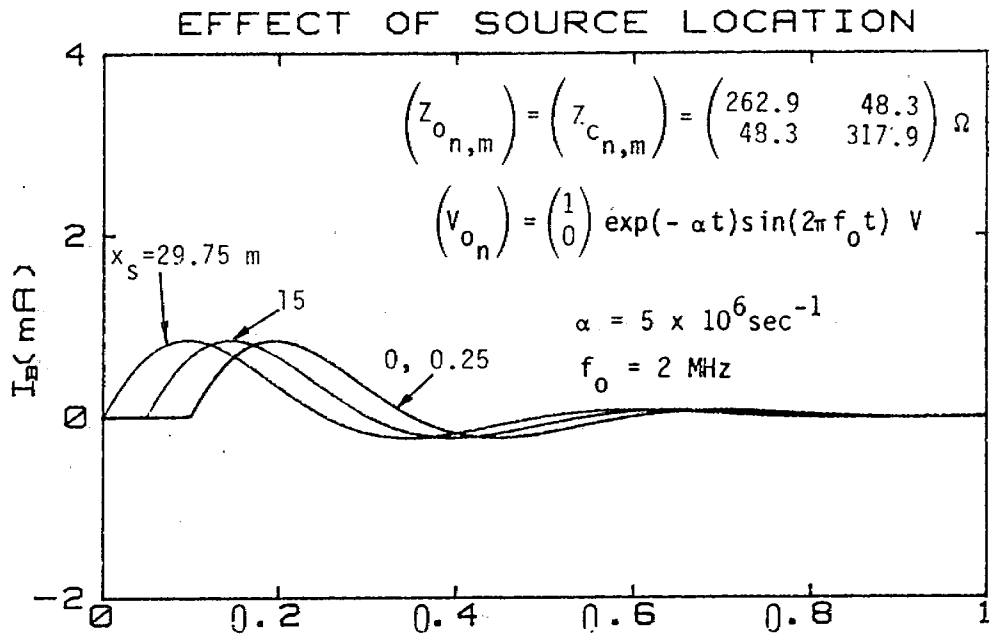

(a) Time history of I_B.

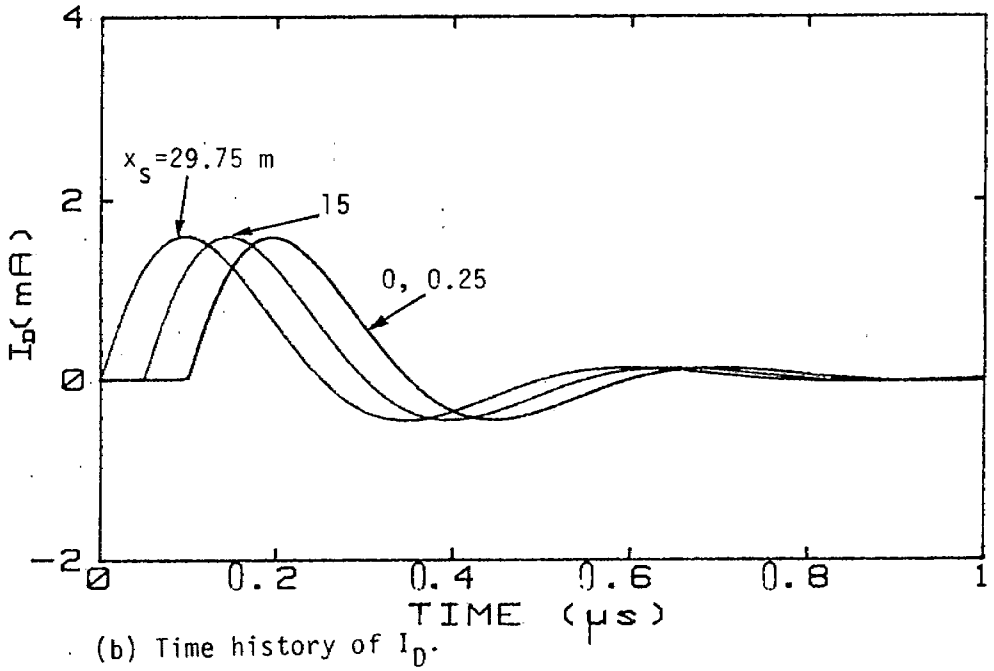

(b) Time history of I_D.

Figure B20. Common and differential mode currents (I_B, I_D) for different source locations when ℓ = 30 m, x_m = 30 m, $Z_{\ell 11} = Z_{\ell 12} = Z_{\ell 22}$ = 400 Ω.

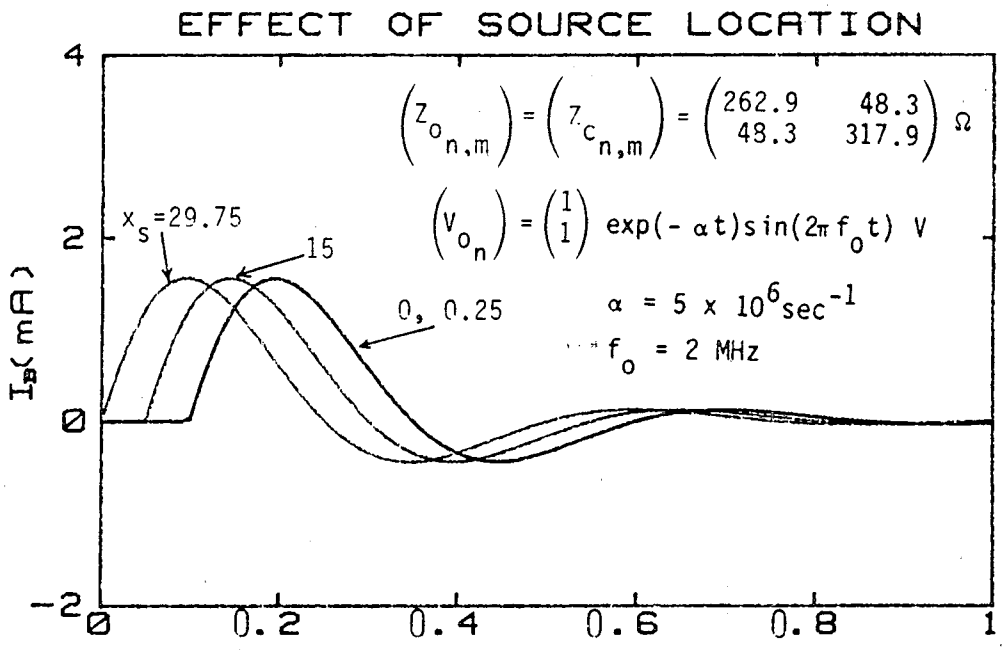

(a) Time history of I_B.

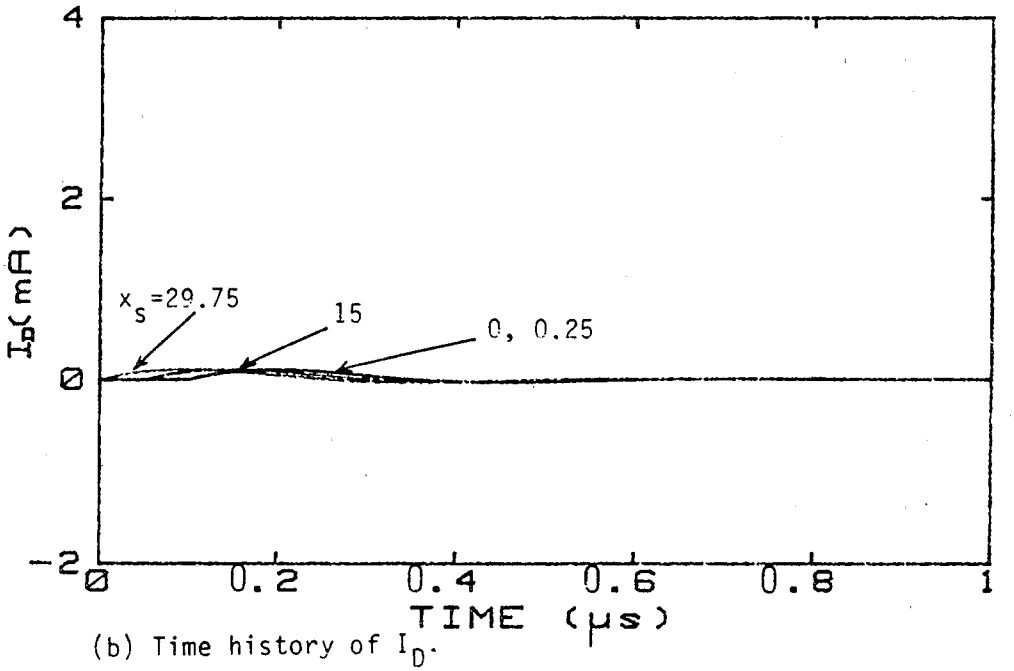

(b) Time history of I_D.

Figure B21. Common and differential mode currents (I_B, I_D) for different source locations when ℓ = 30 m, x_m = 30 m, $Z_{\ell 11} = Z_{\ell 12} = Z_{\ell 22}$ = 400 Ω.

5. EFFECT OF NUMBER OF EXCITED WIRES

Figures B22 through B30 illustrate effects of number of excited wires on common- and differential-mode currents (I_B, I_D).

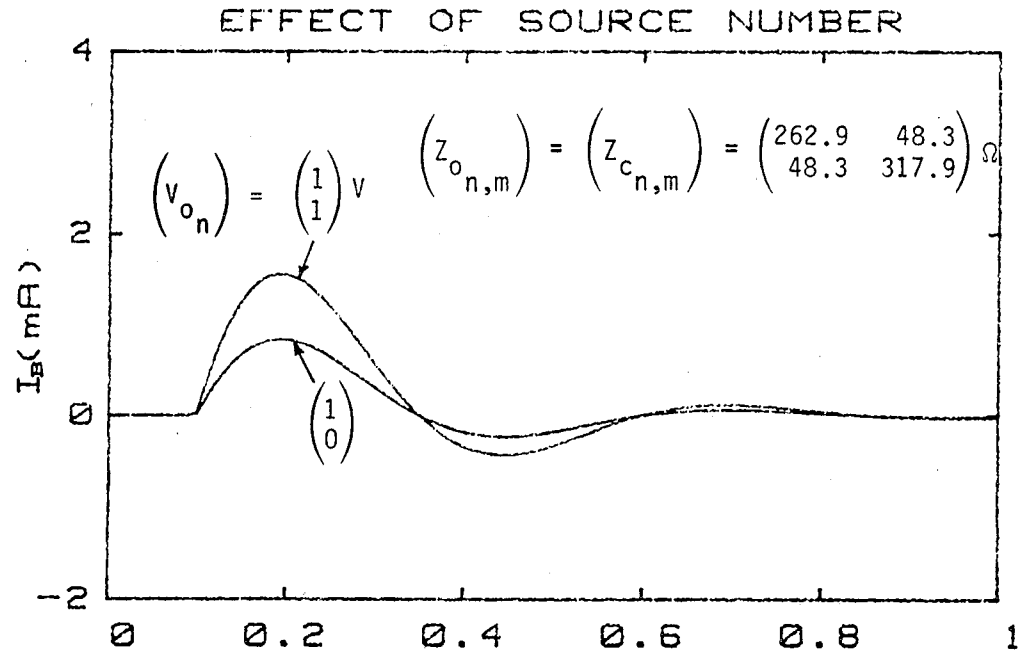

(a) Time history of I_B.

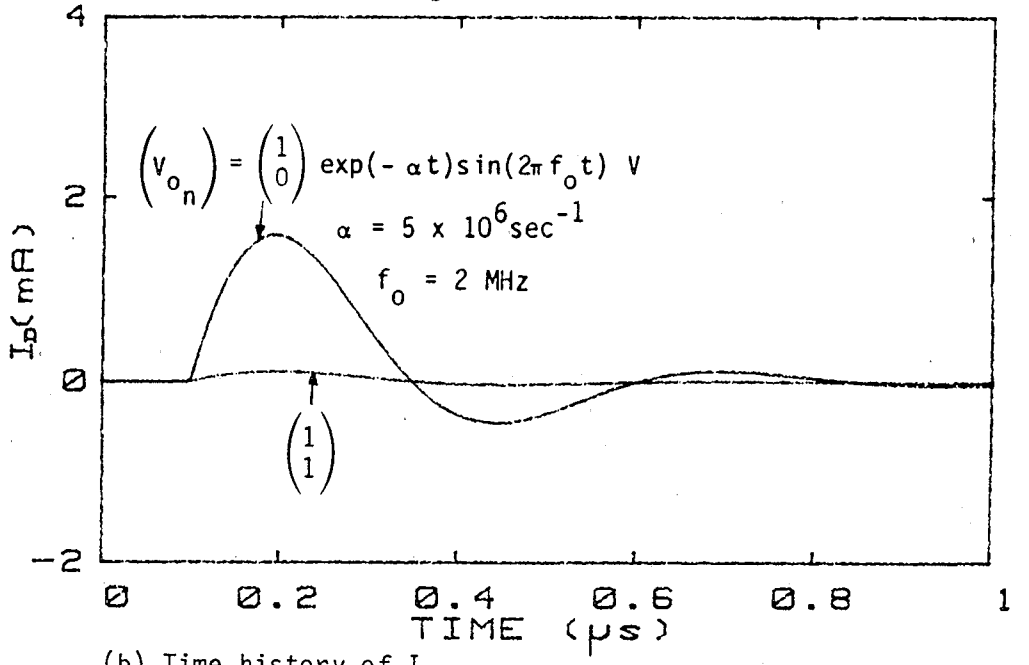

(b) Time history of I_D.

Figure B22. Common and differential mode currents (I_B, I_D) for different numbers of sources when ℓ = 30 m, x_s = 0.25 m, x_m = 30 m, $Z_{\ell 11}$ = $Z_{\ell 12}$ = $Z_{\ell 22}$ = 400 Ω.

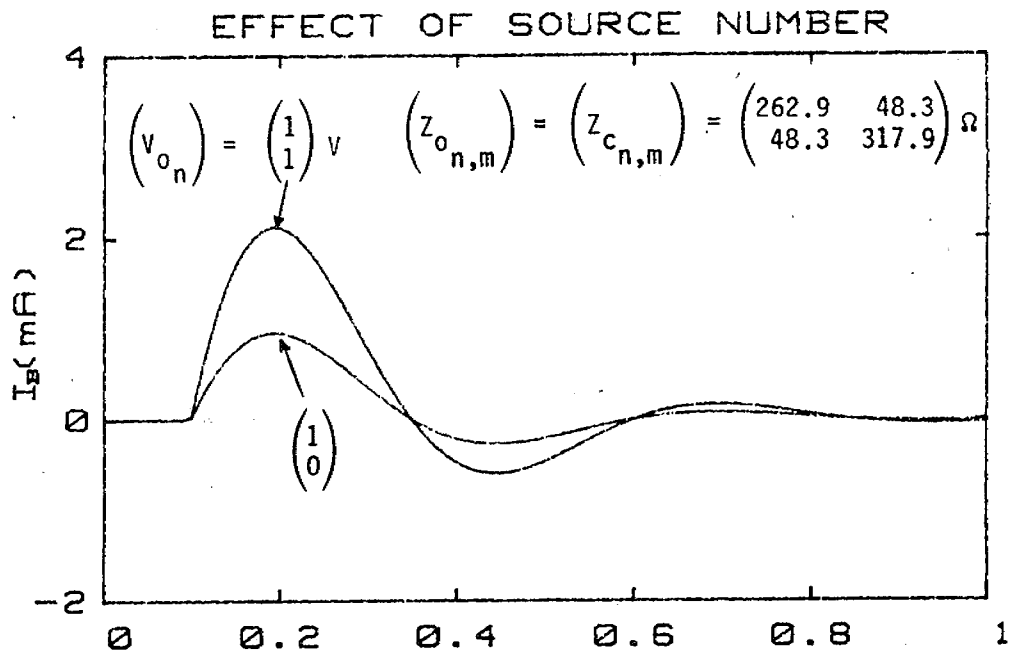

(a) Time history of I_B.

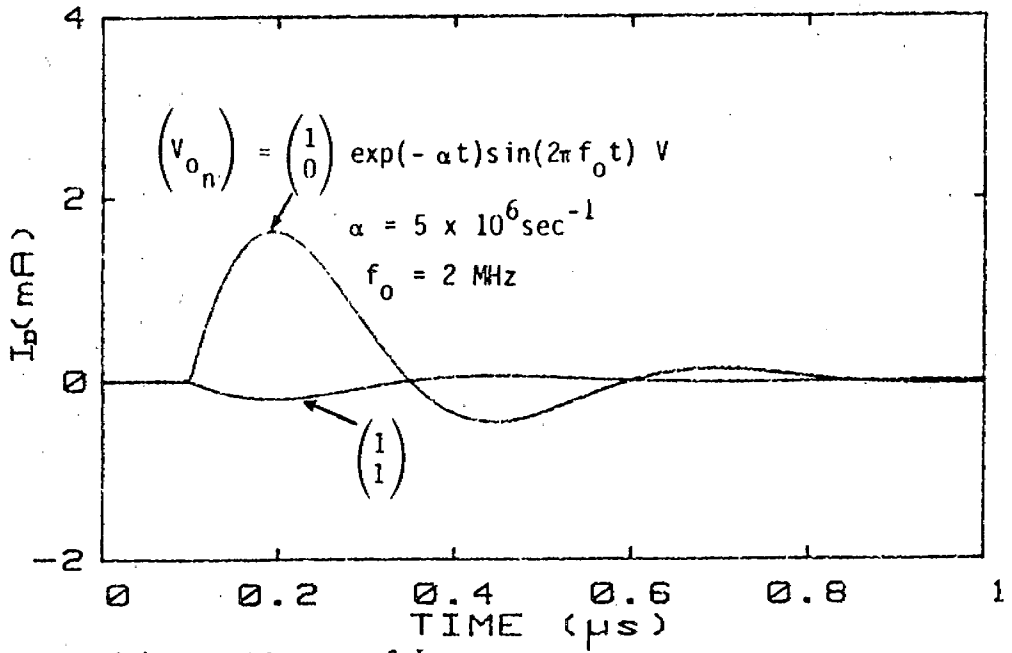

(b) Time history of I_D.

Figure B23. Common and differential mode currents (I_B, I_D) for different numbers of sources when ℓ = 30 m, x_s = 0.25 m, x_m = 30 m, $Z_{\ell 11}$ = 500 Ω, $Z_{\ell 12}$ = 250 Ω, $Z_{\ell 22}$ = 100 Ω.

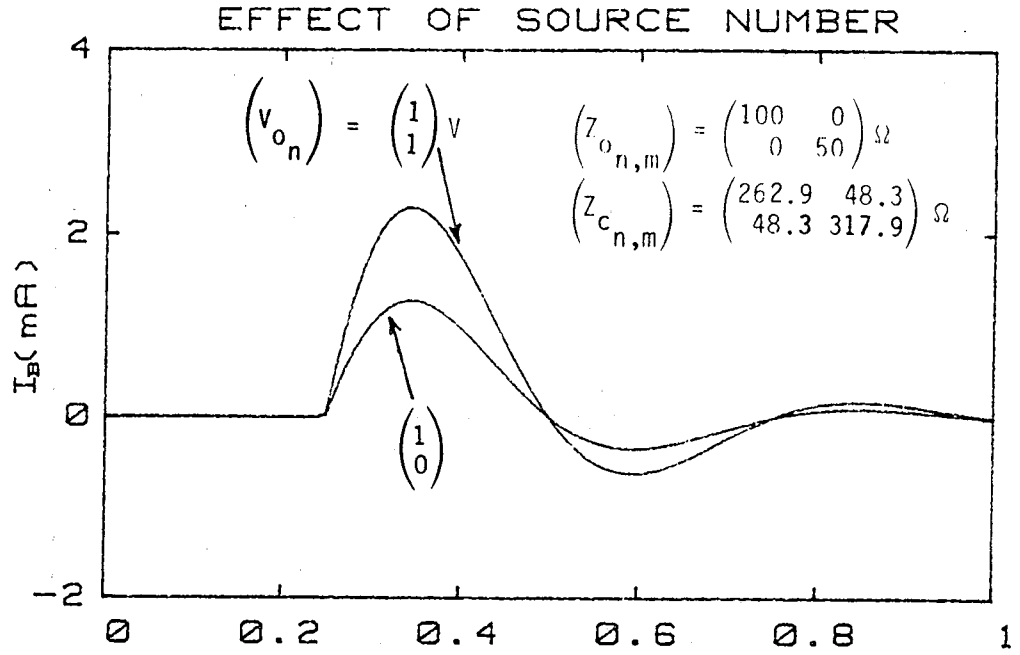

(a) Time history of I_B.

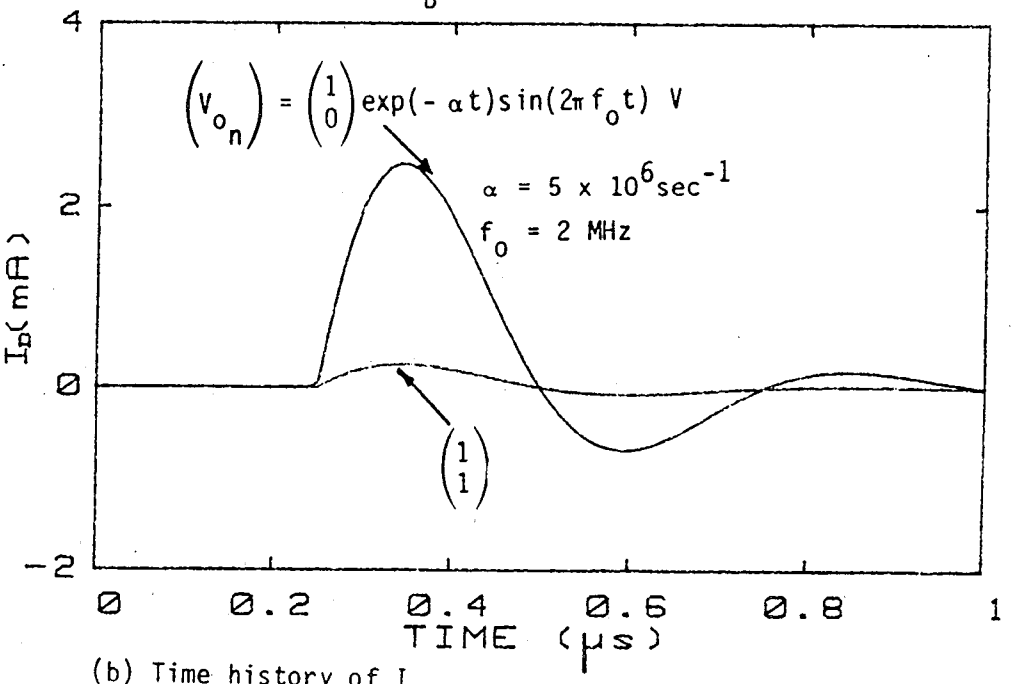

(b) Time history of I_D.

Figure B24. Common and differential mode currents (I_B, I_D) for different numbers of sources when ℓ = 30 m, x_s = 0.25 m, x_m = 75 m, $Z_{\ell 11}$ = 100 Ω, $Z_{\ell 12}$ = 1 Ω, and $Z_{\ell 22}$ = 400 Ω.

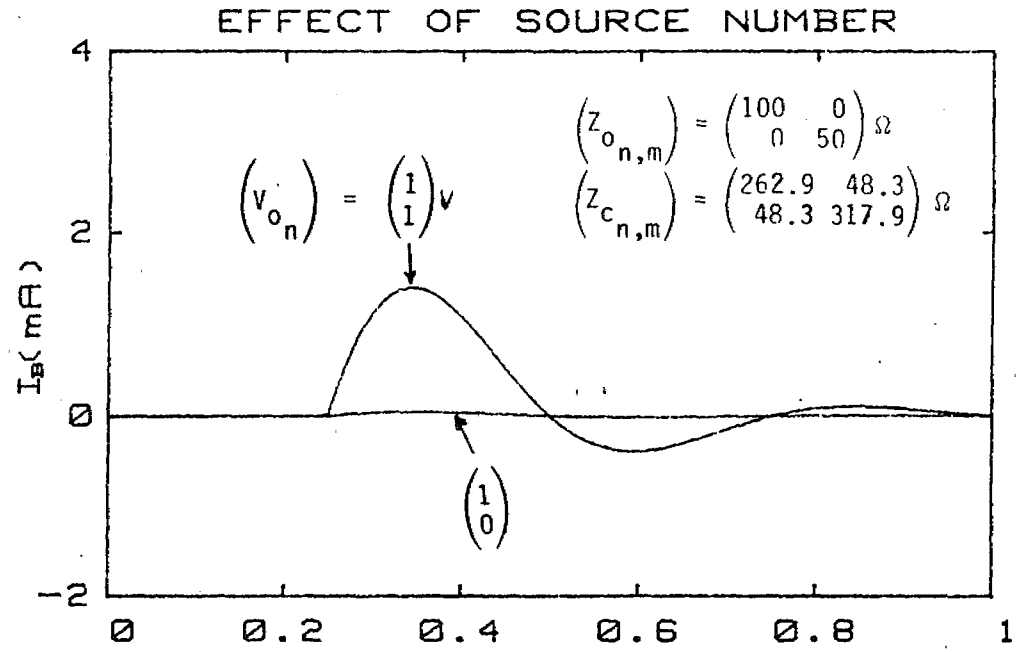

(a) Time history of I_B.

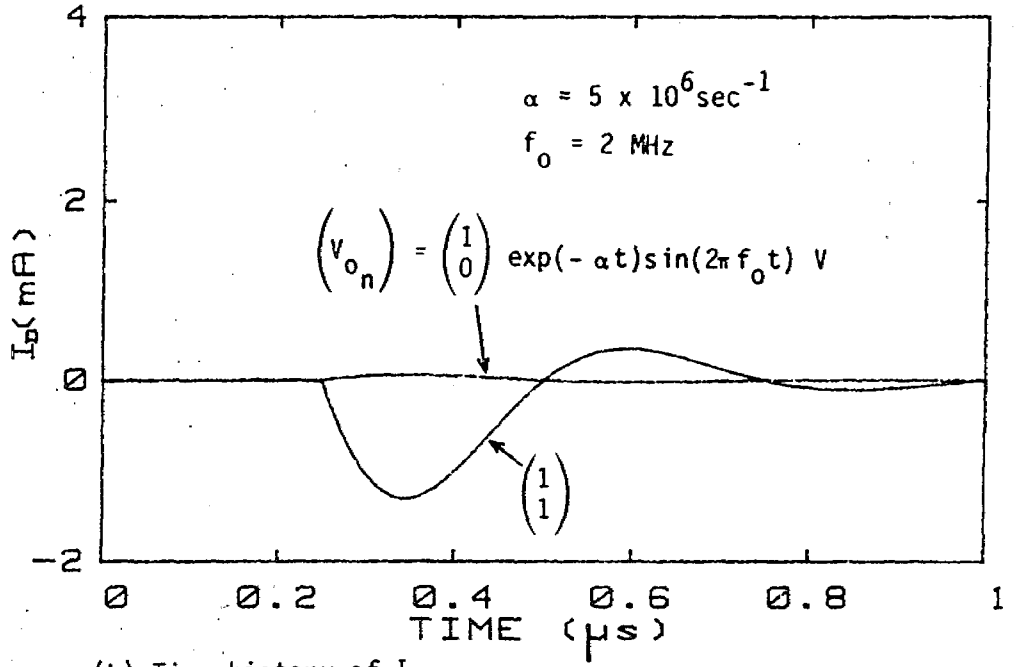

(b) Time history of I_D.

Figure B25. Common and differential mode currents (I_B, I_D) for different numbers of sources when ℓ = 30 m, x_s = 0.25 m, x_m = 75 m, $Z_{\ell 11}$ = 10^4 Ω, $Z_{\ell 12}$ = ∞, and $Z_{\ell 22}$ = 100 Ω.

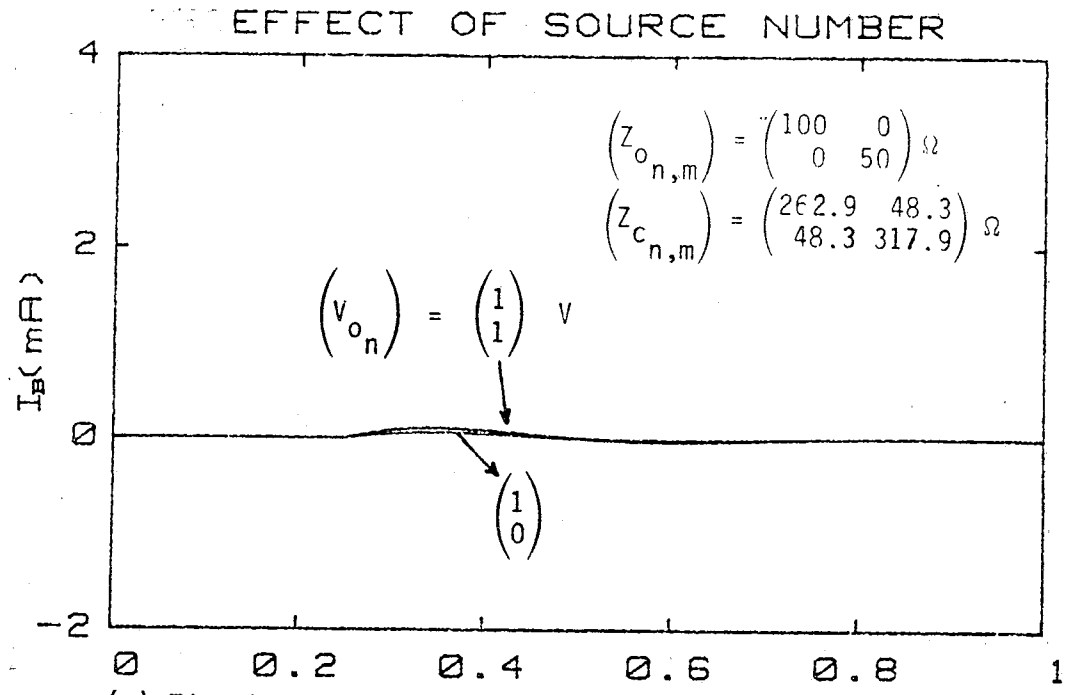

(a) Time history of I_B.

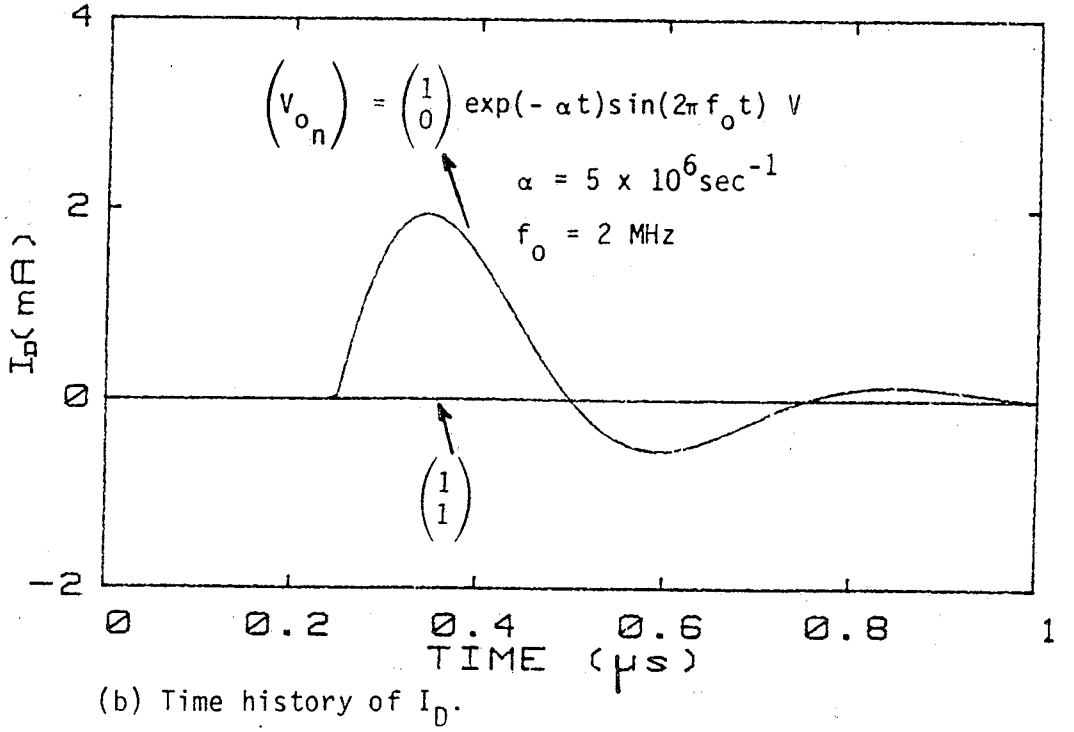

(b) Time history of I_D.

Figure B26. Common and differential mode currents (I_B, I_D) for different numbers of sources when ℓ = 30 m, x_s = 0.25 m, x_m = 75 m, $Z_{\ell 11}$ = $Z_{\ell 22}$ = $10^4\Omega$, and $Z_{\ell 12}$ = 100 Ω.

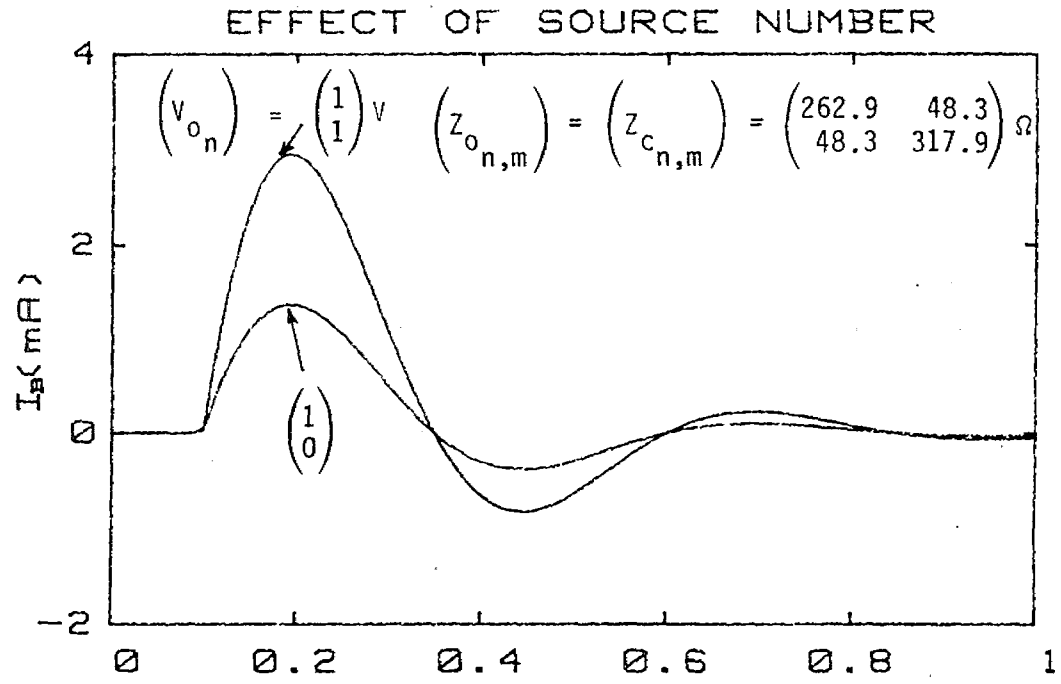

(a) Time history of I_B.

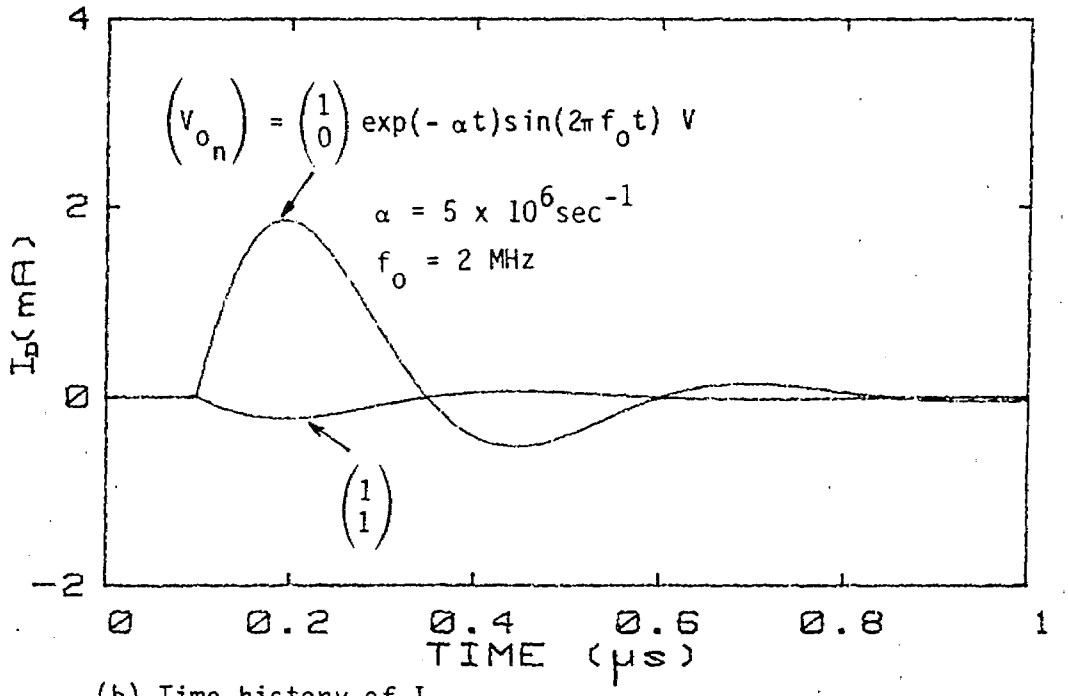

(b) Time history of I_D.

Figure B27. Common and differential mode currents (I_B, I_D) for different numbers of sources when ℓ = 30 m, x_s = 0.25 m, x_m = 30 m, $Z_{\ell 11}$ = $10^4\Omega$, $Z_{\ell 12}$=100 Ω, and $Z_{\ell 22}$ = 1 Ω.

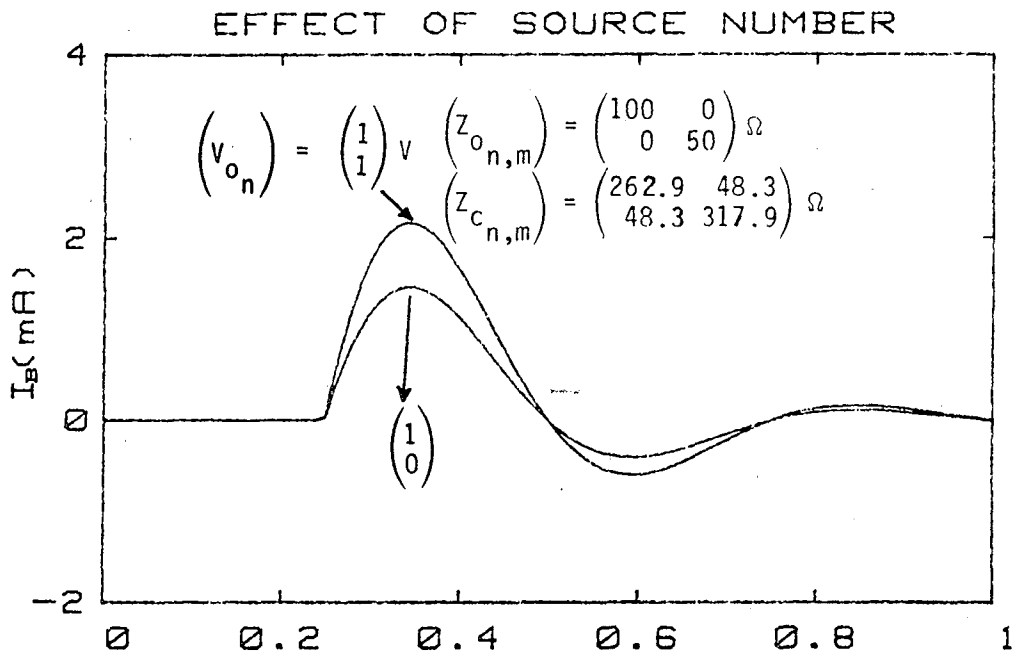

(a) Time history of I_B.

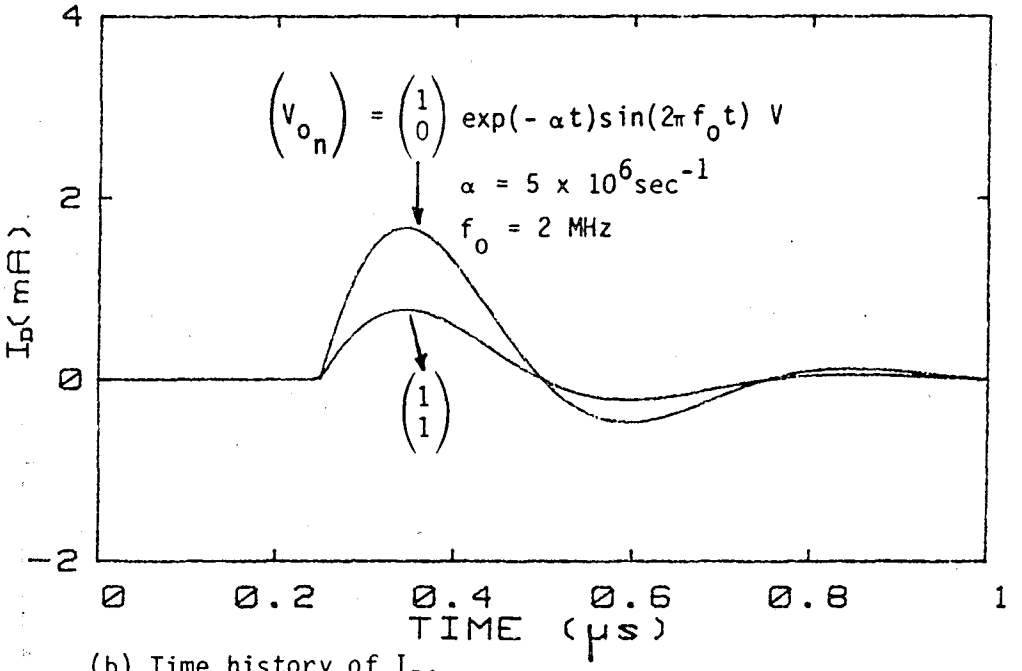

(b) Time history of I_D.

Figure B28. Common and differential mode currents (I_B, I_D) for different numbers of sources when ℓ = 30 m, x_s = 0.25 m, x_m = 75 m, $Z_{\ell 11}$ = 100 Ω, $Z_{\ell 12}$ = ∞ Ω, and $Z_{\ell 22}$ = 400 Ω.

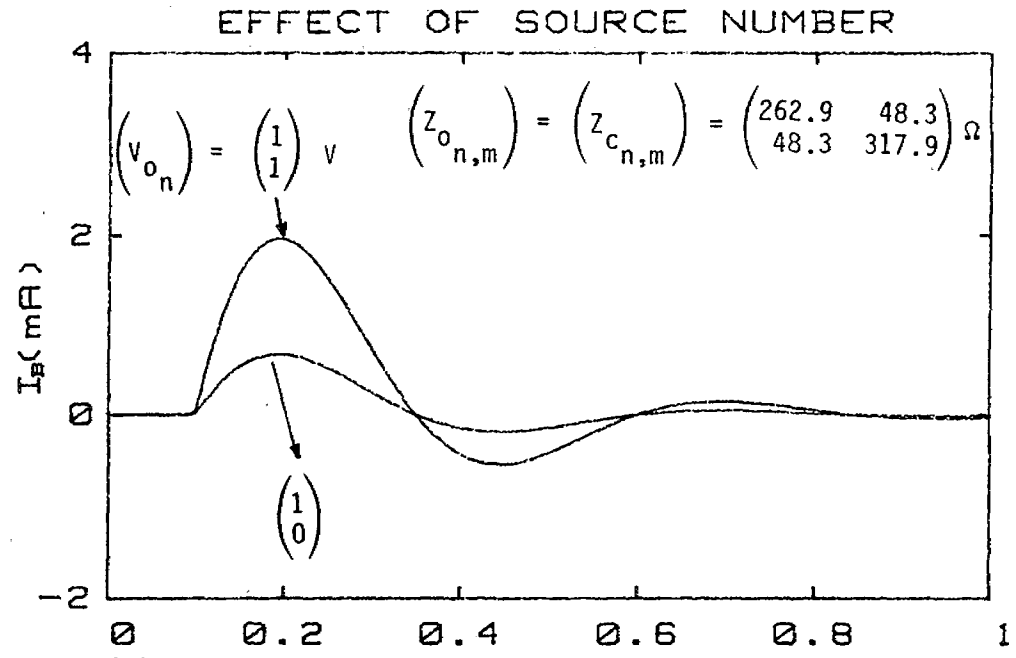

(a) Time history of I_B.

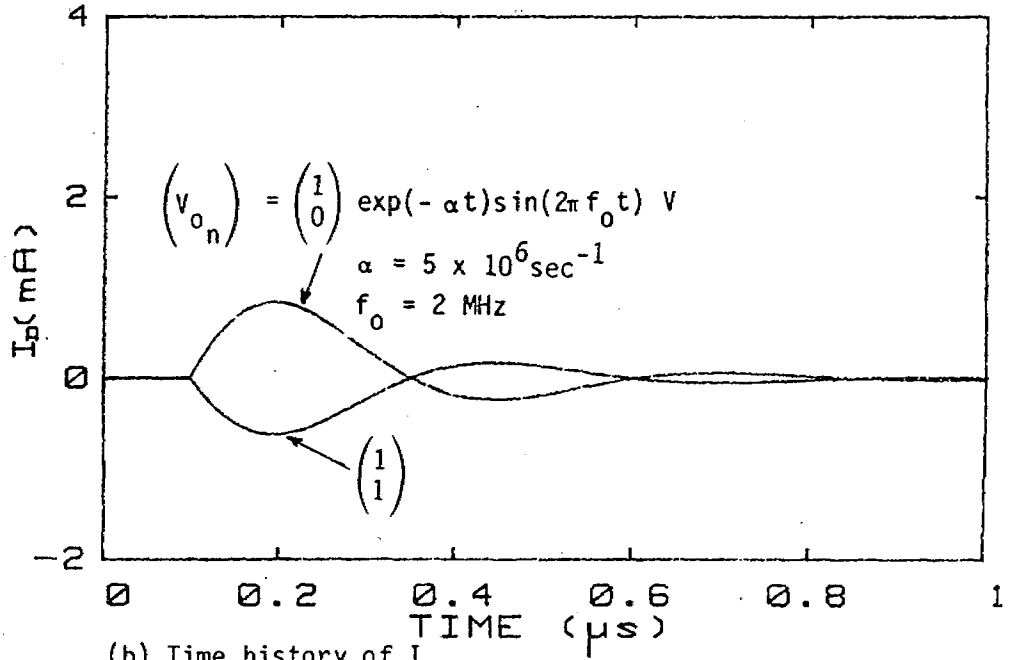

(b) Time history of I_D.

Figure B29. Common and differential mode currents (I_B, I_D) for different numbers of sources when ℓ = 30 m, x_s = 0.25 m, x_m =30 m, $Z_{\ell 11}$ = 500 Ω, $Z_{\ell 12}$ = ∞, and $Z_{\ell 22}$ = 100 Ω.

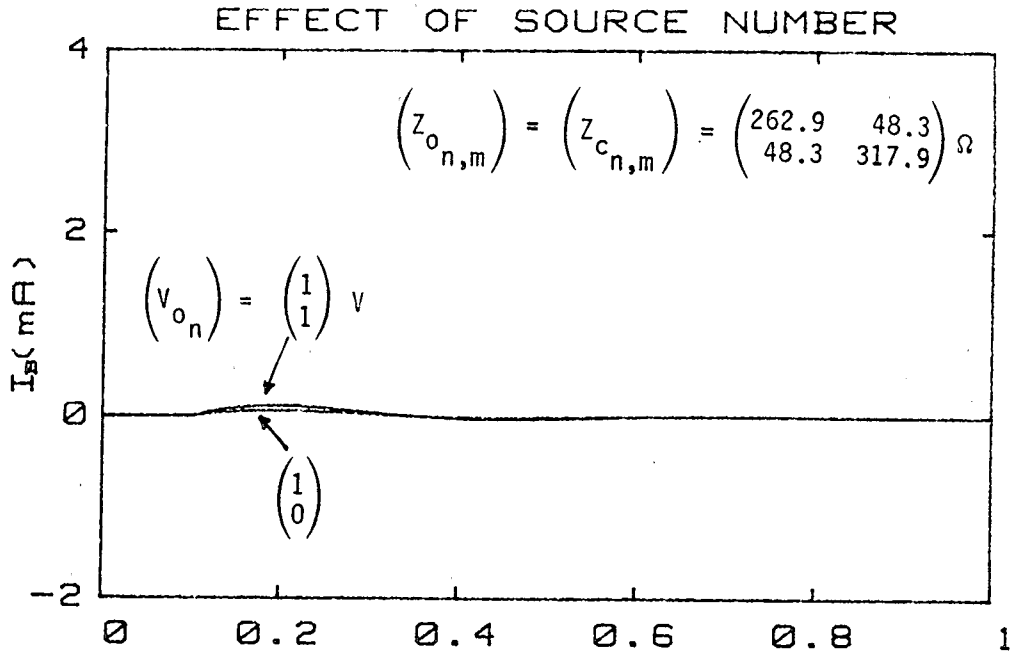

(a) Time history of I_B.

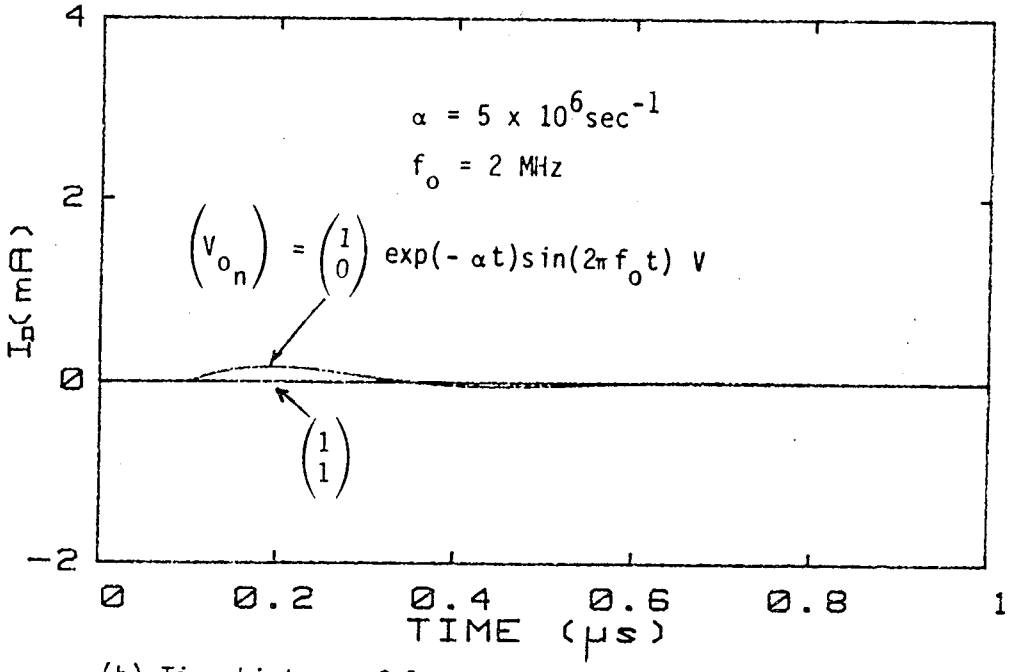

(b) Time history of I_D.

Figure B30. Common and differential mode currents (I_B, I_D) for different numbers of sources when ℓ = 30 m, x_s = 0.25 m, x_m = 30 m, $Z_{\ell 11}$ = $Z_{\ell 12}$ = $Z_{\ell 22}$ = $10^4 \Omega$.

6. EFFECT OF LINE PARAMETERS (CHARACTERISTIC IMPEDANCE)

Figure B31 illustrates the effects of characteristic impedance of the cable ($Z_{C_{m,n}}$) on common- and differential-mode currents (I_B, I_D).

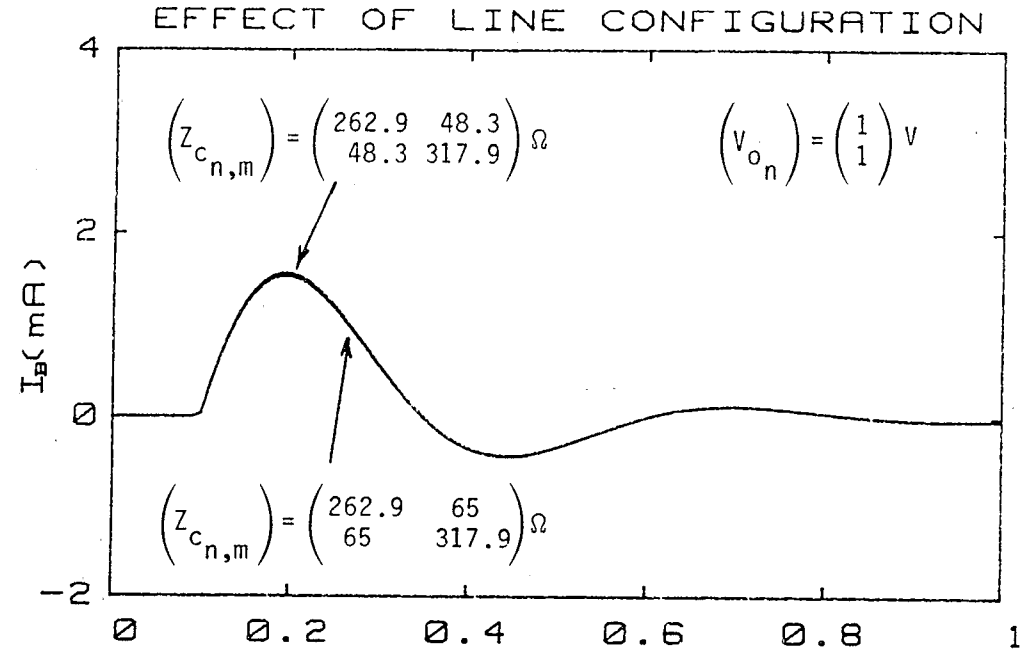

(a) Time history of I_B.

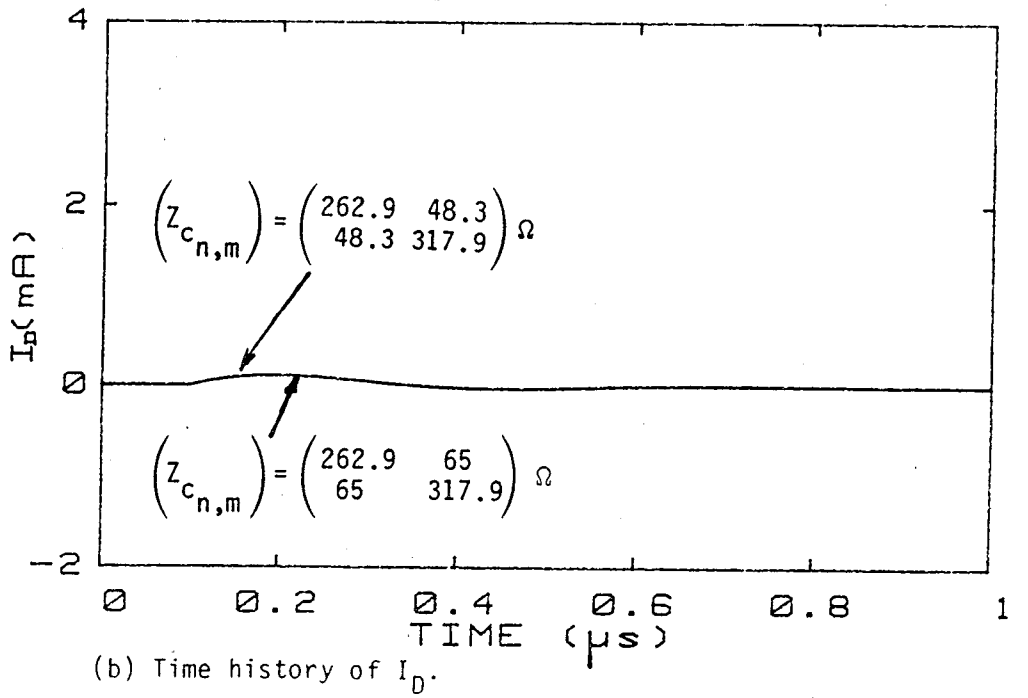

(b) Time history of I_D.

Figure B31. Common and differential mode currents (I_B, I_D) for different characteristic impedances when ℓ = 30 m, x_s = 0.25 m, x_m = 30 m, $Z_{\ell 11} = Z_{\ell 12} = Z_{\ell 22}$ = 400 Ω, and $(Z_{o_{n,m}}) = (Z_{c_{n,m}})$.

7. EFFECT OF MEASUREMENT LOCATION

Figures B32 through B35 illustrate effects of measurement location on common- and differential-mode currents (I_B, I_D).

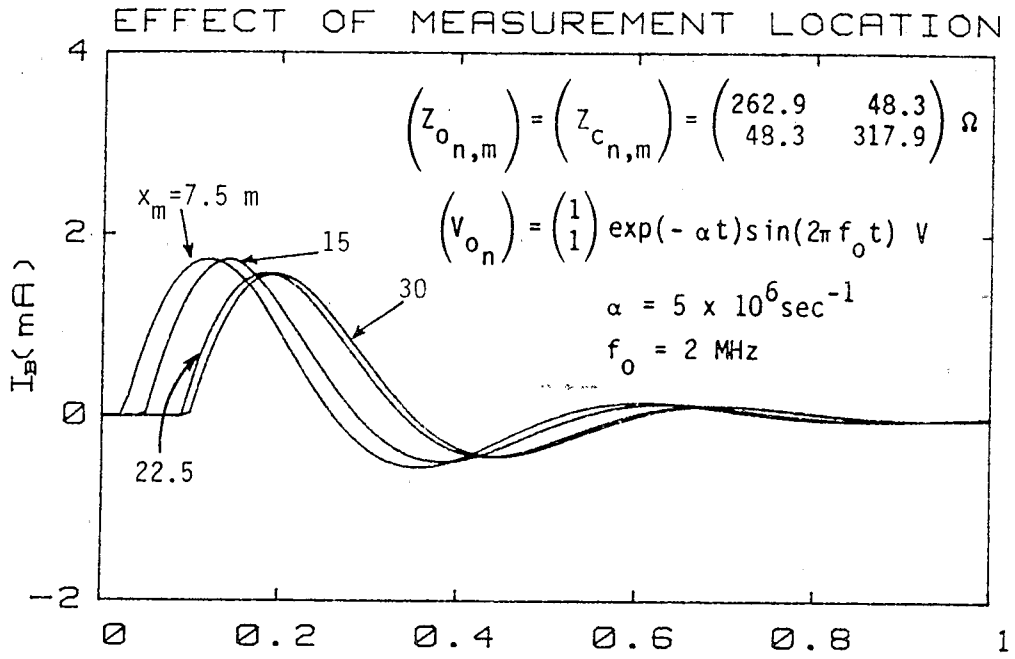

(a) Time history of I_B.

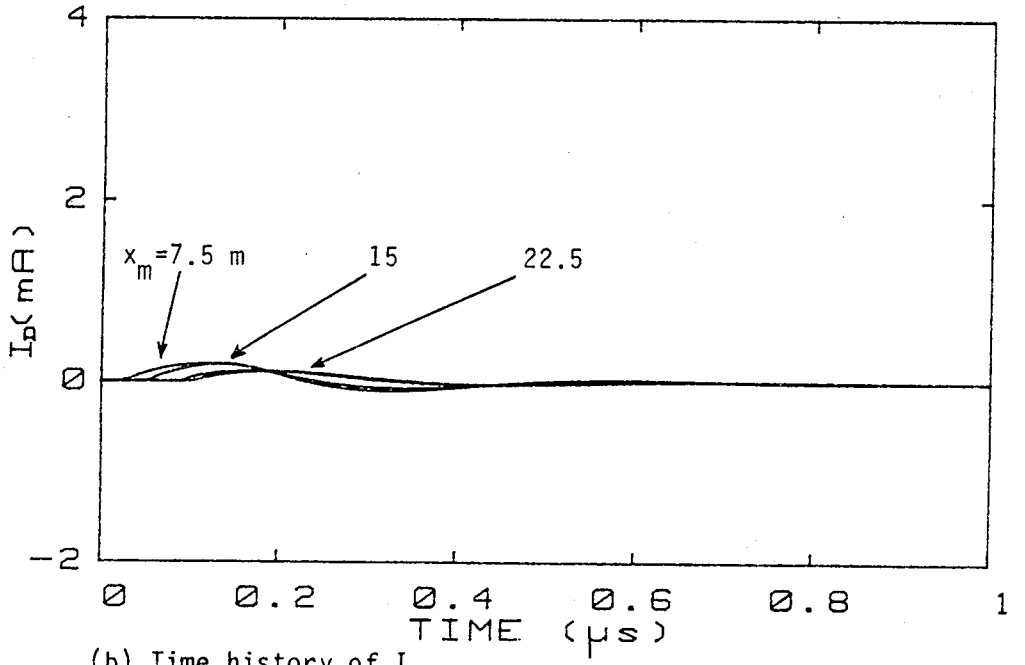

(b) Time history of I_D.

Figure B32. Common and differential mode currents (I_B, I_D) for different measurement locations when ℓ = 30 m, x_s = 0.25 m, $Z_{\ell 11} = Z_{\ell 12} = Z_{\ell 22}$ = 400 Ω.

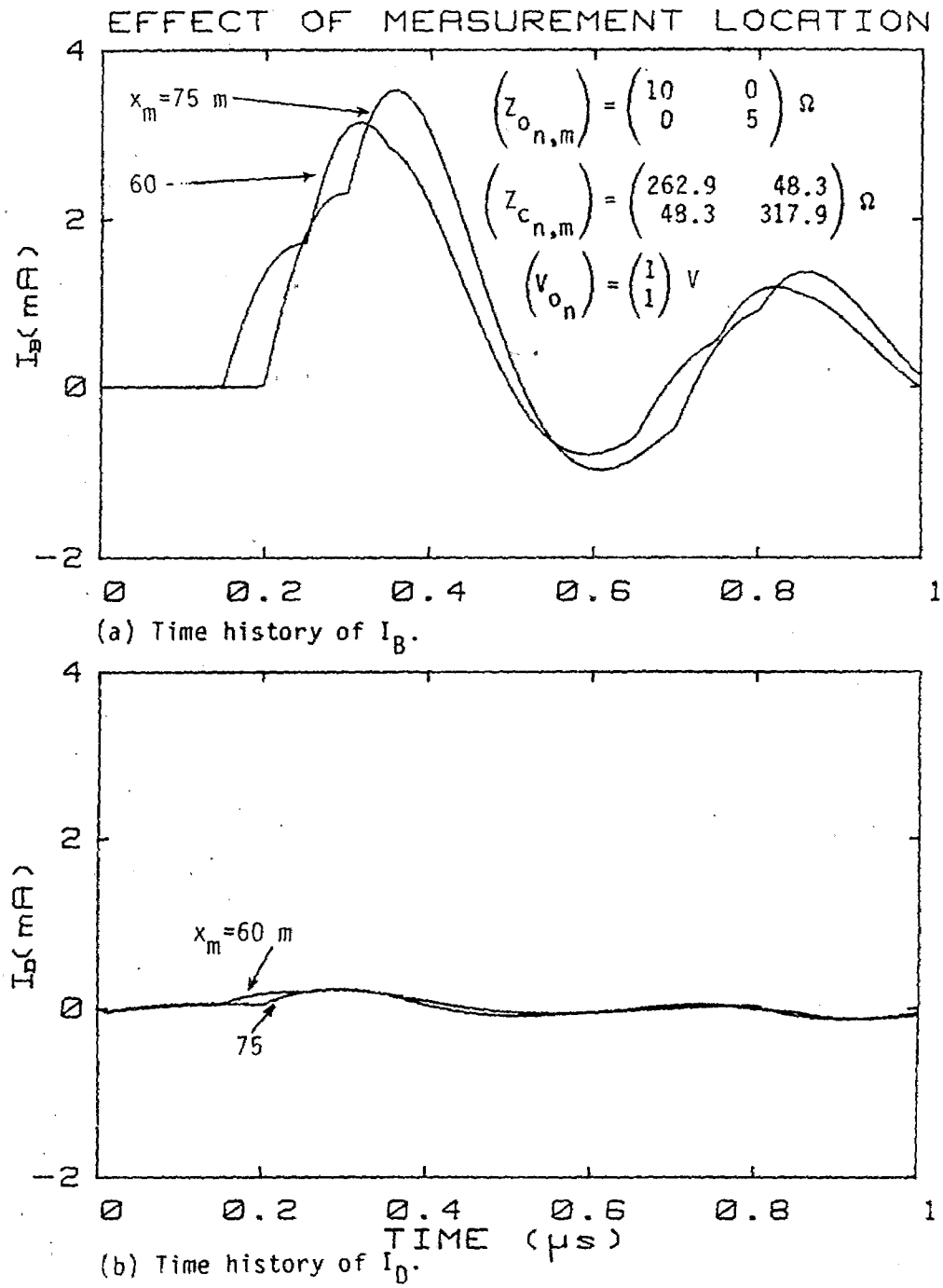

Figure B33. Common and differential mode currents (I_B, I_D) for different measurement locations when ℓ = 75 m, x_s = 15 m, $Z_{\ell 11}$ = 100 Ω, $Z_{\ell 12}$ = 1 Ω, $Z_{\ell 22}$ = 400 Ω.

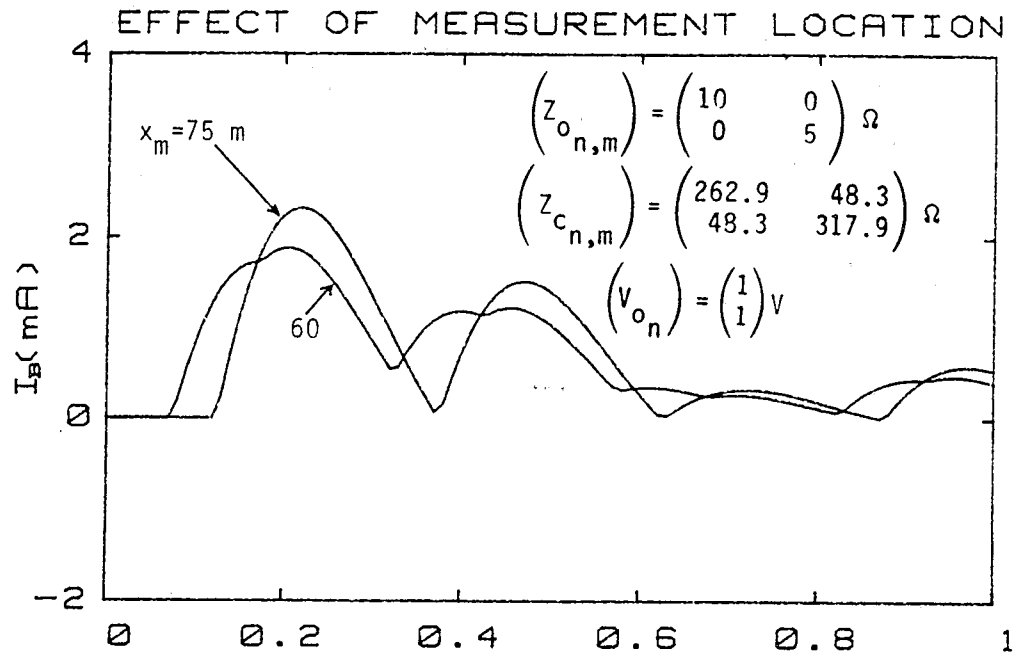

(a) Time history of I_B.

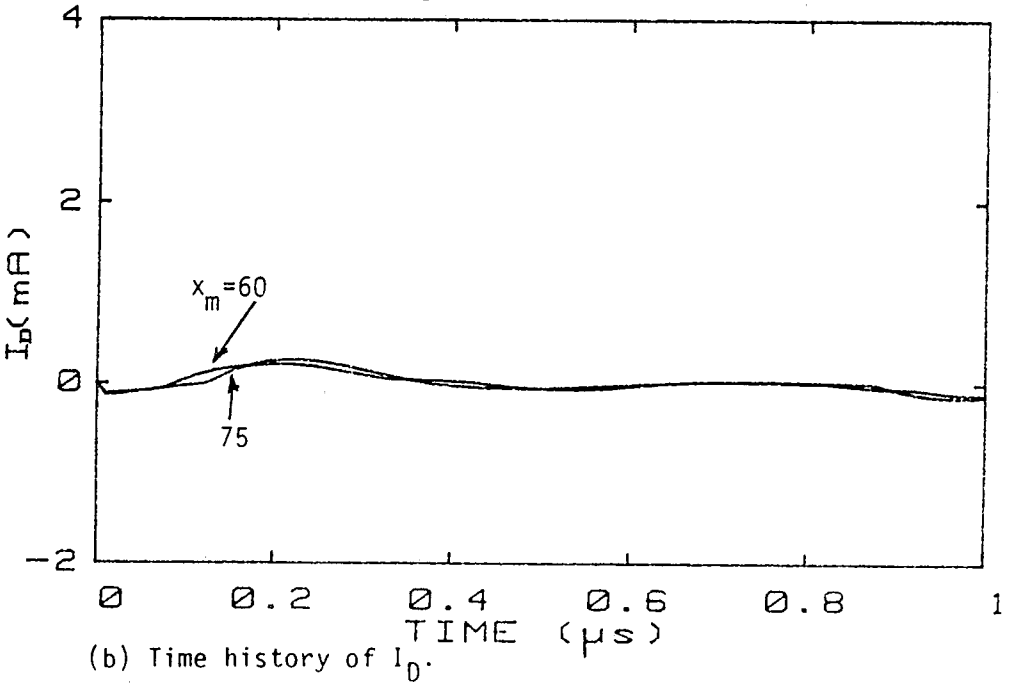

(b) Time history of I_D.

Figure B34. Common and differential mode currents (I_B, I_D) for different measurement locations when ℓ = 75 m, x_s = 37.5 m, $Z_{\ell 11}$ = 100 Ω, $Z_{\ell 12}$ = 1 Ω, and $Z_{\ell 22}$ = 400 Ω.

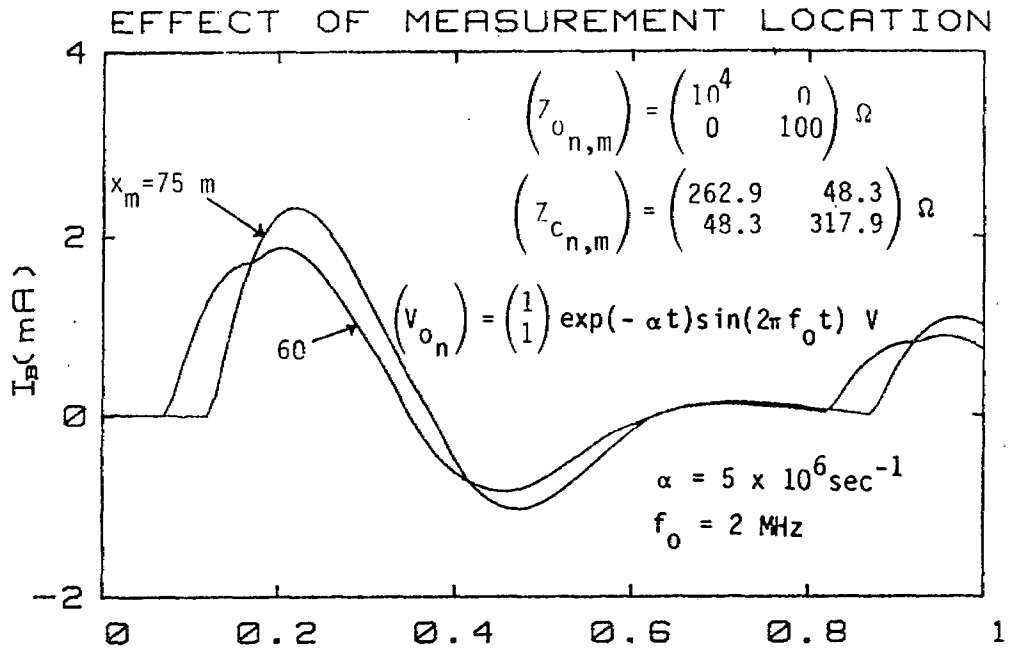

(a) Time history of I_B.

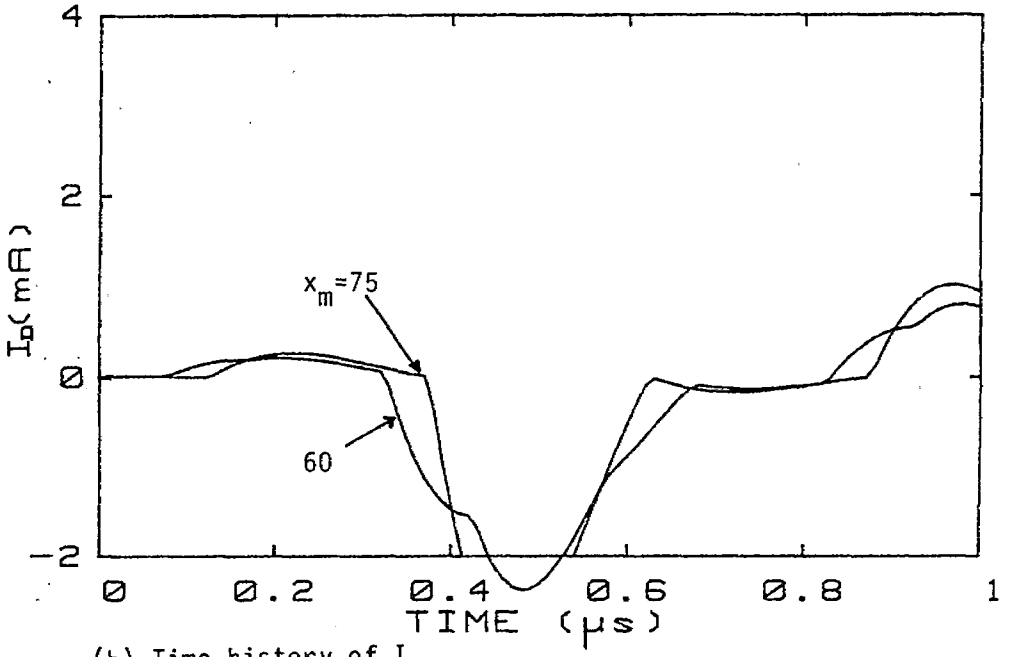

(b) Time history of I_D.

Figure B35. Common and differential mode currents (I_B, I_D) for different measurement locations when ℓ = 75 m, x_s = 37.5 m, $Z_{\ell 11}$ = 100 Ω, $Z_{\ell 12}$ = 1 Ω, and $Z_{\ell 22}$ = 400 Ω.

☆U.S. GOVERNMENT PRINTING OFFICE: 1984–776-131/10,000